Pontifical Catholic University of Chile
Faculty of Physics

Observational constraints in Delta Gravity: CMB and supernovas

by

Marco San Martín Hormazábal

A dissertation presented by Marco San Martín Hormazábal
to The Faculty of Physics
in partial fulfillment of the requirements
for the degree of Ph.D. in Astrophysics.

Thesis advisor	:	Ph.D. Jorge Alfaro (PUC)
Informant Committee	:	Gonzalo Palma (UCH)
		Rolando Dünner (PUC)
		Alejandro Clocchiatti (PUC)
		Leopoldo Infante (PUC)

September 2020, Santiago, Chile

Declaration of authorship

I, Marco San Martín, declare that this thesis titled, 'Observational constraints in Delta Gravity: CMB and supernovas' and the work presented in it are my own. I confirm that:

- This work was done wholly or mainly while in candidature for a research degree at this University.
- Where any part of this thesis has previously been submitted for a degree or any other qualification at this University or any other institution, this has been clearly stated.
- Where I have consulted the published work of others, this is always clearly attributed.
- Where I have quoted from the work of others, the source is always given. With the exception of such quotations, this thesis is entirely my own work.
- I have acknowledged all main sources of help.
- Where the thesis is based on work done by myself jointly with others, I have made clear exactly what was done by others and what I have contributed myself.

Signed: _____

Date: _____

"Have you not learned from your greatest hurts, sometimes even more than from your greatest pleasures? Who, then, is the villain, and who is the victim in your life?"

Pontifical Catholic University of Chile

Abstract

Ph.D. in Astrophysics

by Marco San Martín Hormazábal

We study the cosmological implications of Delta Gravity (DG), which is a gravitational model based on the extension of General Relativity (GR) by a new symmetry called $\tilde{\delta}$. In this model, new matter fields are added to the original matter fields, motivated by the additional symmetry. We call them $\tilde{\delta}$ matter fields. This theory predicts an accelerating Universe without the need to introduce a Cosmological Constant Λ by hand in the equations.

To test the Delta Gravity implications, we examine two critical observations in Cosmology: the rate of the Universe expansion through type Ia supernovae (SNe-Ia) and the power spectrum calculated from the cosmic microwave background radiation (CMB). To compare the observations with these model's predictions, we used a Markov Chain Monte Carlo (MCMC) analysis with the most updated catalog of SNe-Ia and Planck satellite's data.

We obtain the fitted parameters needed to explain both SNe-Ia data and CMB measurements. We analyze the DG model's compatibility with both observations and constrain the cosmological parameters associated with the astrophysical evidence. Finally, we discuss if the Hubble Constant and the Accelerating Universe are compatible with the observational evidence in the DG context.

Acknowledgements

It is a great pleasure to thank my advisor, prof. Jorge Alfaro, for an excellent collaboration. He inspired me to learn about more complicated problems. His experience, ability, and view of how to solve physics problems, approaches, and interpretations improved my understanding of physics. He always was open to answering my questions and supporting my new ideas, sometimes some controversial. His availability lets me approach the problem from different points of view and mix computation, astronomy, and physics in a single project.

I want to thank The Institute of Astrophysics and The Institute of Physics of the Pontifical Catholic University of Chile for its hospitality.

I also want to thank prof. Julio Chanamé and the graduate committee for their institutional management during my doctoral program graduation. Thanks to the Chilean government who supported me by the scholarship Conicyt Ph.D. Fellowship No. 21170604, Fondecyt 1150390, and Conicyt-PIA-ACT14177.

I especially appreciate the help and support that prof. Nelson Padilla, Carlos Rubio, Joaquín Sureda, and Eduardo Núñez gave me during my Ph.D. studies. You all contributed in some way to this thesis and my doctoral studies. I am very grateful for your help, and in some way, everyone helped make this possible.

Finally, Eduardo, Joaquín, Julio, and Constanza have been an important part of my life. Thank you for your love, support, friendship, and the good times we have spent together.

Contents

Chapter 1

Introduction

1.1 ΛCDM

Cosmology is a subject where we can find many data and information to contrast them with theoretical physics. In this context, the scientific community has evidence that shows most of the composition of the Universe is unknown: Dark Matter (DM) and Dark Energy (DE) [67, 53, 45, 20]. most of the matter is in the form of unknown matter, DM, and a mysterious component of the Universe, called DE, governs the dynamics of the accelerating expansion. Although General Relativity (GR) can accommodate both DM and DE, the interpretation of the dark sector in terms of fundamental theories of elementary particles is problematic.[38]

The standard knowledge about cosmology is mainly based on the Standard Cosmological model called ΛCDM. In this model, Λ represents the DE [38]. This constant is strictly necessary to reproduce the acceleration of the Universe. Any other component only creates deceleration (in the GR context). ΛCDM cosmology [53] can fit the observational SNe-Ia data, but there is no fundamental physical reason to add the Λ constant in the Einstein Field Equations or add the Λ constant at the level of the Einstein-Hilbert action [38].

In early times after the Big Bang, this constant is irrelevant, but at the later stages of the evolution of the Universe, Λ will dominate the expansion, explaining the acceleration of the Universe. Such small Λ is very difficult to generate in quantum field theory models, where Λ is the vacuum energy, which is usually very large [26] even to 120 orders of magnitude far from the observed Λ in cosmology [38]. Moreover, in other attempts to obtain a better

value for this vacuum energy, the result is about 54 orders of magnitude far from the Λ observed value (calculated from the CMB or SNe-Ia data in the ΛCDM model). [38]. This explanation is not satisfactory.

Not only SNe-Ia data are useful to understand the cosmology. The CMB data and its power spectrum provide more information to fit even more cosmological parameters [48]. From here, it is possible to obtain (assuming that GR and ΛCDM work well), with reasonable constraints, the value $\Omega_\Lambda = 0.6911 \pm 0.0062$, implying that DE is the main component of the Universe creating acceleration [53]

DG gives good results from the observational data obtained from SNe-Ia [14], and it does not require DE to explain the acceleration. Despite this result, a good cosmological model also has to explain the anisotropies of matter and energy fluctuations observed in the Cosmic Microwave Background (CMB) because the temperature correlations give us information about the constituents of the Universe, such as baryonic and dark matter. These fluctuations have been deeply studied [2], and they have been numerically solved in programs such as CMBFast [71, 59] or CAMB. [1, 35, 49]

From these two pieces of evidence and assuming ΛCDM is correct, and GR works, the scientific community has to accept " Dark Energy". Nevertheless, the main problem with " Dark Energy" remains; what does it mean? Furthermore, the State-of-the-art is controversial; for example, the last H_0 measurements based on local SNe-Ia [56, 54, 55] are incompatible with Planck results from [49]. Also, other works have found inconsistencies in the CMB analysis [65] or in SNe-Ia analysis [21, 31].

A very controversial paper published in 2016 [56] about a H_0 estimation (using new parallaxes from Cepheids) found an observed value $H_0 = 73.24 \pm 1.74$ km Mpc^{-1} s^{-1} which is independent from cosmological model . This value is 3.4 σ higher than 66.93 ± 0.62 km Mpc^{-1} s^{-1} predicted by ΛCDM with Planck. But the discrepancy reduces to 2.1 σ relative to the prediction of 69.3 ± 0.7 km Mpc^{-1} s^{-1} based on the comparably precise combination of WMAP+ACT+SPT+BAO observations. This value has been updated [54] using more precises parallaxes for Cepheids. The H_0 updated value at 2018 is 73.52 ± 1.62 km Mpc^{-1} s^{-1}.

In this context, there are two exciting subjects that we want to study from the DG cosmological model, the first is the Hubble Constant (H_0), and the second, the accelerating

expansion of the Universe, both in the context of the compatibility between the CMB power spectrum and the SNe-Ia data.

1.2 DG model

1.2.1 Why study an alternative model?

First of all, the standard cosmology is based on GR. This theory is valid on scales larger than a millimeter to the solar-system scale [69, 63], but from the fundamental physics point of view, this theory is non-renormalizable, which prevents its unification with the other forces of nature. Many attempts have been developed to solve this problem, for example, string theories trying to quantize GR [28, 50].

Second, recent discoveries in cosmology [67, 53, 45, 20] have revealed that most of the matter is in the form of unknown matter, known as DM. Some alternative explanations have been published based on modifying the dynamics for small accelerations [39, 18]. Although Particle Physics candidates could play the role of DM, none have been detected yet.

A third problem is the accelerating expansion of the Universe and its relation with the DE density [5, 43]. On the other side, DE can be explained if a small Cosmological Constant (Λ) is present. In recent years there have been various proposals to explain the observed acceleration of the Universe. They involve the inclusion of some additional fields in approaches like Quintessence, Chameleon, Vector Dark Energy or Massive Gravity; The addition of higher-order terms in the Einstein-Hilbert action, like $f(R)$ theories and Gauss-Bonnet terms and finally the introduction of extra dimensions for a modification of gravity on large scales (See [62]). Other interesting possibilities, are the search for non-trivial ultraviolet fixed points in gravity (asymptotic safety [66]) and the notion of induced gravity [72, 57, 32, 3, 37, 51, 16].

In this context, DG theory emerges as a model that could give clues about some incompatibilities in cosmology, eventually produced by the GR theory.

1.2.2 What is DG?

In a previous work [12], Jorge Alfaro studied a model of gravitation that is very similar to classical GR but could make sense at the quantum level. In this construction, he considered two different points. The first is that GR is finite on shell at one loop [61], so renormalization is not necessary at this level. The second is a type of gauge theories, $\tilde{\delta}$ Gauge Theories (Delta Gauge Theories), presented in [6, 13], which main properties are: (a) New kinds of fields are created, $\tilde{\phi}_I$, from the originals ϕ_I. (b) The classical equations of motion of ϕ_I are satisfied in the full quantum theory. (c) The model lives at one loop. (d) The action is obtained by extending the original gauge symmetry of the model, introducing an extra symmetry that we call $\tilde{\delta}$ symmetry since it is formally obtained as the variation of the original symmetry. When we apply this prescription to GR, we obtain Delta Gravity.

We studied the classical effects of Delta Gravity at the cosmological level. For this, we assume that the Universe is composed of non-relativistic matter (DM and baryonic matter) and radiation (photons and massless particles), which satisfy a fluid-like equation $p = \omega\rho$. Matter dynamics are not considered, except by demanding that the energy-momentum tensor of the matter fluid is covariantly conserved. In this work, we used the exact solution of the equations, corresponding to the above suppositions, to fit the SNe-Ia data and we obtained an accelerated expansion of the Universe in the model without DE.

1.2.3 Purpose

We are going to provide an analysis using SNe-Ia data updated to 2018 [58] to fit cosmological parameters in an Alternative Cosmological Model known as Delta Gravity [9].

We will also fit the TT CMB power spectrum (Planck satellite's data, [49]) to constraint the DG cosmological parameters. This observational data constraint more parameters, and then, it can be contrasted with SNe-Ia information.

With both observations, we will analyze the compatibility between these observational pieces of evidence and constraint DG parameters to understand if DG is a feasible cosmological model. More specifically, we are interested in analyzing the acceleration of the Universe and the Hubble Constant (H_0) in the DG theory.

1.2.4 Delta Gravity Action

In this subsection, we define the action and the symmetries of the model and derive the equations of motion.

These modified theories consist of the application of a variation represented by $\tilde{\delta}$. As a variation, it has all the properties of a common variation such as:

$$\begin{aligned} \tilde{\delta}(AB) &= \tilde{\delta}(A)B + A\tilde{\delta}(B), \\ \tilde{\delta}\delta A &= \delta\tilde{\delta}A, \\ \tilde{\delta}(\Phi_{,\mu}) &= (\tilde{\delta}\Phi)_{,\mu}, \end{aligned} \tag{1.1}$$

where δ is another variation. The particular point with this variation is that, when we apply it on a field (function, tensor, etc.), it will give new elements that we define as $\tilde{\delta}$ fields, which are an entirely new independent object from the original, $\tilde{\Phi} = \tilde{\delta}(\Phi)$. We use the convention that a tilde tensor is equal to the $\tilde{\delta}$ transformation of the original tensor when all its indexes are covariant.

First, we need to apply the $\tilde{\delta}$ prescription to a general action. The extension of the new symmetry is given by:

$$S_0 = \int d^n x \mathcal{L}_0(\phi, \partial_i\phi) \rightarrow S = \int d^n x \left(\mathcal{L}_0(\phi, \partial_i\phi) + \tilde{\delta}\mathcal{L}_0(\phi, \partial_i\phi)\right), \tag{1.2}$$

where S_0 is the original action, and S is the extended action in Delta Gauge Theories.

GR is based on Einstein-Hilbert action:

$$S_0 = \int d^4 x \mathcal{L}_0(\phi) = \int d^4 x \sqrt{-g}\left(\frac{R}{2\kappa} + L_M\right), \tag{1.3}$$

where $L_M = L_M(\phi_I, \partial_\mu\phi_I)$ is the Lagrangian of the matter fields ϕ_I and $\kappa = \frac{8\pi G}{c^4}$. Then, the DG action is given by

$$S = S_0 + \tilde{\delta} S_0 = \int d^4x \sqrt{-g} \left(\frac{R}{2\kappa} + L_M - \frac{1}{2\kappa} \left(G^{\alpha\beta} - \kappa T^{\alpha\beta} \right) \tilde{g}_{\alpha\beta} + \tilde{L}_M \right), \tag{1.4}$$

where we have used the definition of the new symmetry: $\tilde{\phi} = \tilde{\delta}\phi$ and the metric convention of [67][1] [2] and

$$\tilde{g}_{\mu\nu} = \tilde{\delta} g_{\mu\nu}, \tag{1.5}$$

$$T^{\mu\nu} = \frac{2}{\sqrt{-g}} \frac{\delta \left(\sqrt{-g} L_M \right)}{\delta g_{\mu\nu}}, \tag{1.6}$$

$$\tilde{L}_M = \tilde{\phi}_I \left(\frac{\delta L_M}{\delta \phi_I} \right) + (\partial_\mu \tilde{\phi}_I) \left(\frac{\delta L_M}{\delta (\partial_\mu \phi_I)} \right), \tag{1.7}$$

where $\tilde{\phi}_I = \tilde{\delta}\phi_I$ are the $\tilde{\delta}$ matter fields (also called called Delta matter fields). Then, the equations of motion are:

$$G^{\mu\nu} = \kappa T^{\mu\nu}, \tag{1.8}$$

$$F^{(\mu\nu)(\alpha\beta)\rho\lambda} D_\rho D_\lambda \tilde{g}_{\alpha\beta} + \frac{1}{2} g^{\mu\nu} R^{\alpha\beta} \tilde{g}_{\alpha\beta} - \frac{1}{2} \tilde{g}^{\mu\nu} R = \kappa \tilde{T}^{\mu\nu}, \tag{1.9}$$

with:

$$\begin{aligned} F^{(\mu\nu)(\alpha\beta)\rho\lambda} &= P^{((\rho\mu)(\alpha\beta))} g^{\nu\lambda} + P^{((\rho\nu)(\alpha\beta))} g^{\mu\lambda} - P^{((\mu\nu)(\alpha\beta))} g^{\rho\lambda} - P^{((\rho\lambda)(\alpha\beta))} g^{\mu\nu}, \\ P^{((\alpha\beta)(\mu\nu))} &= \frac{1}{4} \left(g^{\alpha\mu} g^{\beta\nu} + g^{\alpha\nu} g^{\beta\mu} - g^{\alpha\beta} g^{\mu\nu} \right), \\ \tilde{T}^{\mu\nu} &= \tilde{\delta} T^{\mu\nu}, \end{aligned}$$

[1] In [10] you can find more about the formalism of the DG action and the new symmetry $\tilde{\delta}$.

[2] We emphasize that DG is not a metric model of gravity because massive particles do not move on geodesics. Only massless particles move on geodesics of a linear combination of both tensor fields.

where $(\mu\nu)$ denotes that μ and ν are in a totally symmetric combination. Note that our equations are of second order in derivatives which is needed to preserve causality. We can show that the Equation $(1.9)_{\mu\nu} = \tilde{\delta}\left[(1.8)_{\mu\nu}\right]$.

Also, there are two conservation rules given by [10]:

$$D_\nu T^{\mu\nu} = 0 \tag{1.10}$$

$$D_\nu \tilde{T}^{\mu\nu} = \frac{1}{2}T^{\alpha\beta}D^\mu \tilde{g}_{\alpha\beta} - \frac{1}{2}T^{\mu\beta}D_\beta \tilde{g}^\alpha_\alpha + D_\beta(\tilde{g}^\beta_\alpha T^{\alpha\mu}) \tag{1.11}$$

It is easy to see that the Equation (1.11) is $\tilde{\delta}\left(D_\nu T^{\mu\nu}\right) = 0$.

1.3 $T^{\mu\nu}$ and $\tilde{T}^{\mu\nu}$ for a perfect fluid

In DG, the energy-momentum tensors for a perfect fluid are [12] (where $c = 1$ is the speed of light):

$$T_{\mu\nu} = p(\rho)g_{\mu\nu} + (\rho + p(\rho))\, U_\mu U_\nu \tag{1.12}$$

$$\begin{aligned}\tilde{T}_{\mu\nu} &= p(\rho)\tilde{g}_{\mu\nu} + \frac{\partial p}{\partial \rho}(\rho)\tilde{\rho}g_{\mu\nu} + \left(\tilde{\rho} + \frac{\partial p}{\partial \rho}(\rho)\tilde{\rho}\right) U_\mu U_\nu + \\ &(\rho + p(\rho))\left(\frac{1}{2}(U_\nu U^\alpha \tilde{g}_{\mu\alpha} + U_\mu U^\alpha \tilde{g}_{\nu\alpha}) + U^T_\mu U_\nu + U_\mu U^T_\nu\right)\end{aligned} \tag{1.13}$$

where $U^\alpha U^T_\alpha = 0$. p is the pressure, ρ is the density and U^μ is the four-velocity. For more details you can see [12].

1.3.1 Geodesic equation for massless particles

In DG, a massless particle behaves according to the following equation:

$$\mathbf{g}_{\mu\nu}\dot{x}^{\mu}\dot{x}^{\nu} = 0, \tag{1.14}$$

Where the Effective Metric $\mathbf{g}_{\mu\nu}$ is a linear combination given by the two tensors:

$$\mathbf{g}_{\mu\nu} = g_{\mu\nu} + \tilde{g}_{\mu\nu} \tag{1.15}$$

Thus, the massless particles follow null geodesic, like in the GR theory. [3]

1.4 Cosmology in Delta Gravity

1.4.1 Effective Metric to describe the Universe in a cosmological frame

We assume a flat Universe ($k = 0$). The usual metric to describe the Universe in cosmology is the FLRW metric, given by the Equation (1.16):

$$\mathrm{d}s^2 = g_{\mu\nu}\mathrm{d}x^{\mu}\mathrm{d}x^{\nu} = -c^2\mathrm{d}t^2 + a(t)^2\left(dx^2 + dy^2 + dz^2\right), \tag{1.16}$$

where the Scale Factor is called $a(t)$.

The objective is to build an Effective Metric for the Universe; then the equations need to explain the photon trajectories, because these particles are what we observe and provide us the information from the observables (such as the SNe-Ia data), showing us the expansion of the Universe. As in the GR frame, we build the metric for the Universe using the massless particle geodesic in DG. We have to include a "scale factor" in the space-metric component to explain the expansion of the Universe. This factor must be space-independent because we want to preserve the homogeneity and isotropy for the Universe. Therefore this can be only time-dependent.

[3] It is important to consider that massive particles do not follow geodesics. [9]

Thus, we have to find $\tilde{g}_{\mu\nu}$ from the $g_{\mu\nu}$. We are going to do a change of variable in the Standard Metric tensor, $t \to u$, where $T(u) = \frac{dt}{du}(u)$. Then,

$$g_{\mu\nu}dx^\mu dx^\nu = -T^2(u)c^2du^2 + a^2(u)(dx^2 + dy^2 + dz^2).$$

Now we add the new dependencies to the temporal and spatial components of the equation, building the most general metric without losing the homogeneity and isotropy of the Universe:

$$\tilde{g}_{\mu\nu}dx^\mu dx^\nu = -F_b(u)T^2(u)c^2du^2 + F_a(u)a^2(u)(dx^2 + dy^2 + dz^2),$$

thus, we have to fix a gauge to delete the extra degrees of freedom. Fixing an Harmonic gauge (described in [9]) we obtain:

$$T(u) = T_0a^3(u),$$

$$F_b(u) = 3(F_a(u) + T_1),$$

where T_0 and T_1 are gauge constants. Choosing $T_0 = 1$ and $T_1 = 0$ the gauge is fully fixed. Finally, we can go back to the Effective Metric $\mathbf{g}_{\mu\nu} = g_{\mu\nu} + \tilde{g}_{\mu\nu}$ (1.15) to substitute the fixed gauges. This defines the Effective Metric for the Universe in DG:

$$\mathbf{g}_{\mu\nu} = g_{\mu\nu} + \tilde{g}_{\mu\nu} = -\left(1 + 3F_a(t)\right)c^2dt^2 + a^2(t)\left(1 + F_a(t)\right)\left(dx^2 + dy^2 + dz^2\right) \tag{1.17}$$

1.4.2 Delta Gravity equations of motion

To apply this theory to cosmology, we impose only two kinds of Universe components: matter and radiation. With the new symmetry, two kinds of components appear which we call Delta matter and Delta radiation, respectively. To calculate the equations that govern the Universe, we assume $g_{\mu\nu}$ is expressed by the Equation (1.16) and we calculate the First Field Equation given by the Equation (1.8):

$$\left(\frac{\dot{a}(t)}{a(t)}\right)^2 = \frac{\kappa c^4}{3}\left(\rho_r(t) + \rho_m(t)\right). \tag{1.18}$$

If we solve the Equation (1.18), we obtain the following expression:

$$\dot{\rho}_i(t) \;=\; -\frac{3\dot{a}(t)}{a(t)}(\rho_i(t) + p_i(t)). \tag{1.19}$$

Considering an equation of state, it is possible to relate ρ and p for each component i, and assuming that there are only matter (baryonic, and if you want, dark matter) and radiation (photons and other massless particles), we have (same as GR at this point):

for matter:

$$p_m(a) = 0,$$

and for radiation:

$$p_r(a) = \frac{1}{3}\rho_r(a).$$

With these equations we can solve the Equation (1.18) expressing $t(a)$. Summarizing, we have:

$$\rho(a) = \rho_m(a) + \rho_r(a), \tag{1.20}$$

$$p_r(a) = \frac{1}{3}\rho_r(a), \tag{1.21}$$

$$t(Y) = \frac{2\sqrt{C}}{3H_0\sqrt{\Omega_{r,0}}}\left(\sqrt{Y+C}(Y-2C) + 2C^{3/2}\right), \tag{1.22}$$

$$Y(t) = \frac{a(t)}{a_0}, \tag{1.23}$$

$$a_0 \equiv a(t=t_0) \equiv 1, \tag{1.24}$$

$$\Omega_{r,0} \equiv \frac{\rho_{r,0}}{\rho_{c,0}}, \tag{1.25}$$

$$\Omega_{m,0} \equiv \frac{\rho_{m,0}}{\rho_{c,0}}, \tag{1.26}$$

$$\rho_{c,0} \equiv \frac{3H_0^2}{8\pi G}, \tag{1.27}$$

$$\Omega_{r,0} + \Omega_{m,0} \equiv 1, \tag{1.28}$$

where t_0 is the age of the Universe (today). We emphasize that t is the Cosmic Time, a_0 is the Scale Factor at the current time, $C \equiv \frac{\Omega_{r,0}}{\Omega_{m,0}}$, where $\Omega_{r,0}$ and $\Omega_{m,0}$ are the density energies normalized by the Critical Density today, defined as the same as the standard cosmology. Furthermore, we have imposed that Universe must be flat ($k = 0$), so we require that $\Omega_{r,0} + \Omega_{m,0} \equiv 1$. Note that ρ_i is not a physical density. They are only density parameters[4] that are related to physical densities. We are going to discuss this aspect in the CMB Chapter.

Using the second continuity Equation (1.11), where $\tilde{T}_{\mu\nu}$ is a new energy-momentum tensor, we define two new densities called $\tilde{\rho}_m$ (Delta matter density) and $\tilde{\rho}_r$ (Delta radiation density). They are associated with this new tensor. When we solve this equation, we find

$$\tilde{\rho}_m(Y) = \frac{C_1 - \frac{3}{2}\rho_{m,0}F_a(Y)}{Y^3}, \tag{1.29}$$

$$\tilde{\rho}_r(Y) = \frac{C_2 - 2\rho_{r,0}F_a(Y)}{Y^4} \tag{1.30}$$

[4]They are not energy per volume.

where C_1 and C_2 are integration constants. It is crucial to clarify that $\tilde{\rho}_m$ and $\tilde{\rho}_r$ depend on the Normalized Scale Factor Y. We can note that both energy density parameters (remember that these parameters are not real physical densities. But they are related to the physical densities) have terms that behave like the standard cosmology densities $\sim \frac{1}{Y^3}$ and $\sim \frac{1}{Y^4}$ that also are preserved in DG:

$$\rho_r(Y) = \frac{\rho_{r,0}}{Y^4} \tag{1.31}$$

$$\rho_r(Y) = \frac{\rho_{m,0}}{Y^3} \tag{1.32}$$

If we preserve $C_1 \neq 0$ and $C_2 \neq 0$, we have equations that are considering two kinds of dependence: $\sim \frac{1}{Y^3} + \frac{F_a(Y)}{Y^3}$ and $\sim \frac{1}{Y^4} + \frac{F_a(Y)}{Y^4}$. This consideration implies that the total energy density (proportional to the real physical densities) considers the standard energy density and the new dependence given by DG, in other words, this is equivalent to consider that $\tilde{\rho}_r$ is the standard density radiation ρ_r plus the new DG dependence. We only want to consider the new dependence in the $\tilde{\rho}_r$ term without the standard radiation contribution. This same reasoning is valid for the density of matter. Thus, defining $C_1 = C_2 = 0$, we obtain the following equations:

$$\tilde{\rho}_m(Y) = -\frac{3\rho_{m,0}}{2}\frac{F_a(Y)}{Y^3}, \tag{1.33}$$

$$\tilde{\rho}_r(Y) = -2\rho_{r,0}\frac{F_a(Y)}{Y^4}. \tag{1.34}$$

There is another reason to define C_1 and C_2 equal to 0. When $Y \ll C$, the Effective Scale Factor Y_{DG} (defined in Equations (1.39) and (1.37)) represents the evolution of the Universe at the beginning. We know that an accelerated expansion appears at late times, then the non-relativistic matter and radiation must drive the expansion at early times, this means $Y_{DG} = 1 + O(Y)$. We fix $C_1 = 0$ and $C_2 = 0$ to guarantee that the behavior of expansion seems like GR at early times. The full development of this idea can be found in [7, 8].

Using the Equation (1.9) with the solutions from the Equations (1.33) and (1.34) we found (and redefining with respect to Y):

$$F_a(Y) = \left(CC_3\sqrt{\rho_{r,0}}\right)\frac{Y}{C}\sqrt{\frac{Y}{C}+1}, \tag{1.35}$$

where $L_2 \equiv -3C^{-1/2}C_3\sqrt{\rho_{r,0}} = -3C_3\sqrt{\rho_{m,0}}$ (L_2 is defined as a new constant). Thus

$$F_a(Y) = -\frac{L_2}{3}Y\sqrt{Y+C}. \tag{1.36}$$

1.4.3 Relation between the Effective Scale Factor Y_{DG} and the Normalized Scale Factor Y

The Effective Metric for the Universe is given by the Equation (1.17). From this expression, it is possible to define the DG Scale Factor as follows:

$$a_{DG}(t) = a(t)\sqrt{\frac{1+F_a(t)}{1+3F_a(t)}}. \tag{1.37}$$

Defining that $a(t_0) \equiv 1$, we have that $a(t) = Y(t)$, and substituting the Equation (1.35) in the Equation (1.37) we obtain:

$$a_{DG}(t) = Y(t)\sqrt{\frac{1-\frac{L_2}{3}Y\sqrt{Y+C}}{1-L_2Y\sqrt{Y+C}}}. \tag{1.38}$$

Furthermore, we define the Effective Scale Factor:

$$Y_{DG}(t) \equiv \frac{a_{DG}(t)}{a_{DG}(t_0)}. \tag{1.39}$$

Thus, substituting the Equation (1.38) in (1.39), we obtain:

$$Y_{DG}(L_2, C, Y) = \frac{Y}{a_{DG}(t_0)}\sqrt{\frac{1-L_2\frac{Y}{3}\sqrt{Y+C}}{1-L_2Y\sqrt{Y+C}}}. \tag{1.40}$$

With the new definition of L_2, the Delta densities are given by:

$$\tilde{\rho}_m(Y) = \left(\frac{L_2}{2}\right)\rho_{m,0}\frac{\sqrt{Y+C}}{Y^2}, \tag{1.41}$$

$$\tilde{\rho}_r(Y) = \left(\frac{2L_2}{3}\right)\rho_{r,0}\frac{\sqrt{Y+C}}{Y^3}. \tag{1.42}$$

If we know the C and L_2 values it is possible to calculate the Delta densities $\tilde{\rho}_m$ and $\tilde{\rho}_r$. Note that the denominator in the Equation (1.40) is equal to zero when $1 = L_2 Y\sqrt{Y+C}$. Taking into account that $C = \Omega_{r,0}/\Omega_{m,0} \ll 1$, if $Y = 1$ (current time) then $L_2 \approx 1$. Furthermore, we have imposed that $\tilde{\rho}_m > 0$ and $\tilde{\rho}_r > 0$, then L_2 must be greater than 0. Then the valid range for L_2 is approximately $0 \leq L_2 \leq 1$.
C must be positive and small because the radiation is not dominant compared to matter. Then, we can analyze cases close to the standardly accepted value for $\Omega_{r,0}/\Omega_{m,0} \sim 10^{-4}$ (we have assumed GR values to estimate an order of magnitude).

1.4.4 Useful equations for cosmology

Here we present the equations that are useful to fit the SNe-Ia data and to obtain cosmological parameters.

1.4.4.1 Redshift dependence

The relation between the cosmological redshift and the Effective Scale Factor is preserved in DG. The reason is straightforward: it is the same as in GR, but changing the Scale Factor $a(t) \to a_{DG}(t)$ in the GR metric $g_{\mu\nu}dx^\mu dx^\nu \to \mathbf{g}_{\mu\nu}dx^\mu dx^\nu$ [9]. Thus, the dependence is given by:

$$\frac{a_{DG}(t)}{a_{DG}(t_0)} = \frac{1}{1+z}, \tag{1.43}$$

where z is the cosmological redshift. Substituting $Y_{DG}(t) = a_{DG}(t)/a_{DG}(t_0)$ in Equation (1.43), we obtain

$$Y_{DG}(t) = \frac{1}{1+z}. \tag{1.44}$$

It is important to consider that the current time is given by $t_0 \to Y(t_0) \to Y_{DG}(Y=1)=1$.

1.4.4.2 Luminosity distance

The proof is the same as GR, because the main idea is based on the light traveling through a null geodesic described by the Effective Metric given by the Equation (1.17) in DG. Then, the equation that describes the luminosity distance for DG is the same as GR, but changing the Scale Factor $a(t)$ by the $a_{DG}(t)$, because $a_{DG}(t)$ is the factor that is describing the observable expansion (or scaling) of the Universe. Then,

$$d_L = c\frac{a^2(t_0)}{a(t_1)}\int_{t_1}^{t_0}\frac{dt}{a(t)} \to d_L^{DG} = c\frac{{a_{DG}}^2(t_0)}{a_{DG}(t_1)}\int_{t_1}^{t_0}\frac{dt}{a_{DG}(t)}, \tag{1.45}$$

where t_1 is the time when the light was emitted from the source.

We emphasize that the relation between the luminosity distance d_L^{DG} and angular distance d_A^{DG} in DG is the same as in GR. This relation is a direct consequence of the structure of the metric. This relation is given by the Equation (1.46),

$$d_L^{DG} = (1+z)^2 d_A^{DG}. \tag{1.46}$$

Using the Equation (1.22), we obtain

$$\frac{dt}{dY} = \frac{\sqrt{C}}{H_0\sqrt{\Omega_{r,0}}}\frac{Y}{\sqrt{Y+C}}.$$

Substituting $dt = \frac{dt}{dY}dY$, and replacing dt in the Equation (1.45),

$$d_L^{DG} = c\frac{{a_{DG}}^2(t_0)}{a_{DG}(t_1)}\frac{\sqrt{C}}{H_0\sqrt{\Omega_{r,0}}}\int_{Y(t_1)}^{Y(t_0)}\frac{Y}{\sqrt{Y+C}}\frac{dY}{a_{DG}(t)}.$$

Adding that $H_0 = 100h$ (Keep in mind that H_0 is not the observable Hubble Constant in the DG model, it is only an arbitrary constant that must be fixed from the observations. We will define the observable Hubble Constant later), finally, we obtain (we must remember the change of units for H_0 given by km/(Mpc s))

$$d_L^{DG} = c\frac{{R_{DG}}^2(t_0)}{R_{DG}(t_1)}\frac{\sqrt{C}}{100\sqrt{h^2\Omega_{r,0}}}\int_{Y(t_1)}^{Y(t_0)}\frac{Y}{\sqrt{Y+C}}\frac{dY}{R_{DG}(t)}.$$

Substituting the Equations (1.43) and (1.39), we obtain:

$$d_L^{DG}(z, L_2, C) = c\frac{(1+z)\sqrt{C}}{100\sqrt{h^2\Omega_{r,0}}}\int_{Y(t_1)}^{1}\frac{Y}{\sqrt{Y+C}}\frac{dY}{Y_{DG}(t)}, \tag{1.47}$$

where $Y = 1$ denotes today. To solve $Y(t_1)$ at a given redshift z, we need to solve the Equations (1.39) and (1.44) numerically. Furthermore, the integrand contains the Effective Scale Factor $Y_{DG}(t)$ that can be expressed in function of Y through the Equation (1.40). Do not confuse c (speed of light) with C, a free parameter to be fitted by SNe-Ia data.

The parameter $h^2\Omega_{r,0}$ can be simplified through the C definition: [5]

$$d_L^{DG}(z, L_2, C) = c\frac{(1+z)}{100\sqrt{h^2\Omega_{m,0}}}\int_{Y(t_1)}^{1}\frac{Y}{\sqrt{Y+C}}\frac{dY}{Y_{DG}(t)}. \tag{1.48}$$

If the integration takes $Y \gg C$ (a good approximation for SNe-Ia), this equation can be approximated to:

$$d_L^{DG}(z, L_2) \approx c\frac{(1+z)}{100\sqrt{h^2\Omega_{m,0}}}\int_{Y(t_1)}^{1}\frac{\sqrt{Y}}{Y_{DG}(t)}dY, \tag{1.49}$$

where d_L^{DG} is independent of C because in the Equation (1.40) we can replace $C = 0$. Also, if $C \to 0$, then $\Omega_{m,0} = 1/(1+C) \to 1$. In this context, to determine $h^2\Omega_{m,0}$ is equivalent to determine h.

We only need to know the values C and L_2 (or only L_2 in the approximation) to estimate SNe-Ia distances. Note that in this case it is impossible to know the value of $\Omega_{r,0}$ only with SNe-Ia data, but we will constraint this value using the TT CMB power spectrum [49].

[5] The $h^2\Omega_{r,0}$ value is not the physical density of radiation. It is related with that, but they are not the same. This will be discussed in the CMB chapter.

1.4.5 Distance modulus

This relation is fundamental because it lets us calculate the dependence between the apparent magnitude and the distance to the object. It is essential to consider that we need to know the value of the absolute magnitude M. We will discuss this aspect in the next pages.

$$\mu = m - M = 5 \log_{10} \left(\frac{d_L^{DG/GR}}{10\,\mathrm{pc}} \right) \tag{1.50}$$

1.4.6 Normalized Effective Scale Factor

In DG, the "size" of the Universe is given by $Y_{DG}(t)$, then every cosmological parameter that in the GR theory was built up from the standard scale factor $a(t)$, in DG will be built from $Y_{DG}(t)$. This value is equal to 1 at the current time, because the DG Scale Factor a_{DG} is normalized by itself: $a_{DG}(Y = 1)$.

1.4.7 Hubble Parameter

The Hubble parameter (and also, the Hubble Constant) is defined in GR cosmology as:

$$H(t) = \frac{\dot{a}(t)}{a(t)}. \tag{1.51}$$

Thus, in DG we define the Hubble Parameter as follows:

$$H^{DG}(t) \equiv \frac{\dot{a}_{DG}(t)}{a_{DG}(t)}. \tag{1.52}$$

The Hubble Constant is the Hubble Parameter $H^{DG}(t)$ evaluated today, in other words, when $Y = 1$. To evaluate the derivative, we apply the chain rule:

$$\frac{da_{DG}}{dt} = \frac{da_{DG}}{dY} \left(\frac{dt}{dY} \right)^{-1}.$$

Therefore, the Hubble Parameter is given by

$$H^{DG}(t) = \frac{\frac{da_{DG}}{dY}\left(\frac{dt}{dY}\right)^{-1}}{a_{DG}}. \tag{1.53}$$

Observe that all the DG parameters are written as a function of Y.

1.4.8 Deceleration Parameter

In the standard cosmology the Deceleration Parameter is given by:

$$q^{GR}(t) = -\frac{\ddot{a}a}{\dot{a}^2}. \tag{1.54}$$

Thus, in DG we define the Deceleration Parameter as follows:

$$q^{DG}(t) = -\frac{\ddot{a}_{DG}a_{DG}}{\dot{a}_{DG}^2}, \tag{1.55}$$

where

$$\ddot{a}_{DG} = \frac{d\dot{a}_{DG}}{dt} = \frac{d\dot{a}_{DG}}{dY}\frac{dY}{dt} = \frac{d}{dY}\left(\frac{da_{DG}}{dY}\left(\frac{dt}{dY}\right)^{-1}\right)\left(\frac{dt}{dY}\right)^{-1}.$$

Then,

$$q^{DG}(t) = -\frac{\frac{d}{dY}\left(\frac{da_{DG}}{dY}\left(\frac{dt}{dY}\right)^{-1}\right)\left(\frac{dt}{dY}\right)^{-1}a_{DG}}{\left(\frac{da_{DG}}{dY}\left(\frac{dt}{dY}\right)^{-1}\right)^2} \tag{1.56}$$

1.4.9 Dependence between redshift and Cosmic Time

All the equations are parametrized as a function of Y, so we need to use the Equations (1.22), (1.40) and (1.44) to relate redshift and Cosmic Time.

1.4.10 Non-physical Densities of Common Components: $\Omega_{m,0}$ and $\Omega_{r,0}$

We have imposed that $\Omega_{m,0} + \Omega_{r,0} = 1$ and $C = \frac{\Omega_{r,0}}{\Omega_{m,0}}$, then

$$\Omega_{r,0} = \frac{1}{1 + \frac{1}{C}}; \qquad \Omega_{m,0} = 1 - \Omega_{r,0}. \tag{1.57}$$

It is vital to consider that this equation only expresses a relation, or a proportion, between the non-physical energy density for Common matter and Common radiation densities, and does not express a real percentage of composition of the Universe because in DG we also have Delta matter and Delta radiation. We will discuss the composition of the Universe in the following chapters.

This condition is imposed when we assumed that $T^{\mu\nu}$ only expresses a standard composition, and when we assumed that the DE does not exist either at the level of Action or Field Equations.

Chapter 2

First Supernovae Analysis

This chapter focus on the published paper [14]. Here we presented an MCMC analysis to fit an updated SNe-Ia catalog. The results were compatible with the local expansion of the Universe, in other words, DG finds a H_0^{DG} close to the local H_0 measured by Riess et al. [56] because it can explain the SNe-Ia curve, and also predicts an accelerated Universe considering the high-redshift SNe-Ia.

Note: This work was done before the CMB analysis. The results of this thesis are slightly different from the values presented in this chapter (see Chapter 3). All the changes are a consequence of the physical meaning of the parameter C. This is crucial to understand the CMB and SNe-Ia compatibility. The C parameter will play an essential role in the next chapters.

2.1 Luminosity distance

We use the definition given by the Equation (1.47). In this definition, $Y = 1$ indicates today. To solve $Y(t_1)$ at a given redshift z, we need to solve the Equations (1.40) and (1.44) numerically. Furthermore, the integrand contains $Y_{DG}(t)$ that can be expressed in function of Y in the Equation (1.40). In this expression, C is a free parameter that will be fitted using the SNe-Ia data. To use this equation, we calculate the parameter $h^2\Omega_{r,0}$ from the CMB spectrum. The CMB spectrum can be described by a black body spectrum, where the energy density of photons is given by

$$\rho_{\gamma,0} = aT^4$$

From statistical mechanics, we know the neutrinos density is related with photons density by [48]:

$$\rho_{\nu,0} = 3\frac{7}{8}\left(\frac{4}{11}\right)^{4/3}\rho_{\gamma,0},$$

then,

$$h^2\Omega_{r,0} = h^2\Omega_{\gamma,0} + h^2\Omega_{\nu,0}. \tag{2.1}$$

The $h^2\Omega_{r,0}$ parameter given by the Equation (2.1) is a value that only depends on the temperature of the black body spectrum of the CMB. Thus, we can fix this value as a known cosmological parameter.

Therefore, we only need to find the C and L_2 values. In this context, it is impossible to know the $\Omega_{r,0}$ value without any other information.

Finally, with the Distance Modulus given in the Equations (1.50) and (1.47), we can fit the SNe-Ia data.

2.2 Fitting the SNe-Ia data

We are interested in the viability of Delta Gravity as a real alternative cosmology theory that could explain the accelerating Universe without Λ. Then it is natural to check if this model fits the SNe-Ia data.

2.2.1 SNe-Ia data

To analyze this, we used the most updated type Ia supernovae catalog. We obtained the data from Scolnic et al. [58]. We only needed the distance modulus μ and the redshift z to the SN-Ia to fit the model using the luminosity distance d_L^{DG} predicted from the theory.

The SNe-Ia are very useful in cosmology [53] because they can be used as standard candles and allow to fit the ΛCDM model finding out free parameters such as Ω_Λ. We are interested in doing this in DG. The main characteristic of the SNe-Ia that makes them so useful is that they have a very standardized absolute magnitude close to -19 [56, 19, 15, 52, 64].

From the observations, we only know the apparent magnitude and the redshift of each SN-Ia. Thus, we have the option to use a standardized absolute magnitude obtained by an independent method that does not involve ΛCDM model, or any other assumptions. To fit the SNe-Ia data, we use M as a free parameter, and then we have 3 degrees of freedom [1].

We used 1048 SNe-Ia data in [58][2]. All the SNe-Ia are spectroscopically confirmed. [3]

In [58] they used the SNe-Ia data to try to obtain a better estimation of the DE state equation. They define the distance modulus as follows:

$$\mu \equiv m_B - M + \alpha x_1 - \beta c + \Delta_M + \Delta_B, \tag{2.2}$$

where μ is the distance modulus, Δ_M is a distance correction based on the host-galaxy mass of the SN, and Δ_B is a distance correction based on predicted biases from simulations. Furthermore, α is the coefficient of the relation between luminosity and stretch, β is the coefficient of the relation between luminosity and color, and M_V is the absolute B-band magnitude of a fiducial SN-Ia with $x_1 = 0$ and $c = 0$. [58]

In this work, we are not interested in the specific corrections to observational magnitudes of SN-Ia. We only take the values extracted from [58] to analyze the DG model. The SNe-Ia data are the redshift z_i and $(\mu + M)_i$ with the respective errors.

[1] (Also, we are going to analyze the case where $M = -19.23 \pm 0.05$[56]. The value was calculated using 210 SNe-Ia data from [56]. This value is independent of the model since it was calculated by building the distance ladder from local Cepheids measured by parallax and using them to calibrate the distance to Cepheids hosted in nearest galaxies (by Period-Luminosity relations) that are also SN-Ia host. Riess et al. calculated the M and the H_0 local value, and they did not use any particular cosmological model. Keep in mind that the value of M found by Riess et al. is an intrinsic property of SNe-Ia, and that is why they are used as standard candles.

[2] Scolnic's data are available at https://archive.stsci.edu/hlsps/ps1cosmo/scolnic/.

[3] In this paper [14], we have used the full set of SNe-Ia presented in [58]. They present a set of spectroscopically confirmed PS1 SN-Ia and combine this sample with spectroscopically confirmed SN-Ia from CfA1-4, CSP, PS1, SDSS, SNLS, and HST SN surveys.

2.2.2 Delta Gravity equations

We need to establish a relation between the redshift and the apparent magnitude for the SNe-Ia:

$$[\mu + M] - M = 5 \log_{10} \left(\frac{d_L^{DG}(z, C, L_2)}{10\,\mathrm{pc}} \right), \tag{2.3}$$

where $d_L^{DG}(z, L_2, C)$ is given by the Equation (1.48) and $[\mu + M]$ are the SNe-Ia data given at [58].

We have as free parameters in this expression: C and L_2 to be found by fitting the model to the points $(z_i, [\mu + M]_i)$.

2.2.3 GR equations

For GR we use the following expression:

$$[\mu + M] - M = 5 \log_{10} \left(\frac{d_L(z, H_0, \Omega_{m0})}{10\,\mathrm{pc}} \right), \tag{2.4}$$

where $d_L(z, H_0, \Omega_{m0})$ is given by

$$d_L(z, H_0, \Omega_{m0}) = \frac{c(1+z)}{H_0} \int_{\frac{1}{1+z}}^{1} \frac{du}{\sqrt{(1-\Omega_{m,0})u^4 + \Omega_{m,0} u}}, \tag{2.5}$$

and $[\mu + M]$ are the SNe-Ia data given at [58]. Remember that we are always working on a flat Universe, and in the GR standard model the $\Omega_{r,0}$ is negligible. We have the same degrees of freedom as in DG. We are including DE as $\Omega_{\Lambda,0} \equiv \Omega_\Lambda \equiv 1 - \Omega_{m,0}$ in GR.

2.2.4 MCMC method

To fit the SNe-Ia data to GR and DG, we used Markov Chain Monte Carlo (MCMC). This routine was implemented in Python 3.6 using PyMC2.[4]

[4] https://pymc-devs.github.io/pymc/.

MCMC consists of fitting a model, characterizing its posterior distribution. It is based on bayesian statistics. We used the Metropolis-Hastings algorithm.

We used this bayesian approach because it allows us to know the posterior probability distribution for every parameter of the model [29, 47]. Furthermore, it is possible to identify dependencies between the fitted parameters, which it is not possible using other method such as the least-square used in [12].

Initially, we propose initial distributions for the parameters that we want to fix, and then PyMC2 will give us the posterior probability distribution for: C, L_2 and M for DG and $H_0, \Omega_{m,0}$ and M for GR.

2.2.4.1 About the extra degrees of freedom

This subsection is dedicated to clarifying the differences between the original model published in [7], and the model used in this chapter. **It is not essential to understand these equations because they are not useful in this full-form. The objective is to show the evolution of the research during these years**.

Initially, the F_a function was given by

$$F_a(Y) = -\frac{3}{2}C_1\frac{Y}{C}\left(\sqrt{\left(\frac{Y}{C}+1\right)}ln\left(\frac{\sqrt{\frac{Y}{C}+1}+1}{\sqrt{\frac{Y}{C}+1}-1}\right)-2\right)+C_3\frac{Y}{C}\sqrt{\frac{Y}{C}+1}, \tag{2.6}$$

where C_1 y C_3 were integration constants. This implied that the Effective Scale Factor was given by

$$Y_{DG}(Y,\ L_1,\ L_2,\ C) = Y\sqrt{\frac{1-L_2\frac{Y}{3}\sqrt{Y+C}+L_1\frac{Y}{c}\left(\sqrt{\frac{Y}{c}+1}\ln\left(\frac{\sqrt{\frac{Y}{c}+1}+1}{\sqrt{\frac{Y}{c}+1}-1}\right)-2\right)}{1-L_2Y\sqrt{Y+C}+3L_1\frac{Y}{c}\left(\sqrt{\frac{Y}{c}+1}\ln\left(\frac{\sqrt{\frac{Y}{c}+1}+1}{\sqrt{\frac{Y}{c}+1}-1}\right)-2\right)}}, \tag{2.7}$$

where $C_1 = -\frac{2L_1}{3}$ and $C_3 = \frac{-C^{3/2}L_2}{3}$ (L_1 and L_2 were new constants).

This definition implied different Delta matter and Delta radiation contents, given by the Equations (1.29) and (1.30). These expressions were discarded because of the reasons exposed in section 1.4.2. Furthermore, any fit that included these parameters were degenerate with the result shown in this chapter. Initially, the degeneration given by these extra parameters creates some undesirable effects, for instance, the other parameters could take an arbitrarily large number implying that the Delta densities could change arbitrarily, while the fitted curve always would be the same. Before this work, the parameters were degenerate, and I found physical arguments to discard these parameters (Section 1.4.2). Furthermore, the extra parameters implied arbitrary densities.

Note 1: A possible inflation effect caused by the F function's log term was also discarded because it does not imply an exponential expansion rate.

Note 2: We want to use DG as a model to fit SNe-Ia data, then we want to preserve extra effects that create acceleration, but not effects that change the early Universe (this constraint was done before the CMB analysis). In other words, we impose that $\tilde{Y} = Y + O(Y^2)$. Then, C_2 have to be 0 because $\tilde{Y} \simeq \sqrt{\frac{1-2C_2}{1-6C_2}}Y + O(Y^2)$ when $Y \ll C$. This observation about the scale factor was no sufficient to delete all the degeneracy between the parameters. Finally (today), we only preserve the L_2 as a free parameter.

Note 3: In previous works, $\tilde{Y}$ is equivalent to the new notation Y^{DG}. (This was the notation at the beginning of the DG publications).

2.3 Results and analysis

We present the results for DG and GR fitted data, and with these values, we obtain different cosmological parameters. We divide the results in two fits: DG fit and GR fit.

From the MCMC analysis, we obtain a non-convergent result. In DG model, the C, and M parameters are dependent, but L_2 is independent. Figure 2.1 shows the degeneration.

A second-order polynomial can fit the dependence for DG parameters. This dependence is given by:

$$C = 8.59 \times 10^{-5} M^2 + 3.15 \times 10^{-3} M + 2.9 \times 10^{-2} \tag{2.8}$$

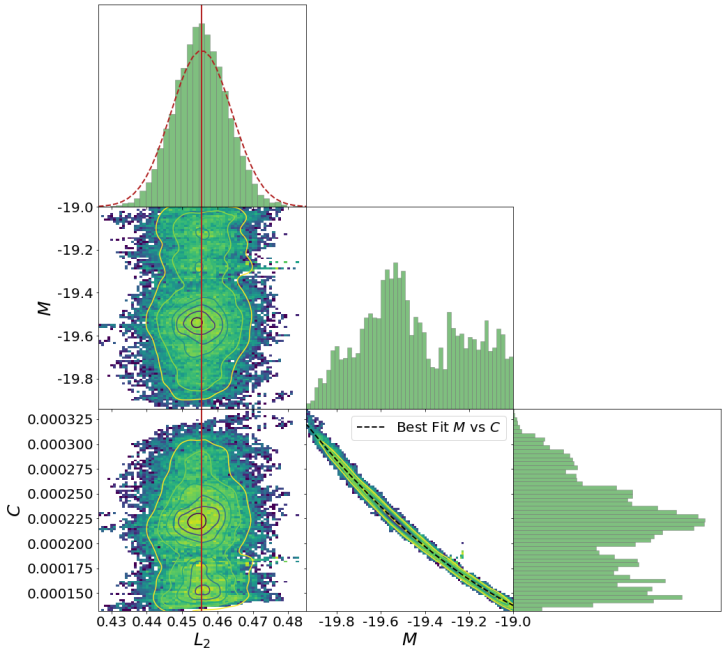

Figure 2.1: This MCMC analysis assumes M as a free parameter in the DG Model. The Figure shows the posterior probability densities.

If we use $M = -19.23 \pm 0.05$ [56], it fixes C which agrees with the SNe-Ia results. This implies a $H_0^{DG} = 74.47 \pm 1.63$ km/(Mpc s).

For GR, we did the same procedure, but in this model, the dependence appears between h^2 and M. These parameters degenerates; indeed, it easy to see from the Equation (1.50)[5]. The polynomial is showed in Figure 2.2 and is given by:

$$h^2 = 0.177M^2 + 7.335M + 75.896 \tag{2.9}$$

Again, if we evaluate the Equation (2.9) at $M = -19.23 \pm 0.05$, we obtain $h^2 \to H_0 \approx 74.08 \pm 0.24$ km/(Mpc s).

[5]We decide to include this degeneration as an MCMC and not as an equation only to show that the program works and to obtain figures that can be easily compared because they were generated with the same code: GR vs. DG.

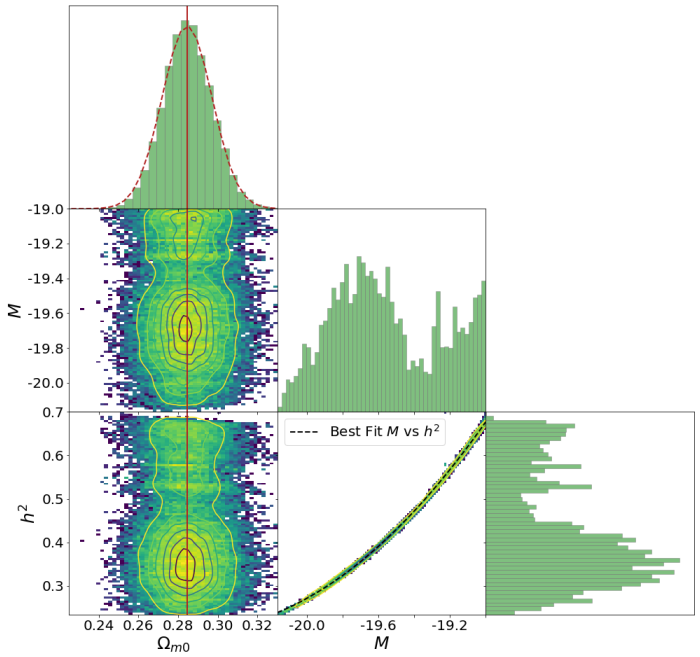

Figure 2.2: MCMC analysis assumes M as a free parameter in GR. The Figure shows the posterior probability densities.

2.3.1 Fitted curves

As we see in Figures 2.3 and 2.4, both models describe very well the m_B vs. z SNe-Ia data. While in GR frame $\Lambda \neq 0$ is needed to find this well-behaved curve ($\Omega_{m,0} \neq 1$), in DG, Λ is not needed to fit the SNe-Ia data. Essentially, DG predicts the same behavior, but the accelerating Universe is explained without the need to include Λ, or anything like "Dark Energy".

The Table 2.1 shows the coefficients of determination (r^2) and residual sum of squares (RSS) for both fitted models.

Table 2.1: Statistical parameters.

Model	r^2	RSS
DG	0.99709	21.39
GR	0.99708	21.44

Both coefficients of determination are excellent, and the RSS is similar for both cases.

The fitted parameters for GR and DG models are shown in Tables 2.2 and 2.3, respectively.

Table 2.2: Fitted parameters using MCMC for DG.

DG	Value	Error
L_2	0.455	0.008
C	0.000169	0.000003

Table 2.3: Fitted parameters using MCMC for GR.

GR	Value	Error
$\Omega_{m,0}$	0.28	0.01
h^2	0.549	0.004

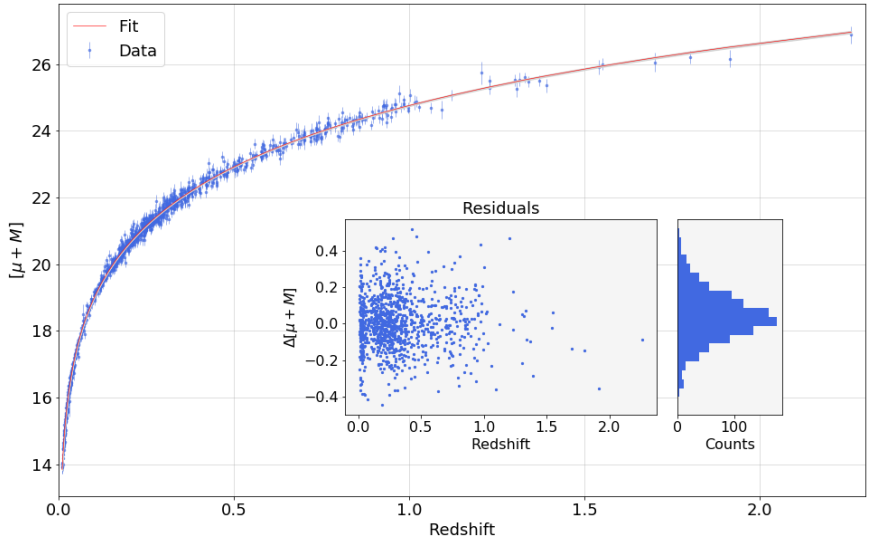

Figure 2.3: The fitted curve for the DG model assuming $M = -19.23$. On the right corner, the residual plot for the fitted data.

The convergence test were included in the Appendix C.

2.3.2 The Hubble Constant and H_0 and the Deceleration Parameter

With the fitted parameters found by MCMC for GR and DG, we can find $H(t)$ and H_0. Note the superscript for GR as ^{GR} and DG as ^{DG}. For GR, H_0 is easily obtained from the h^2 fitted ($H_0 = 100h$). We evaluate H^{DG} at $Y_{DG} = 1$ obtaining the Hubble Constant H_0^{GR} and H_0^{DG}. We present the results for both models and we compare these values with previous measurements in Table 2.4.

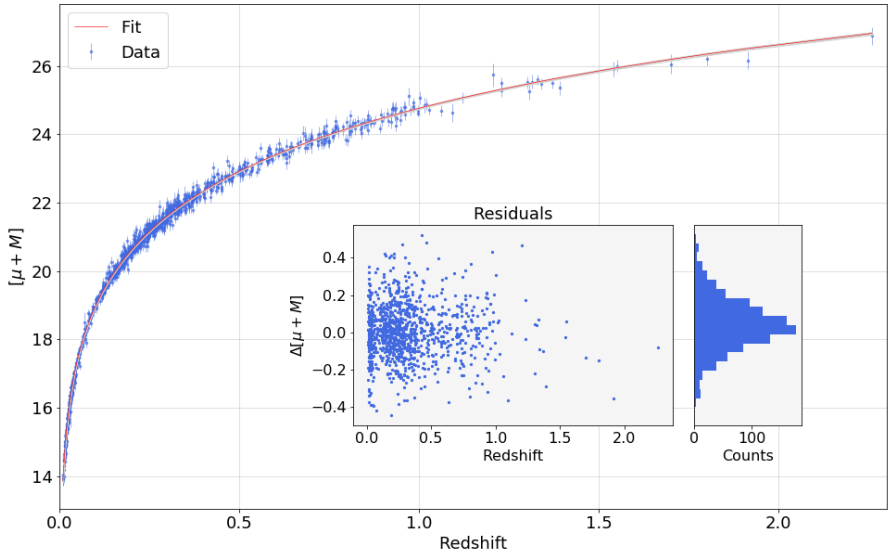

Figure 2.4: The fitted curve for the GR model assuming $M = -19.23$. On the right corner, the residual plot for the fitted data.

Table 2.4: H_0 values found by MCMC with SNe-Ia data, assuming $M_V = -19.23$. Furthermore, we tabulate Planck [49] and Riess [54] H_0 values.

Model	$\boldsymbol{H_0}$ **(km/(s Mpc))**	**Error**
Planck 2018 [49]	67.36	0.54
Riess 2018[6] [54]	73.52	1.62
Riess 2018[7] [54]	73.83	1.48
GR	74.08	0.24
Delta Gravity	74.47	1.63

Also, we show the Deceleration Parameter for both models in Table 2.5.

Table 2.5: q_0 values found by MCMC with SNe-Ia data, assuming $M_V = -19.23$.

Model	$\boldsymbol{q_0}$	**Error**
DG	-0.664	0.002
GR	-0.57	0.02

In both models $q_0 < 0$, then in DG the Universe is accelerating at a similar rate (compared to GR).

2.3.3 Relation with Delta Components

In DG, we are interested in determining the Delta Composition of the Universe. Using the Equations (1.41) and (1.42), we can obtain the densities for Delta matter and Delta radiation with the C and L_2 fitted values:

$$\tilde{\rho}_{m,0} = 0.22777\rho_{m,0} = 0.22773\rho_{c,0} \tag{2.10}$$

$$\tilde{\rho}_{r,0} = 0.68330\rho_{r,0} = 0.000115\rho_{c,0} \tag{2.11}$$

The Common Components are dominant compared with Delta Components. Matter is always dominant compared with radiation (in both cases). See Figure 2.5.

In both, Common Components and Delta Components, there is a transition between matter and radiation that is indicated in the zoom-in included in the Figure 2.5. These transitions occur at a very early stage of the Universe.

Remember that in DG we do not know $\rho_{c,0}$, but we know the densities of each component in units of $\rho_{c,0}$, because they are given by C and L_2 fitted values from SNe-Ia data.

2.3.4 Importance of L_2 and C

To understand the role that L_2 and C are playing in the DG model, we need to plot some cosmological parameters as a function of both coefficients. We are interested in analyzing the accelerating expansion of the Universe as a function of these two parameters, then we plotted H_0^{DG} in Figures 2.6 and 2.7 and q_0^{DG} in Figures 2.8 and 2.9.

The Figure 2.6 shows that there is a big zone that is prohibited because the results become complex values at a certain level of the equations. Only the allowed values are colored. Almost all the allowed H_0^{DG} values are close to the axis $L_2 = 0$. Only the contour of the colored area shows $H_0^{DG} \neq 0$. The Figure 2.7 is the same as the upper one, but with a big zoom-in close the fitted values obtained from MCMC analysis. These ranges of C and L_2 are reasonable to make an analysis. We emphasize that H_0^{DG} has a strong dependence with C and L_2 values.

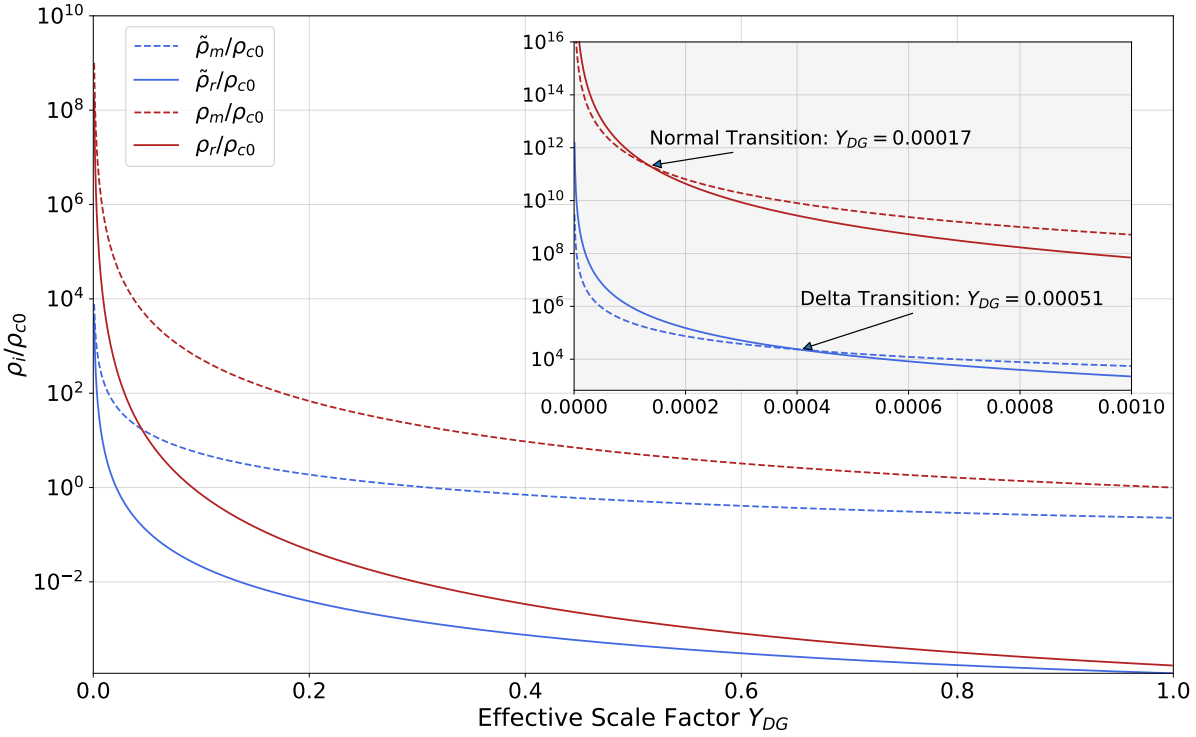

Figure 2.5: Temporal evolution of density components for Delta Gravity. The vertical axis is normalized by the critical density at the current time $\rho_{c,0}$. On the top right corner, there is a zoom-in very close to $Y_{DG} = 0$ showing the transition between Delta matter and Delta radiation (Delta Components), and the transition between matter and radiation (Common Components). In general, the Common Density is higher than the Delta Density.

Remember that L_2 only makes sense between values 0 and 1, because we only want to allow positive Delta densities and, from the Equation (1.40), the denominator could be equal to 0.

Figure 2.8 is very interesting because it shows the dependence of the current value of the acceleration of the Universe expressed by the deceleration parameter q_0^{DG}. If we examine the zone close to the fitted values in the Figure 2.9, we can highlight that the acceleration of the Universe only depends on the value of L_2. The most significant result is that the accelerating Universe is determined by the L_2 parameter. This parameter appeared naturally like an integration constant from the differential equations when we solved the DG field equations. Then, in this model, and exploring the closest area to the Universe with a little amount of radiation compared to matter, we found that a higher L_2 value, higher the acceleration of the Universe (today): q_0^{DG} becomes more negative when $L_2 \to 1$ independently of C.

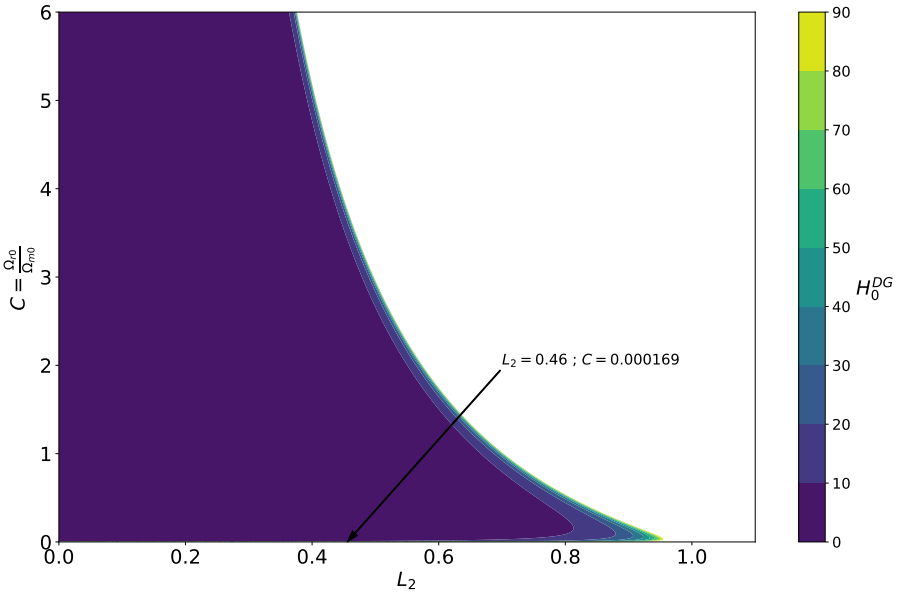

Figure 2.6: H_0^{DG} for a different combination of L_2 and C values. The fitted values found by MCMC analysis are indicated in the Figure. C values go from 0 to 6 to explore various types of Universe, even one dominated by radiation.

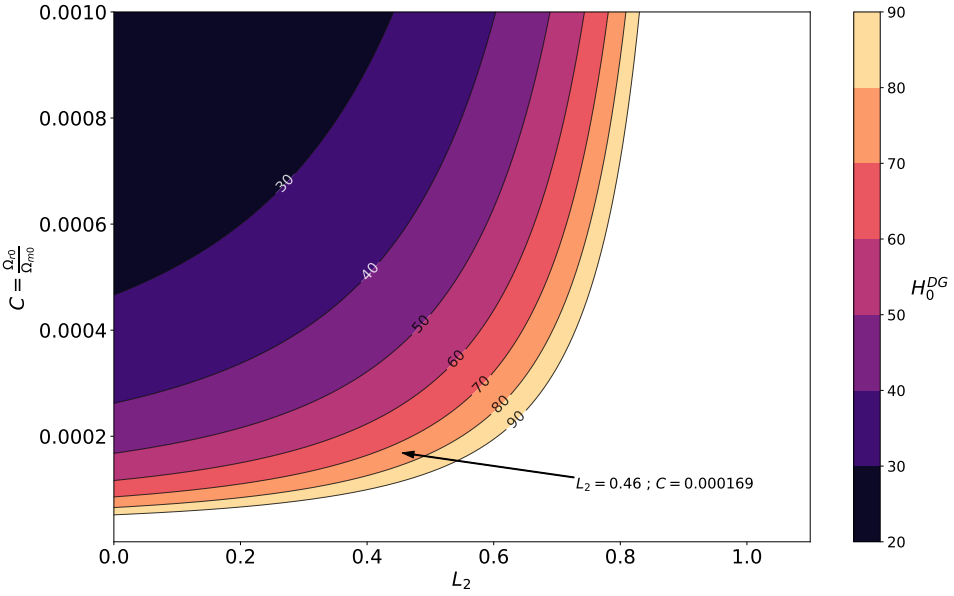

Figure 2.7: H_0^{DG} for a different combination of L_2 and C values. The fitted values found by MCMC analysis are indicated in the Figure. The C values are bounded to very small values, nearly close to the C fitted value obtained by MCMC.

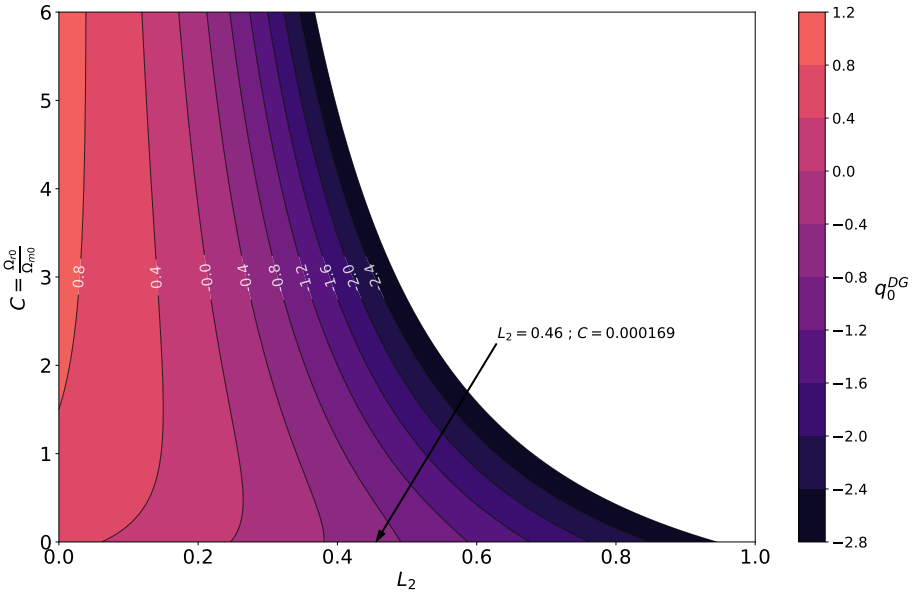

Figure 2.8: q_0^{DG} for different combination of L_2 and C values. The fitted values found by MCMC analysis are indicated in the Figure. C values go from 0 to 6 to explore various Universes, even a Universe dominated by radiation.

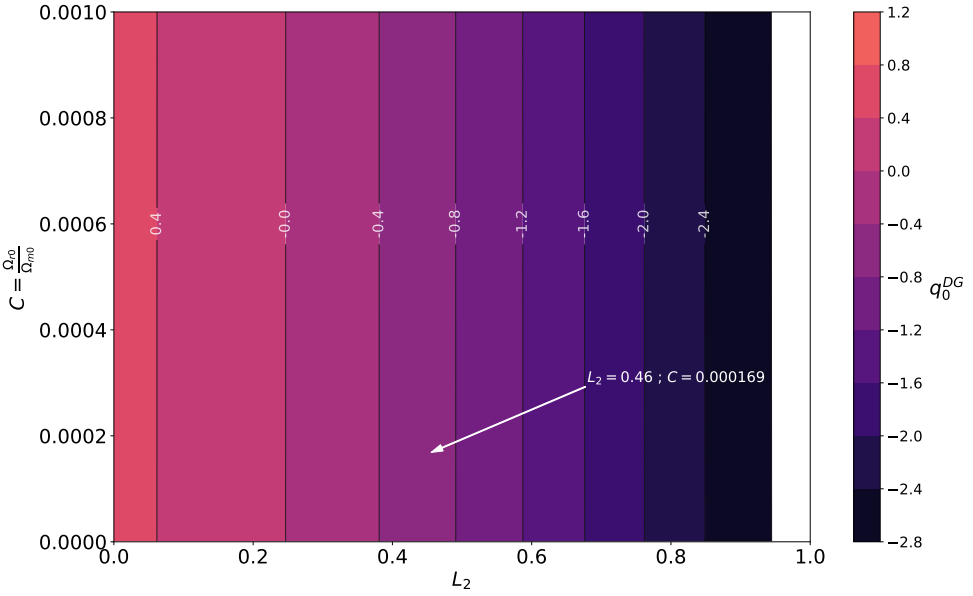

Figure 2.9: q_0^{DG} for different combination of L_2 and C values. The fitted values found by MCMC analysis are indicated in the Figure. The C values are bound to minimal values, nearly close to the C fitted value obtained by MCMC.

Chapter 3

Supernovas

We are interested in the viability of DG as a real alternative cosmology theory that could explain the accelerating Universe without Λ. The first Section shows the SNe-Ia data and the equations, the Section 2 shows the results and the last Section contains the analysis and the conclusions. This chapter is similar to the previous one, but the meaning of some parameters and their numerical values change. This change is **relevant** to be able to explain the CMB later.

3.1 Fitting the SNe-Ia data

3.1.1 SNe-Ia data

To analyze the expansion of the Universe, we used 1048 SNe from the most updated type Ia supernovae catalog presented in the Subsection 2.2.1.

From the observations, we only know the apparent magnitude and the redshift for each SN-Ia. We have two options: try to fit the absolute magnitude M or use a standardized absolute magnitude obtained by an independent method that does not involve ΛCDM model or any other assumptions. In this chapter we even do not assume a C value, because it is related with the CMB and other cosmological constraints that can be derived from the CMB and

not from SNe-Ia.

In consequence, in DG we assume a scenario with M fixed, and try to find L_2 value assuming $C = 0$. We will use $M = -19.23 \pm 0.05$. This value was calculated using 210 SNe-Ia data from [56]. This absolute magnitude is significant for us because it is independent of the Model.

We emphasize that we are always working in a flat Universe, and in the GR standard model, the $\Omega_{r,0}$ is negligible. Then, we have the same degrees of freedom as DG: 2, where we are including DE as $\Omega_{\Lambda,0} \equiv \Omega_\Lambda \equiv 1 - \Omega_{m,0}$. Summarizing, in DG we fit L_2 and h while in GR we fit Ω_Λ and h. Both models with 2 degrees of freedom.

3.1.2 GR fit

To fit the SNe-Ia data, we used the Least Squares Method. The Figure 3.1 assumes $M = -19.23$, curvature 0 and $\Omega_{r,0} = 0$. It is important to note that in GR h and M are degenerated. We fix M because it is an independent value obtained from a local measurement [54, 55, 56]. The objective is to compare this SNe-Ia fit with the DG fit.

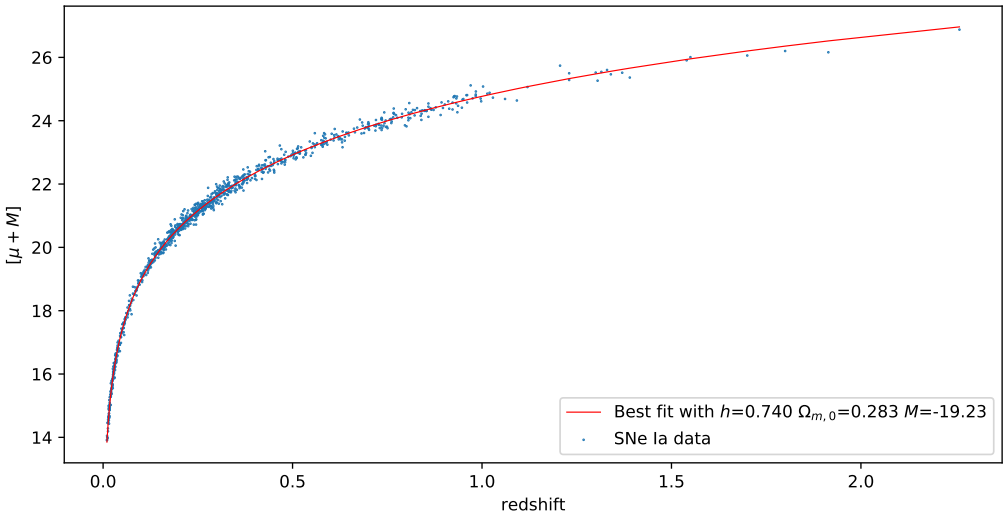

Figure 3.1: The fitted curve for the GR model assumes $M = -19.23$.

Both parameters, h and $\Omega_{m,0}$, are not degenerated and are well-determined. These are shown in Table 3.1.

Parameter	Value	Standard Error	Relative Error
$\Omega_{m,0}$	0.28	0.01	4.20%
h	0.740	0.002	0.33%

Table 3.1: Fitted values for GR model.

3.1.3 DG fit

To fit the SNe-Ia data we used Least Squares Method. We present two fitted curves. The Figure 3.2 assumes a luminosity distance with $C = 0$. The Figure 3.3 assumes a luminosity distance with $C = 4.5 \times 10^{-4}$. Both curves are very similar, but we decided to include both plots to show that the fit does not change.

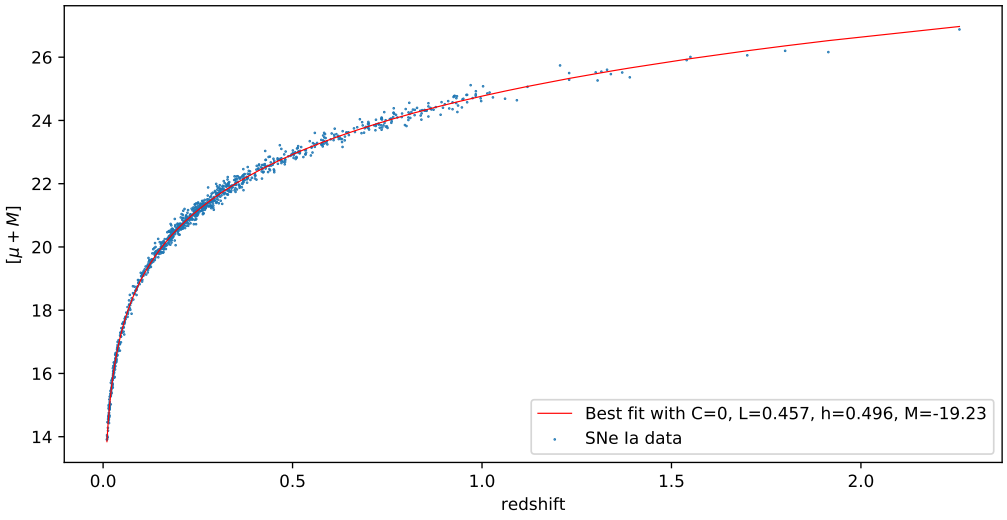

Figure 3.2: The fitted curve for the DG model assumes $C = 0$ and $M = -19.23$.

Both parameters, h and L_2, are not degenerated and are well-determined.

The results of the fit for the case $C = 0$ are the same as for $C = 4.5 \times 10^{-4}$, then both cases are presented in only one Table 3.2 (considering the standard error).

Note: the Figure 3.2 is a fit and the Figure 3.3 is a plot where we changed the C value.

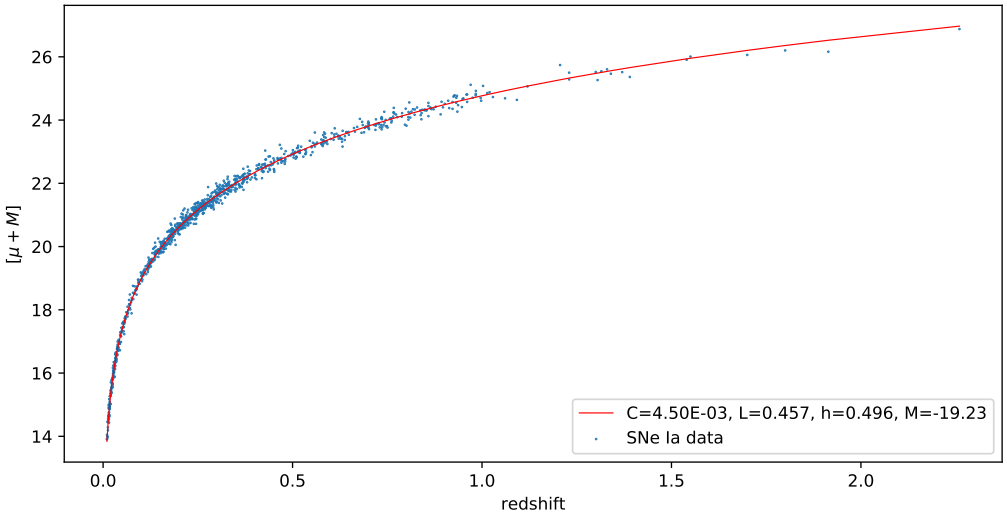

Figure 3.3: This curve assumes that C is 4.5×10^{-4} instead of 0. The other parameters are not changed.

Parameter	Value	Standard Error	Relative Error
L_2	0.457	0.007	1.57%
h	0.496	0.004	0.77%

Table 3.2: Fitted values for DG model.

The differences between both cases are tiny. We decided to show the error distribution vs. the redshift in the Figure 3.4, and we calculated the squared error associated with different C values in the Figure 3.5.

3.2 Analysis

The results from SNe-Ia analysis indicate that DG explains the accelerating expansion of the Universe without including Λ or anything like "Dark Energy". The acceleration is naturally produced in DG, caused by a coefficient named L_2, which appears when we solve the differential equations that describe the cosmology. L_2 was not introduced by hand, as the case of Λ in the standard cosmological model. The accelerating Universe occurs naturally, and comes from the variation of the E-H action, assuming that the Delta symmetry is a real symmetry about the physics that describes the Universe. Note that L_2 and h are not degenerated.

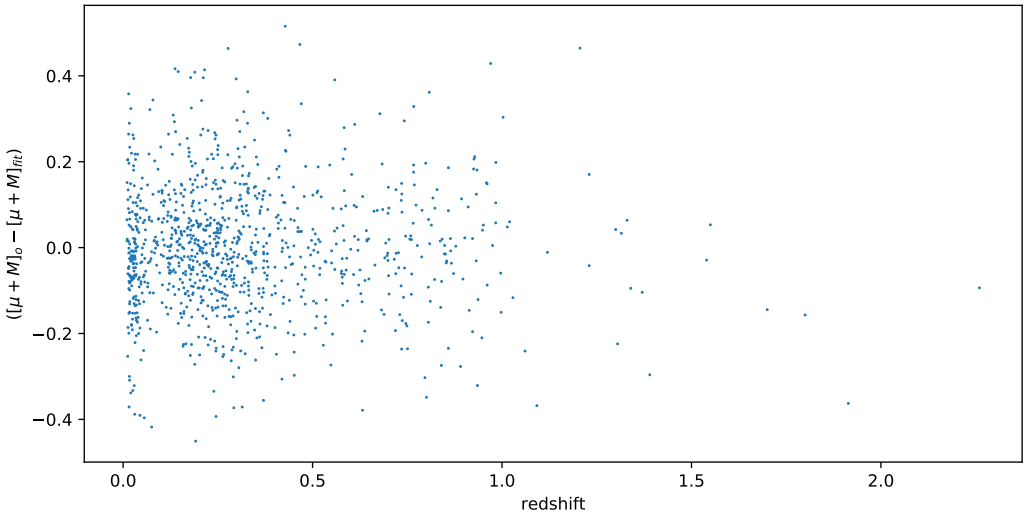

Figure 3.4: Error dispersion for DG model assuming a fitted model with $C = 0$,$L_2 = 0.457$ and $M = -19.23$.

We assumed that $M = -19.23$ is a right value calculated from [56]. This value was obtained by local measurements (this is essential) and SNe-Ia calibrations, and then, it is independent of any cosmological model. Therefore the procedure presented does not use ΛCDM assumptions. We only assume that the calibrations from Cepheids and SN-Ia are correct; then, the absolute magnitude is given by $M = -19.23$ for SNe-Ia.

DG needs $L_2 \neq 0$ to explain Dark Energy, and this implies that it must exist a new kind of energy density that we have called Delta matter and Delta radiation. It is not clear if this Delta Composition is made of real particles or is a kind of energy that underlies the space-time. We are going to clarify this aspect in the Chapter 4.

Also, DG can predict a high value for H_0, and it is in concordance with the last measurement of the local Hubble Constant. This value is not necessarily preserved in a local expansion of the luminosity distance. In DG, a low redshift expansion of the d_L term gives the same equation as a polynomial in z as GR. This aspect is crucial because the current H_0 value is in tension [56][54] between SNe-Ia analysis and CMB data, thus in the next chapter, we are going to use the L_2 value, which is the only option to preserve the Riess et al. observations as a correct measurement. In the next Section, we will show a local expansion in terms of z and a local fit of the H_0^{DG}. It is essential to understand that the parameters that we usually

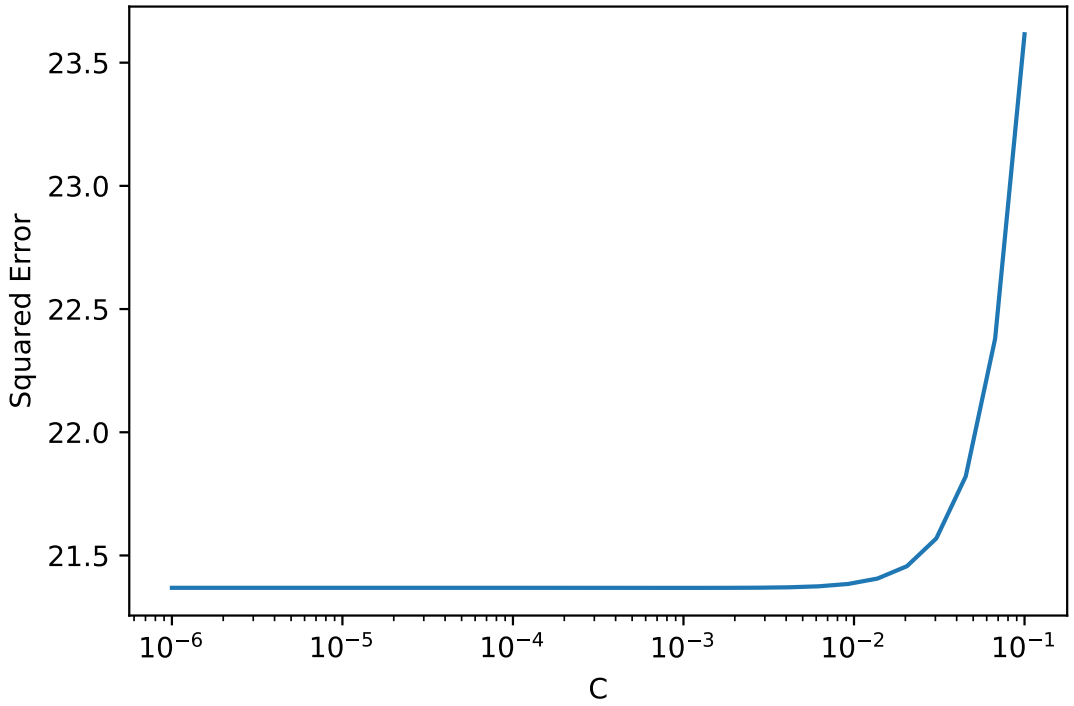

Figure 3.5: Squared errors for DG model assuming a fitted model with $C = 0$,$L_2 = 0.457$ and $M = -19.23$.

know in standard cosmology could change in DG. For example, the rate of expansion of the Universe is given by H_0^{DG}, and not by h. Indeed, $H_0^{DG} \neq 100h$ because they are entirely different in our model. h is a parameter inherited from GR background, but the real rate of expansion H_0^{DG} is determined by the Effective Scale Factor Y_{DG} and not by a or Y.

An important result from the fitted curves is the independence between the curve fitting and C value in a wide range of $0 \leq C \ll 10^{-2}$. First of all, we analyzed if the errors were normally distributed around the observed SNe-Ia magnitudes. This distribution is not necessarily true for every combination of h, C, and L_2, but it is true for all $C \ll 10^{-2}$. If C is about 10^{-4} it is impossible to distinguish a curve with $C = 0$ or with $C \sim 10^{-4}$. This indistinguishable is crucial because the range of C allows us to fit the CMB without changing the SNe-Ia fit (if C is small). Nonetheless, we decide to show how much the fit changes (the squared error) if C value changes. This was depicted in the Figure 3.5, while the effect of the C value in the fitted curve can be visualized in the Figure 3.6. A higher C value moves the predicted curve to lower values. Then, the mean of the normal distribution of the errors moves to lower prediction values, resulting in a worse fit if the C value is sufficiently high. In other

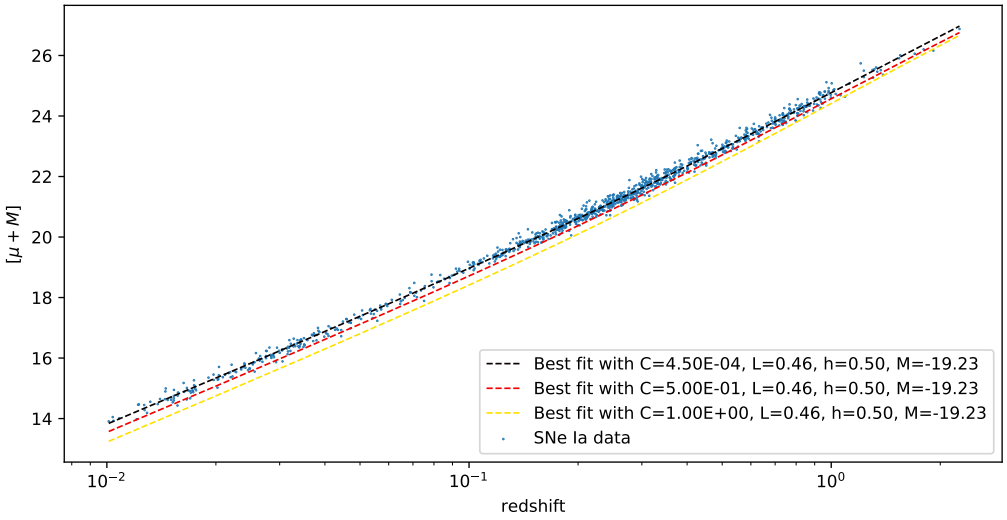

Figure 3.6: There are three different curves fitted to SNe-Ia data in a log-scaled horizontal plot. All the curves assume the parameters obtained for the best fit for DG, but changing C. At a higher C value, the predicted curve tends to be lower than the observed values. If C is small, it appears almost similar to the $C = 0$ case.

words, the SNe-Ia data constraint the DG model to consider only small values of C, but it does not give more information about it.

3.3 Cosmological parameters

With the parameters fixed from the SNe-Ia data, we can find the Hubble Constant, the Deceleration parameter, the Age of the Universe, and the evolution of these parameters with time. Also, we decided to show the luminosity distance as a local expansion in terms of z.

3.3.1 Local expansion

3.3.1.1 Approximation up to first order in redshift

The luminosity distance is given by the Equation (1.48):

$$d_L^{DG}(z, L_2, C) = c\frac{a_{DG,0}(1+z)}{H_0\sqrt{\Omega_m}}\int_{Y(z)}^{1}\frac{Y}{\sqrt{Y+C}}\frac{dY}{a_{DG}}, \tag{3.1}$$

Taking the limit where $C = 0$ and using the relation between the DG Scale Factor and redshift given by the Equation (1.43):

$$a_{DG} = \frac{a_{DG,0}}{1+z}, \tag{3.2}$$

we obtain an expression around $z = 0$ given by

$$m = 5\log\frac{cz}{H_0^{DG}} + M + 25. \tag{3.3}$$

This expression is in concordance with the standard Hubble Parameter and the Deceleration Parameter definitions, where we have replaced the a by a_{DG} (See appendix A).

3.3.1.2 Local fit of SNe-Ia data

Riess et al. [54] found values for M and H_0 that are independent of any assumptions (only depends on the d_L definition, where they assumed a flat Universe) and that are not degenerate. Therefore, the local analysis for DG is valid, where the Hubble Constant measured in this context is H_0^{DG} and not H_0. Only to clarify any doubt, we have fitted 150 SNe-Ia with redshift less than 0.05 [58], as is shown in the Figure (3.7).

This local measurement constraints the Hubble Constant to $H_0^{DG} = 73.5 \pm 0.4(0.6\%)$ assuming $M = -19.23$, because H_0^{DG} and M are degenerated by the equation (3.3) but this relation is constrained by the Cepheids calibration [56, 54, 55].

The local measurement is vital because any conclusion from Riess et al. can be extrapolated to DG. After all, the local behavior between redshift and magnitude is preserved.

We expect that M must be constant because it is an intrinsic property of the SNe-Ia. This result depends on the local data used to obtain this constraint: a local measurement could be slightly different from a high redshift measurement because cosmological effects must be considered, where the luminosity distance plays an important role. Also, note that H_0 is very different from H_0^{DG}, which is not a problem in DG. DG can accept that the real (physical or observable) rate of expansion H_0^{DG} is high and not necessarily is contradictory with the CMB measurements). Until here, we are trying to conciliate local and high redshift measurements

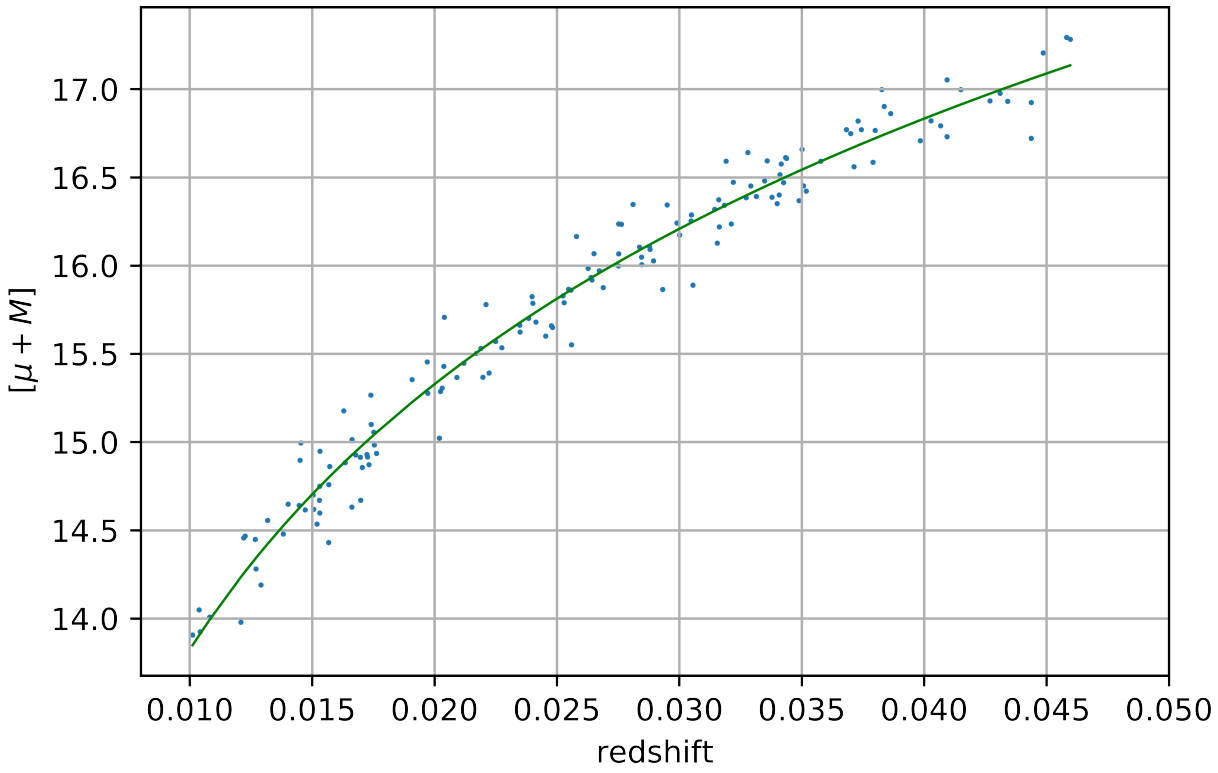

Figure 3.7: 150 SNe-Ia data fitted with equation (3.3) in DG model.

of SNe-Ia data. If any of these observations or data are wrong, all the analyses presented here must be revisited because it depends on both observations.

3.3.2 H^{DG} and q^{DG}

3.3.2.1 Hubble parameter and H_0

With the fitted parameters found in Section 3.1, we can find $H(t)$ and H_0. For GR, H_0^{GR} is easily obtained from the h^2 fitted ($H_0 = 100h$) and $H^{GR}(t)$ can be obtained using the first Friedmann equation

$$H^2 = \left(\frac{\dot{a}}{a}\right)^2 = \frac{8\pi G}{3}\left(\frac{\rho_{m,0}}{a^3} + \frac{\rho_{r,0}}{a^4} + \rho_{\Lambda,0}\right) \tag{3.4}$$

Taking into account that $\Omega_{m,0} + \Omega_{r,0} + \Omega_{\Lambda,0} = 1$, $\Omega_{r,0} \approx 0$ and $\rho_{c,0} = \frac{3H_0^2}{8\pi G}$, where $\Omega_{i,0} = \frac{\rho_{i,0}}{\rho_{c,0}}$ for every i component in the Universe, we obtain

$$H^2 = H_0^2 \left(\frac{\Omega_{m,0}}{a^3} + (1 - \Omega_{m,0}) \right) \tag{3.5}$$

With the Equation (3.5), we obtain $H^{GR}(t)$ and using the Equation (1.53) we obtain $H^{DG}(t)$. For the current time we evaluate H^{GR} at $a = 1$ and for DG we evaluate H^{DG} at $Y_{DG} = 1$ obtaining the Hubble Constants H_0^{GR} and H_0^{DG}, respectively. It is important to highlight that these values are not local fitted parameters. They were obtained using all the SNe-Ia data, and both fitted analysis have the same degrees of freedom. They were made to compare both models. Therefore, this GR fit does not imply that H_0^{GR} must be the same value that Riess et al. obtained, because it is not local. However, this value is higher than the CMB Hubble Constant. Still, in this section, we are only working with SNe-Ia, and we are not going to discuss this aspect until the last part of this thesis, nevertheless we show all the Hubble Constant estimations.

The H_0^{DG} value can be found using (1.53), but also, we can obtain an approximate equation that depends on h and L_2 (that assumes $C = 0$). This estimation is very precise[1]:

$$H_0^{DG} \approx 50h \frac{(-6 + 11L_2 - 7L_2^2 + 2L_2^3)}{(-3 + L_2)(-1 + L_2)^2} \tag{3.6}$$

We present the results from both models, and we compare these values with measurements in the Table 3.3. Finally, we plot the values in the Figure 3.8.

Model	H_0 (km/(s Mpc))	Error (km/(s Mpc))
Planck 2015 [48]	67.74	0.46
Planck 2018 [49]	67.4	0.5
Riess 2016 [56] [2]	73.24	1.74
Riess 2018[3] [54]	73.52	1.62
Riess 2019[4] [54]	74.03	1.42
GR	74.0	0.2
DG	74.3	1.3

[1] This equation is straightforward from the definition of (1.53).

[2] First local determination of the Hubble Constant: "A 2.4% Determination of the Local Value of the Hubble Constant"

[3] The calibration was made including the new MW parallaxes from *HST* and *Gaia*.

[4] Precision HST photometry of Cepheids in the Large Magellanic Cloud (LMC) reduce the uncertainty in the distance to the LMC from 2.5% to 1.3%

DG approx	74.2	-
DG local	73.5	0.4

Table 3.3: H_0 values found by Least Squares Method with SNe-Ia data. Furthermore, we tabulate Planck satellite's data [48] and [49], and Riess et al. [54] H_0 values. *GR* and *DG* are the H_0 values obtained in Section 3.1 using all the SNe-Ia data. *DGapprox* was calculated from the Equation (3.6) and *DGlocal* was obtained fitting local SNe-Ia using the Equation (3.3).

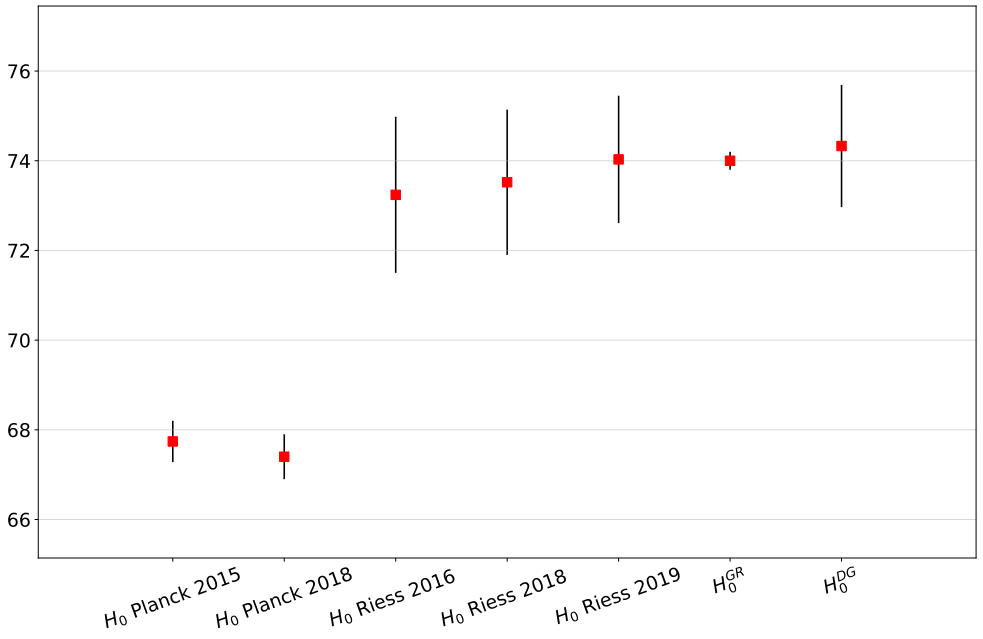

Figure 3.8: Different measurements of the Hubble Constant from Planck [48, 49] and local SNe-Ia [56, 54, 55]. We include the two results obtained in the fitting analysis presented in the Section 3.1

The Figure 3.8 shows the DG prediction for H_0, and clearly, this is in concordance with the last H_0 measurement. This compatibility is a consequence of the excellent fit obtained from the model (we are only working with h and L_2). GR also predicts a high H_0 value with the same assumptions, but it needs to include Λ to fit the SN-Ia data. The last two data labeled as *GR* and *DG* in Figure 3.8 are related to the full SNe-Ia data set, and not with a local measurement. DG describes the acceleration given by high redshift data and fits the local (low redshift) regime. This acceleration is a consequence of the definition of d_L in DG. This term can be expanded as a z series, with the same physical significance, such as the Hubble Constant and the Deceleration Parameter (but these parameters depend in a

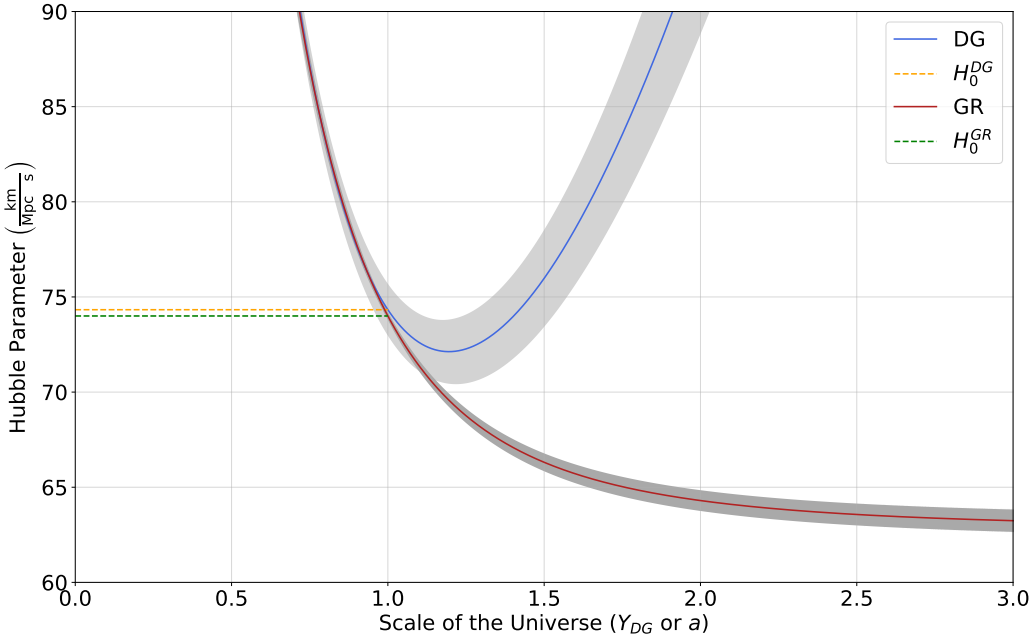

Figure 3.9: Hubble Parameter for DG and GR fitted models assuming $M = -19.23$

very different form compared to GR) [5]. Furthermore, the discrepancy about H_0 value could be indicating new physics behind the Standard Cosmology Model Assumptions, and maybe, one possibility could be the modification of GR.

The Figure 3.9 shows the change in the Hubble parameter for both models. In the DG case, the Hubble parameter increases after $Y_{DG} \approx 1.2$, and the Universe starts to increases its size to end with a Big Rip. In contrast, as we know, LCDM does not predict a Big Rip. The $H(a)$ tends to be constant when $a \to \infty$.

The Figures 3.10 and 3.11 shows how the Deceleration Parameter depends on C and L_2. In the regime of interest, where $C \to 10^{-4}$, H_0^{DG} is independent of C and it increases with L_2.

[5] "The direct measurement is very model-independent, but prone to systematics related to local flows and the standard candle assumption. On the other hand, the indirect method is very robust and precise, but relies completely on the underlying model to be correct. Any disagreement between the two types of measurements could in principle point to a problem with the underlying ΛCDM model." [41]

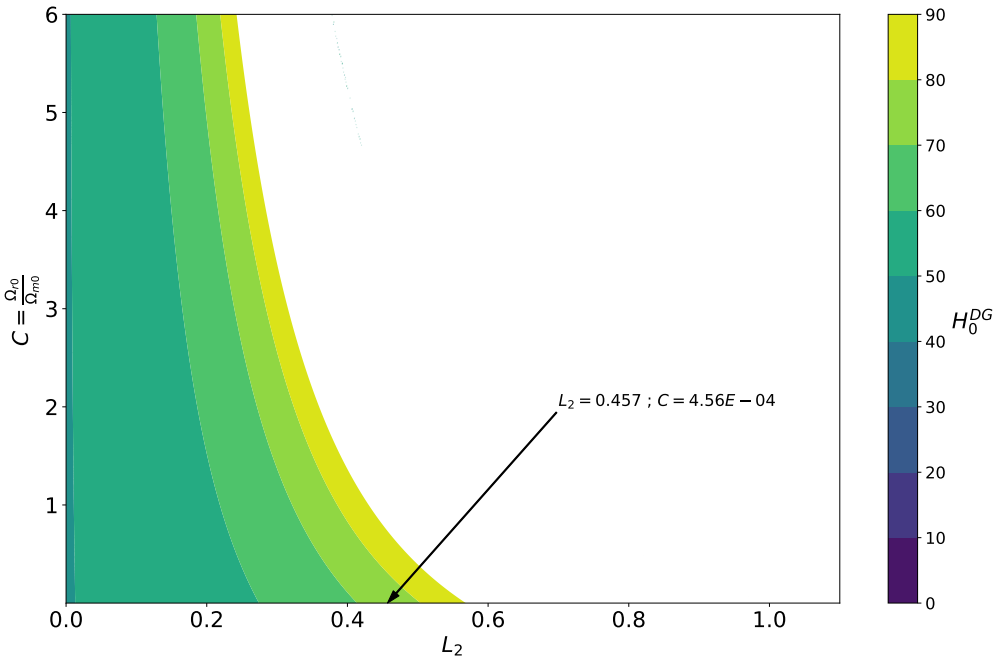

Figure 3.10: Dependence of the Hubble Parameter for DG with C and L_2.

3.3.3 Deceleration Parameter $q(t)$

In GR the Deceleration Parameter is calculated from the Equation (1.54) and the Friedmann equations (see Appendix B).

$$q_0 = \frac{1}{2}\Omega_{m,0} - \Omega_{\Lambda,0}. \tag{3.7}$$

This equation is straightforward from (1.54).

For DG, we used the Equation (1.56). To evaluate at current time, we choose $a = 1$ for GR, and $Y = 1$ for DG.

We show the Deceleration Parameters for both models in the Table 3.4

Model	q_0	Error
DG	-0.700	0.001
GR	-0.58	0.02

Table 3.4: q_0 values were found using Least Squares Method with SNe-Ia data.

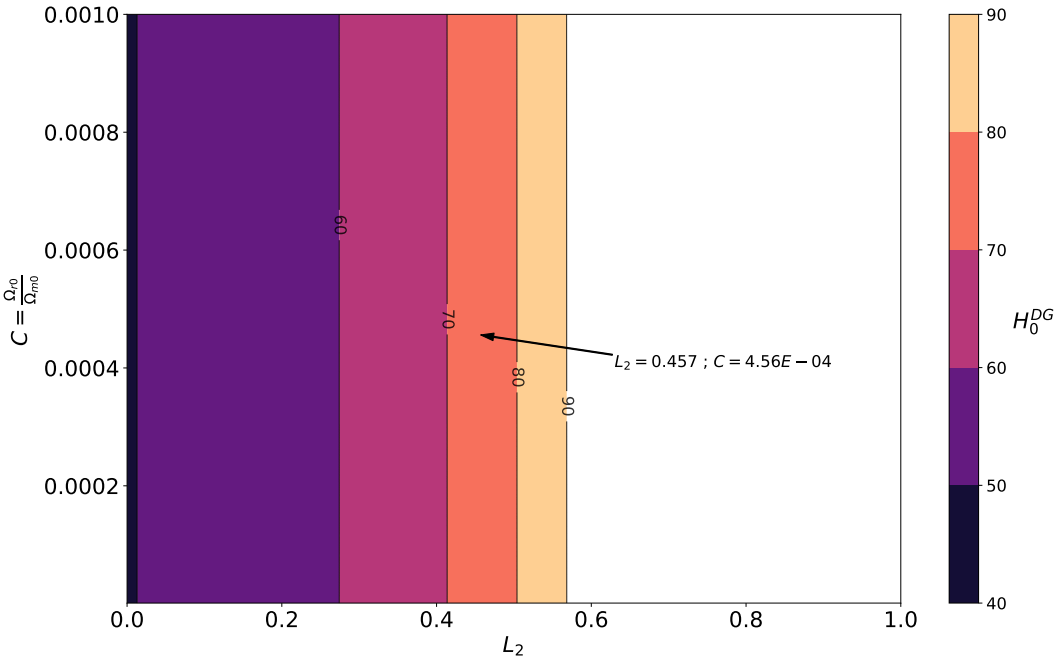

Figure 3.11: This is a zoom of the Figure 3.10 in the area near to $C \sim 10^{-4}$.

Both models have $q_0 < 0$; in other words, the Universe is accelerating but with slightly different rates.

In the Figure 3.12 we show how the Deceleration Parameter depends on C and L_2. It is important to take into account that acceleration only depends on L_2. This plot is extended to an arbitrary C value. However, our physical interest is in a small range of C, see Figure 3.13.

In Figure 3.13 the dependence with C disappear, in contrast with Figure 3.12. L_2 drives all the acceleration of the Universe, also if we have $L_2 = 0$, there is no acceleration, and also, there is no Delta Composition. This parameter is driving the acceleration, and it is describing the SNe-Ia data. If $L_2 \to 1$, then q_0 is more negative, and the Universe has a higher acceleration.

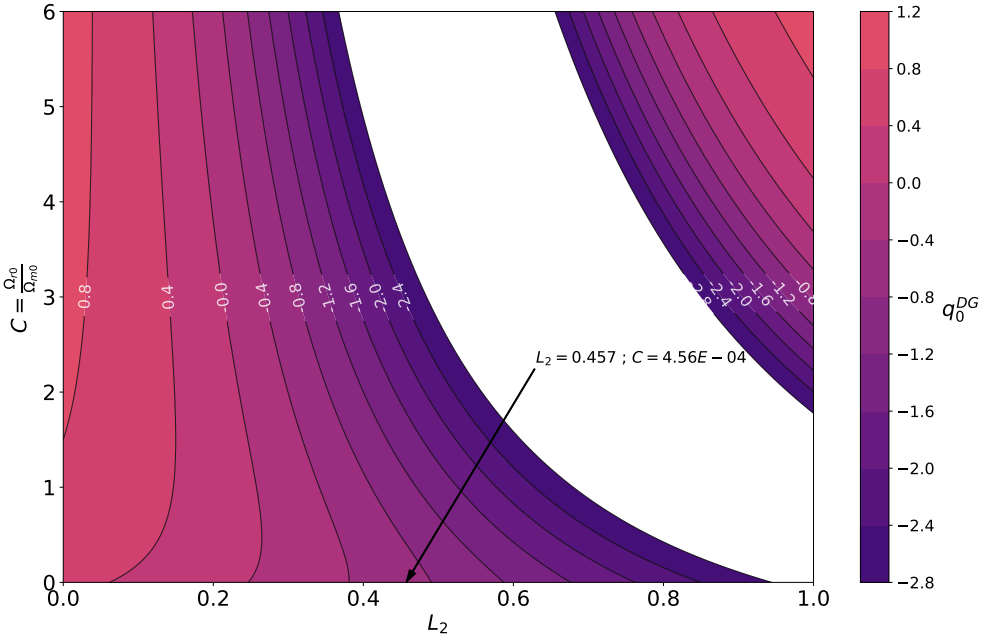

Figure 3.12: The Figure shows the dependence of the Deceleration Parameter for DG with C and L_2.

3.3.4 Other interesting relations

3.3.4.1 Cosmic Time and redshift

To calculate the Cosmic Time in DG, we used the Equation (1.22). The redshift is obtained by numerical solution from the Equation (1.44).

Meanwhile, for the GR model, we obtained the Cosmic Time integrating the first Friedmann equation and solving $t(\Omega_{m,0}, H_0)$. Here we have included $\Omega_\Lambda = 1 - \Omega_{m,0}$ and we chose a flat cosmology and $\Omega_{r,0} = 0$. The integral for the first Friedmann equation can be analytically solved (from the Equation 3.5):

$$t = \int_0^a \frac{1}{\sqrt{\frac{\Omega_{m,0}}{x} + (1-\Omega_{m,0})x^2}} dx = \frac{2}{3\sqrt{1-\Omega_{m,0}}} \ln\left(\frac{\sqrt{-\Omega_{m,0}a^3 + \Omega_{m,0} + a^3} + \sqrt{1-\Omega_{m,0}}a^{3/2}}{\sqrt{\Omega_{m,0}}}\right), \tag{3.8}$$

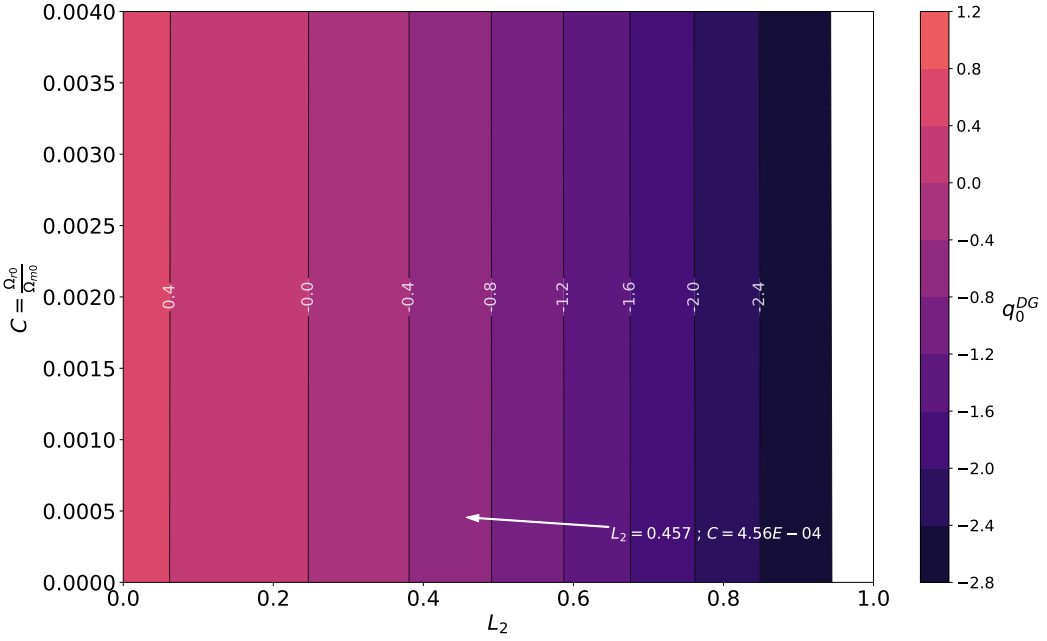

Figure 3.13: This is a zoom in the physical area of interest, close $C \sim 10^{-4}$. In this regime, the Deceleration Parameter is independent of C, and L_2 drives all the acceleration of the Universe.

where t in (3.8) is the Cosmic Time for GR. The behavior of Cosmic Time dependence with redshift for both models is very similar. This is shown in Figure 3.14, while, the relations between the size of the Universe and the cosmic time is shown in Figure 3.15.

3.3.4.2 Age of the Universe

The age of the Universe in DG is calculated using the Equation (1.22). $t(Y)$ only depends on h and C, but not on L_2. In GR, we calculate the age of the Universe using (3.8). The age for DG model is 13.1 ± 0.1 Gyrs and for GR is 13.0 ± 0.2 Gyrs. With these same expressions, we can compare the behavior between Cosmic Time and the Scale Factor in GR (or the Effective Scale Factor in DG).

The Figure 3.15 shows the evolution for $Y_{DG}(t)$ with the time. At $t \approx 28.7$ Gyr, Y_{DG} goes to infinity, and the Universe ends with a Big Rip dominated by the L_2 value. Then, in this model, the Universe has an end (in time). Also, we plot the dependence between the Scale Factor a and the Cosmic Time t. In this last case, the Universe has no Big Rip.

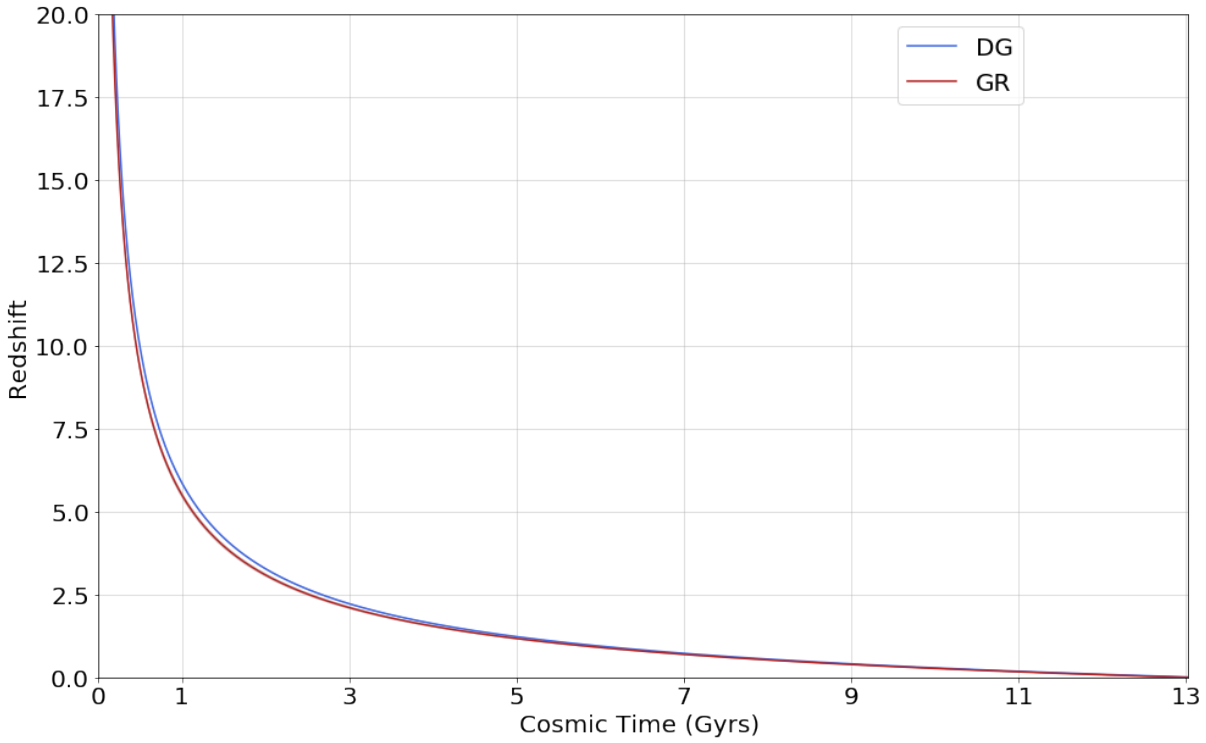

Figure 3.14: Cosmic Time for GR and DG assuming $M = -19.23$.

The higher the Hubble Constant, the lower the age of the Universe. This relation is vital since if the local fit of supernovae radically changes H_0, then the age of the Universe changes. The age of the Universe for DG and GR are small (13.1 Gyrs for DG and 13.0 Gyrs for GR) compared with the age calculated from Planck (13.8 Gyrs). A crucial and precise estimation based on the measurement of globular clusters' age in the Milky Way [42], which is independent of cosmology, indicates that the Universe has to be older than 13.6 ± 0.8 Gyrs. DG, assuming the results of SNe's local measurements, is on the verge of this observational constraint. We emphasize that the problem goes beyond DG because this discrepancy is related to the local measurements and it is due to the calibration made by Riess et al. [56]. For instance, other researchers have tried to measure the H_0 value using methods independent of distance ladders and the CMB. They found that the Hubble Constant exceeds the Planck results, with the confidence of 95% [46]. However, other measurements based on the tip of the red giant branch (TRGB) have found that H_0 is close to 69.6 km/(Mpc s) [24, 25]. Other methods based on lensed quasars found that $H_0 = 73.3$ Mpc/(km s) agrees with local measurements but tension with Planck observations [70].There is no agreement about this problem in the ΛCDM model (for DG is the same).

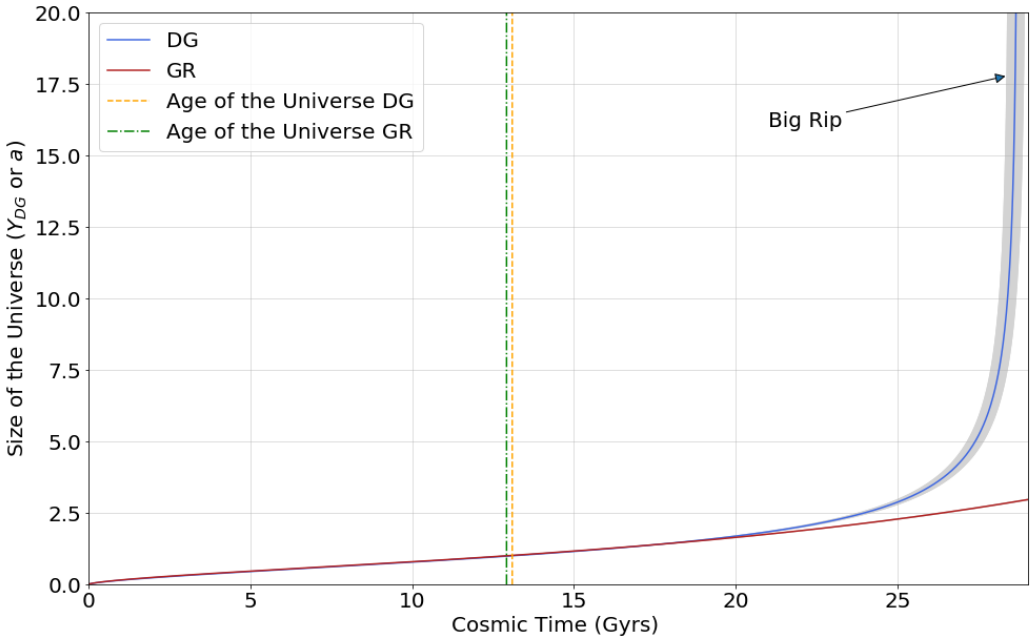

Figure 3.15: The size of the Universe vs. age of the Universe. In the DG model, the size of the Universe Y_{DG} depends on the Cosmic Time t and C. The blue line indicates the Effective Scale Factor in DG. The gray zone shows the error associated with Y_{DG}. For GR, the Scale Factor a depends on the Cosmic Time t and on $\Omega_{m,0}$. The red line indicates the Scale Factor evolution in GR. The gray zone shows the error associated with a (these are tiny).

3.3.4.3 Relation with Delta Components

With these values, through the Equations (1.41) and (1.42), we obtain the following parameters for Delta matter and Delta radiation:

$$\tilde{\rho}_{m,0} = 0.23\rho_{m,0} \tag{3.9}$$

$$\tilde{\rho}_{r,0} = 0.69\rho_{r,0} \tag{3.10}$$

Chapter 4

CMB

To fit the CMB power spectrum with DG equations, we have to define the physical density in this theory. In other words, until here, the theory explains the acceleration of the Universe with $C \approx 0$ and a L_2 value obtained in the Chapter 3. There are many possibilities to find parameters that adjust the CMB values, but we want to preserve one important aspect: the acceleration of the Universe that preserves the H_0 value found by Riess et al. [55]. Then, L_2 and h are no more free parameters, but C is free. There are constraints over C. First, it cannot be 0 because the CMB is sensible to the presence of radiation and cannot be a high value because the SNe-Ia analysis showed that we require a small C value. It is not an arbitrary condition; it is an observational constraint required to preserve the M and H_0 observed. Only the results from Chapter 3 are valid, but keep in mind that the L_2 value never changed between Chapters 2 and 3. Finally, it is crucial to remark that an arbitrary C value can be contradictory for the SNe-Ia measurements. In this context, we will assume the L_2 value obtained from Chapter 3, and we are going to constraint the C value fitting the CMB spectrum.

4.1 Comments about the thermodynamics in DG

This section is essential to fit the CMB. Any change in this definition affects everything in numerical precision because the CMB shape is very accurate. Now, we develop the physical argument.

The physical element of volume is $dV = a_{DG}^3 dxdydz$ (given by the effective metric), which is described by the DG Scale Factor:

$$a_{DG}(t) = a(t)\sqrt{\frac{1+F(t)}{1+3F(t)}}.$$

With the volume, we can define the density of any kind of matter as

$$\rho = \frac{U}{c^2 V}, \tag{4.1}$$

where U is the internal energy, and V is the volume (defined in the cosmology model).

Therefore, if we apply the first law of thermodynamics,

$$\frac{dU}{dt} = T\frac{dS}{dt} - P\frac{dV}{dt}, \tag{4.2}$$

and assuming that the evolution of the Universe is adiabatic as in GR [1], the entropy must be preserved, then

$$\dot{\rho} = -3H_{DG}\left(\rho + \frac{P}{c^2}\right). \tag{4.3}$$

To solve this equation for a fluid, we need to know the equation of state of it. In order to know the evolution of ρ, we need an equation of state $P(\rho)$. In cosmology, the equations of state are written as $P = \omega\rho$, then

$$\rho a_{DG}^{3(1+\omega)} = \rho_0 a_{DG\,0}^{3(1+\omega)}, \tag{4.4}$$

where ρ_0 is the density today.

In DG, we preserve the standard solutions of GR, then the standard evolution of the "GR densities" behaves as usual, but with the GR Scale Factor $a(t)$:

[1] See for instance T. Padmanabhan, Theoretical Astrophysics, Volume III: Galaxies and Cosmology, First Edition, Chapter 4 (Cambridge University Press, Cambridge, England, 2002).

$$\rho_{GR} a^{3(1+\omega)} = \rho_{GR\,0} a_0^{3(1+\omega)}. \tag{4.5}$$

Note: ρ_{GR} goes for GR background in DG equations. These are not physical densities. The physical densities in the perturbative theory are indicated as ρ without sub or super index.

Finally, we can relate both densities by the ratio between them as follows

$$\frac{\rho}{\rho_{GR}} \left(\sqrt{\frac{1+F_a(t)}{1+3F_a(t)}} \right)^{3(1+\omega)} = constant(\omega). \tag{4.6}$$

This ratio is essential for the study of the perturbations. The evolution of fractional perturbations at the last-scattering moment are defined as

$$\delta_{GR\,\alpha} = \frac{\delta\rho_{GR\,\alpha}}{\bar{\rho}_{GR\,\alpha} + \bar{p}_{GR\,\alpha}}, \tag{4.7}$$

where $\alpha = \gamma$, ν, B or D (photons, neutrinos, baryons and dark matter, respectively). The crucial part of this development is that the physical densities perturbations depend on this relation, but at the time of the Last Scattering surface $Y \sim 10^{-3}$ (denoted as a ls subindex) this extra factor tends to 1. This is essential in the development of the perturbative equations, because at that moment the physical densities were proportional to the GR densities, and by definition, the density perturbations are fractional, then this factor is simplified, and then we obtain

$$\delta_{phys\,\alpha}(t_{ls}) = \delta_{GR\,\alpha}(t_{ls}) = \delta_\alpha(t_{ls}). \tag{4.8}$$

This very accurate approximation is valid from the beginning of the Universe ($z \to \infty$) to $z \sim 10$.

4.1.1 The shape of the black body spectrum

We want to preserve the shape of the Black Body spectrum because it is an observable (the CMB). The black body spectrum is given by

$$n_T(\nu)d\nu = \frac{8\pi\nu^2 d\nu}{e^{\frac{h\nu}{k_B T}} - 1}. \tag{4.9}$$

After the Last Scattering surface, the photons traveled without being perturbated until us (photons were not coupled with baryons), then the spectrum only changes because the frequency is redshifted cause of the expansion of the Universe. Then the frequency changes as $\nu = \nu_{ls} a_{DG}(t_{ls})/a_{DG}$, and the volume $V = V_{ls} a^3_{DG}/a^3_{DG}(t_{ls})$, then, the number of photons dN must be preserved, and this implies that the number of photons $dN = n_T(\nu)d\nu dV$ must preserve the following relation:

$$T a_{DG} = constant \rightarrow T = \frac{T_0}{Y_{DG}}\ , \tag{4.10}$$

where T_0 is the CMB temperature.

In other words, the temperature of the Universe evolves as usual, but with the Effective Scale Factor described by Y_{DG}.[2]

All these definitions and interpretations are essential to fit the CMB because we understand how the real physical densities evolve, and then, we can obtain indirect physical implications (that will appear in the CMB) that are measurable.

Some observations correlate the T with redshift in this sense. This correlation is important because DG preserves this relation. This deviation has been studied [36] as an arbitrary dependence in the T, where the results indicate that $T = T_0(1+z)$ is correct. [22, 17]

[2] $e^{\frac{h\nu}{kT}} = e^{\frac{h\nu_0 a_{DG}}{kT_0 a_{DG}}} = e^{\frac{h\nu_0}{kT_0}}$. Keep in mind that $a_{DG,0} \neq 1$ today, but $Y_{DG,0} = 1$.

4.2 Perturbative equations

The perturbation theory has been developed in previous work, where the perturbation terms have been decomposed as the standard Scalar-Vector-Tensor method. Here we show a summary of the main equations required to obtain the CMB and fit the parameters. [3]

$$g_{\mu\nu} = \bar{g}_{\mu\nu} + h_{\mu\nu}, \tag{4.11}$$

$$\tilde{g}_{\mu\nu} = \tilde{\bar{g}}_{\mu\nu} + \tilde{h}_{\mu\nu}. \tag{4.12}$$

4.3 Evolution of cosmological fluctuations

We are interested in the study of the evolution of the cosmological fluctuations, including the Delta evolutions. The perturbation equations are complicated, and they can be solved only using numerical methods, such as CMBfast [59, 71] and CAMB [1, 35]. However, such computer programs can not give a clear understanding of the physical phenomena involved.

In particular, the following equations were obtained using the Weinberg's approach [67] (he developed this method in the synchronous gauge [4]), which consist in two main aspects: the first one is the so-called hydrodynamic limit, which consists on that near recombination time photons were in local thermal equilibrium with the baryonic plasma, then photons could be treated hydro-dynamically, like plasma and cold dark matter. The second assumption is a sharp transition from thermal equilibrium to complete transparency at last scattering moment t_L.

In this context, the standard components of the Universe are photons, neutrinos, baryons, and cold dark matter, but we had to include Delta-counterpart. The approximation used here neglected anisotropic both energy-momentum tensor and took the usual state equation for pressures and energy densities and perturbations. Besides, as we treated photons and Delta photons hydro-dynamically, we used $\delta u_\gamma = \delta u_B$ and $\delta\tilde{u}_\gamma = \delta\tilde{u}_B$ (velocity perturbations).

[3] For a full development about the DG perturbation theory, the reader can visit the preprint in https://arxiv.org/abs/2001.08354.

[4] There are other methods, to solve the equations analytically, assuming some approximations [40, 67].

Moreover, as the synchronous scheme did not fully fix the gauge, the remaining degree of freedom were used to fix $\delta u_D = 0$, which means that cold dark matter evolves at rest with respect to the Universe expansion. In our theory, the extended synchronous scheme also had an extra degree of freedom, which we used to put $\delta\tilde{u}_D = 0$ as its standard part.

It is useful to rewrite these equations in terms of the following dimensionless term:

$$\delta_{\alpha q} = \frac{\delta\rho_{\alpha q}}{\bar{\rho}_\alpha + \bar{p}_\alpha}\,, \tag{4.13}$$

where α can be γ, ν, B and D (photons, neutrinos, baryons and dark matter, respectively). Also we use $R = 3\bar{\rho}_B/4\bar{\rho}_\gamma$ and $\tilde{R} = 3\tilde{\bar{\rho}}_D/4\tilde{\bar{\rho}}_\gamma$. By the other side, in the Delta sector we used a dimensionless fractional perturbation. However, this perturbation was defined as the Delta transformation of Equation (4.13) [5],

$$\tilde{\delta}_{\alpha q} \equiv \tilde{\delta}\delta_{\alpha q} = \frac{\delta\tilde{\rho}_{\alpha q}}{\bar{\rho}_\alpha + \bar{p}_\alpha} - \frac{\tilde{\bar{\rho}}_\alpha + \tilde{\bar{p}}_\alpha}{\bar{\rho}_\alpha + \bar{p}_\alpha}\delta_{\alpha q}\,. \tag{4.14}$$

The equations for the GR sector are

[5] We choose this definition because the system of equations now seems as an homogeneous system exactly equal to the GR sector (where now the variables were the Delta-fields) with external forces mediated by the GR solutions. Maybe the most intuitive solution should be

$$\tilde{\delta}^{int}_{\alpha q} = \frac{\delta\tilde{\rho}_{\alpha q}}{\tilde{\bar{\rho}}_\alpha + \tilde{\bar{p}}_\alpha}\,,$$

however these definitions are related by

$$\tilde{\delta}_{\alpha q} = \frac{\tilde{\bar{\rho}}_\alpha + \tilde{\bar{p}}_\alpha}{\bar{\rho}_\alpha + \bar{p}_\alpha}\left(\tilde{\delta}^{int}_{\alpha q} - \delta_{\alpha q}\right)\,.$$

$$\frac{d}{dt}\left(a^2\dot{\Psi}_q\right) = -4\pi G a^2\left(\bar{\rho}_D\delta_{Dq}+\bar{\rho}_B\delta_{Bq}+\frac{8}{3}\bar{\rho}_\gamma\delta_{\gamma q}+\frac{8}{3}\bar{\rho}_\nu\delta_{\nu q}\right), \tag{4.15}$$

$$\dot{\delta}_{\gamma q}-(q^2/a^2)\delta u_{\gamma q} = -\dot{\Psi}_q\,, \tag{4.16}$$

$$\dot{\delta}_{Dq} = -\Psi_q\,, \tag{4.17}$$

$$\dot{\delta}_{Bq}-(q^2/a^2)\delta u_{\gamma q} = -\dot{\Psi}_q\,, \tag{4.18}$$

$$\dot{\delta}_{\nu q}-(q^2/a^2)\delta u_{\nu q} = -\dot{\Psi}_q\,, \tag{4.19}$$

$$\frac{d}{dt}\left(\frac{(1+R)\,\delta u_{\gamma q}}{a}\right) = -\frac{1}{3a}\delta_{\gamma q}\,, \tag{4.20}$$

$$\frac{d}{dt}\left(\frac{\delta u_{\nu q}}{a}\right) = -\frac{1}{3a}\delta_{\nu q}. \tag{4.21}$$

While, the equations for the DG sector are

$$\left[2\dot{F}\frac{\dot{a}}{a}+\ddot{F}\right]a^2\Psi_q+\left[6F\frac{\dot{a}}{a}+\frac{5}{2}\dot{F}\right]a^2\dot{\Psi}_q+3Fa^2\ddot{\Psi}_q-\frac{d}{dt}\left(a^2\dot{\tilde{\Psi}}_q\right) = \frac{\kappa}{2}a^2\Big[\bar{\rho}_D\tilde{\delta}_{Dq}$$
$$+\bar{\rho}_B\tilde{\delta}_{Bq}+\frac{8}{3}\bar{\rho}_\gamma\tilde{\delta}_{\gamma q}+\frac{8}{3}\bar{\rho}_\nu\tilde{\delta}_{\nu q}-\frac{F}{2}\left(\bar{\rho}_D\delta_{Dq}+\bar{\rho}_B\delta_{Bq}\right)-\frac{8}{3}F\left(\bar{\rho}_\gamma\delta_{\gamma q}+\bar{\rho}_\nu\delta_{\nu q}\right)\Big], \tag{4.22}$$

$$\dot{\tilde{\delta}}_{\gamma q}-\frac{q^2}{a^2}\left(\delta\tilde{u}_{\gamma q}+F\delta u_{\gamma q}\right)+\dot{\tilde{\Psi}}_q-\partial_0(F\Psi_q) = 0 \tag{4.23}$$

$$\dot{\tilde{\delta}}_{Dq}+\dot{\tilde{\Psi}}_q-\partial_0(F\Psi_q) = 0 \tag{4.24}$$

$$\dot{\tilde{\delta}}_{Bq}-\frac{q^2}{a^2}\left(\delta\tilde{u}_{\gamma q}+F\delta u_{\gamma q}\right)+\dot{\tilde{\Psi}}_q-\partial_0(F\Psi_q) = 0 \tag{4.25}$$

$$\dot{\tilde{\delta}}_{\nu q}-\frac{q^2}{a^2}\left(\delta\tilde{u}_{\nu q}+F\delta u_{\nu q}\right)+\dot{\tilde{\Psi}}_q-\partial_0(F\Psi_q) = 0 \tag{4.26}$$

$$\frac{\tilde{\delta}_{\gamma q}}{3a}+\frac{d}{dt}\left(\frac{(1+R)\delta\tilde{u}_{\gamma q}}{a}\right)+2F\frac{d}{dt}\left(\frac{(R-\tilde{R})\delta u_{\gamma q}}{a}\right)-F\frac{d}{dt}\left(\frac{(1+R)\delta u_{\gamma q}}{a}\right)$$
$$-2\dot{F}(\tilde{R}-R)\frac{\delta u_{\gamma q}}{a} = 0 \tag{4.27}$$

$$\frac{\tilde{\delta}_{\nu q}}{3a}+\frac{d}{dt}\left(\frac{\delta\tilde{u}_{\nu q}}{a}\right)-F\frac{d}{dt}\left(\frac{\delta u_{\nu q}}{a}\right) = 0 \tag{4.28}$$

4.3.1 Matter era

In this era $a \gg C$ [6], and the perturbative equations for GR can be approximated and solved. These solutions are given by [7]

$$\delta_{Dq} = \frac{9q^2t^2\mathcal{R}_q\mathcal{T}(\kappa)}{10a^2}, \tag{4.29}$$

$$\dot{\Psi}_q = -\frac{3q^2t\mathcal{R}_q\mathcal{T}(\kappa)}{5a^2}, \tag{4.30}$$

$$\delta_{\gamma q} = \delta_{\nu q} = \frac{3\mathcal{R}_q}{5}\left[\mathcal{T}(\kappa) - \mathcal{S}(\kappa)\cos\left(q\int_0^t \frac{dt}{\sqrt{3}a} + \Delta(\kappa)\right)\right], \tag{4.31}$$

$$\delta u_{\gamma q} = \delta u_{\nu q} = \frac{3t\mathcal{R}_q}{5}\left[-\mathcal{T}(\kappa) + \mathcal{S}(\kappa)\frac{a}{\sqrt{3}qt}\sin\left(q\int_0^t \frac{dt}{\sqrt{3}a} + \Delta(\kappa)\right)\right], \tag{4.32}$$

where $\mathcal{T}(\kappa)$, $\mathcal{S}(\kappa)$ and $\Delta(\kappa)$ are functions that only depend on the following dimensionless value:

$$\kappa \equiv \frac{q\sqrt{2}}{a_{EQ}H_{EQ}}, \tag{4.33}$$

where a_{EQ} and H_{EQ} are, respectively, the Scale Factor and the expansion rate at the matter-radiation equality.[67].

To get all the Transfer functions, we have to compare solutions with the full equation system (with $\rho_B = \tilde{\rho}_B = 0$). To do this, we define $y \equiv a/a_{EQ} = a/C$ and use the following change of variable:

$$\frac{d}{dt} = \frac{H_{EQ}}{\sqrt{2}}\frac{\sqrt{1+y}}{y}\frac{d}{dy}. \tag{4.34}$$

Also, the following new variables are useful:

[6] and $R = \tilde{R} = 0$.

[7] $\mathcal{R}_q$ is defined as $q^2\mathcal{R}_q \equiv -a^2H\Psi_q + 4\pi Ga^2\delta\rho_q + q^2H\delta u_q$. It is a gauge invariant quantity, which take a time independent value for $q/a \ll H$. [67]

$$\delta_{Dq} = \kappa^2 \mathcal{R}_q^0 d(y)/4 \ , \quad \delta_{\gamma q} = \delta_{\nu q} = \kappa^2 \mathcal{R}_q^0 r(y)/4 \ ,$$
$$\dot{\Psi}_q = (\kappa^2 H_{EQ}/4\sqrt{2})\mathcal{R}_q^0 f(y) \ , \quad \delta u_{\gamma q} = \delta u_{\nu q} = (\kappa^2\sqrt{2}/4H_{EQ})\mathcal{R}_q^0 g(y) \ ,$$

and

$$\tilde{\delta}_{Dq} = \kappa^2 \mathcal{R}_q^0 \tilde{d}(y)/4 \ , \quad \tilde{\delta}_{\gamma q} = \tilde{\delta}_{\nu q} = \kappa^2 \mathcal{R}_q^0 \tilde{r}(y)/4$$
$$\dot{\tilde{\Psi}}_q = (\kappa^2 H_{EQ}/4\sqrt{2})\mathcal{R}_q^0 \tilde{f}(y) \ , \quad \delta \tilde{u}_{\gamma q} = \delta \tilde{u}_{\nu q} = (\kappa^2\sqrt{2}/4H_{EQ})\mathcal{R}_q^0 \tilde{g}(y) \ .$$

Then perturbative equations given in the matter era for GR and DG can be rewritten as

$$\sqrt{1+y}\frac{d}{dy}\left(y^2 f(y)\right) = -\frac{3}{2}d(y) - \frac{4r(y)}{y}, \tag{4.35}$$
$$\sqrt{1+y}\frac{d}{dy}r(y) - \frac{\kappa^2 g(y)}{y} = -yf(y), \tag{4.36}$$
$$\sqrt{1+y}\frac{d}{dy}d(y) = -yf(y), \tag{4.37}$$
$$\sqrt{1+y}\frac{d}{dy}\left(\frac{g(y)}{y}\right) = -\frac{r(y)}{3}\,, \tag{4.38}$$

and

$$-\left[(1+2y)yF'(y)+y(1+y)F''(y)\right]d(y)+\left[6F(y)+\frac{5}{2}yF'(y)\right]y\sqrt{1+y}f(y)$$
$$+3F(y)y^2\sqrt{1+y}f'(y)-\sqrt{1+y}\frac{d}{dy}\left(y^2\tilde{f}(y)\right)=\frac{3\tilde{d}(y)}{2}+\frac{4\tilde{r}(y)}{y}$$
$$-\frac{3F(y)d(y)}{4}-\frac{4F(y)r(y)}{y}, \tag{4.39}$$
$$\sqrt{1+y}\frac{d}{dy}\tilde{d}(y)=-y\tilde{f}(y)-\sqrt{1+y}\frac{d}{dy}d(y), \tag{4.40}$$
$$\sqrt{1+y}\frac{d}{dy}\tilde{r}(y)=\frac{\kappa^2}{y}[\tilde{g}(y)+F(y)g(y)]-y\tilde{f}(y)-\sqrt{1+y}\frac{d}{dy}d(y), \tag{4.41}$$
$$\sqrt{1+y}\frac{d}{dy}\left(\frac{\tilde{g}(y)}{y}\right)=-\frac{\tilde{r}(y)}{3}+\sqrt{1+y}F(y)\frac{d}{dy}\left(\frac{g(y)}{y}\right). \tag{4.42}$$

Now, we have to calculate the initial condition-behavior described by the radiation-dominated era (we have to approximate the original equations in this regime). In other words, at the beginning of the matter-dominated era, we have the following initial conditions

$$d(y)=r(y)\to y^2,$$
$$f(y)\to -2,$$
$$g(y)\to -\frac{y^4}{9},$$

$$\tilde{d}(y)=\tilde{r}(y)\to -\frac{L_2C^{3/2}}{3}y^3,$$
$$\tilde{f}(y)\to \sqrt{2}L_2C^{3/2}y,$$
$$\tilde{g}(y)\to \frac{L_2C^{3/2}}{2}y^5.$$

Now, we have to include the R and $\tilde{R}$ factors that were not considered as a part of the equations. This step was done with WKB approximation [67]. Also, we have to include the damping effect acting on the fluid of baryons and photons. This effect is known as the *Silk damping* and considers coefficients of shear viscosity, heat conduction, bulk viscosity, and

Thomson scattering associated with the fluid. [30, 60, 68]. Then the full solutions for the photon density perturbations are

$$\begin{aligned}\delta_{\gamma q} &= \frac{3\mathcal{R}_q^o}{5}\left[\mathcal{T}(\kappa)(1+3R)\right. \\ &\left. -(1+R)^{-1/4}e^{-\int_0^t \Gamma dt}\mathcal{S}(\kappa)\cos\left(\int_0^t \frac{qdt}{\sqrt{3(1+R(t))}a_{DG}(t)}+\Delta(\kappa)\right)\right], \quad (4.43)\\ \delta u_{\gamma q} &= \frac{3\mathcal{R}_q^o}{5}\left[-t\mathcal{T}(\kappa)\right. \\ &\left. +\frac{a_{DG}}{\sqrt{3}q(1+R)^{3/4}}e^{-\int_0^t \Gamma dt}\mathcal{S}(\kappa)\sin\left(\int_0^t \frac{qdt}{\sqrt{3(1+R(t))}a_{DG}(t)}+\Delta(\kappa)\right)\right] \quad (4.44)\end{aligned}$$

where

$$\Gamma = \frac{q^2 t_\gamma}{6a_{DG}^2(1+R)}\left[\frac{16}{15}+\frac{R^2}{1+R}\right]. \quad (4.45)$$

Note that at this level, we used $a \sim a_{DG}$ because these solutions are valid when DG approaches to GR. In particular, we will see that those solutions at the moment of the last scattering will play a crucial role when we compute the temperature multipole coefficients of the CMB.

4.3.2 The TT CMB spectrum in DG model

To calculate the TT CMB spectrum in the hydrodynamical approach, we have to express the temperature's perturbation as a function of the densities perturbations. This procedure is long and takes many pages. It is not the objective of this thesis to show the steps to obtain this result. However, it is vital to understand the physics behind the equations, the approximations, and the numerical contributions behind every term. First of all, we show four essential functions called Form Factors that are the contributions to calculate the TT CMB spectrum,

$$\mathcal{F}(q) = -\frac{1}{2}a_{DG}^2(t)\ddot{B}_q(t_{ls}) - \frac{1}{2}a_{DG}(t)\dot{a}_{DG}(t_{ls})\dot{B}_q(t_{ls}) + \frac{1}{2}E_q(t_{ls}) + \frac{\delta T_q(t_{ls})}{\bar{T}(t_{ls})}, \quad (4.46)$$

$$\tilde{\mathcal{F}}(q) = -\frac{1}{2}a_{DG}^2(t)\ddot{\tilde{B}}_q(t_{ls}) - \frac{1}{2}a_{DG}(t_{ls})\dot{a}_{DG}(t_{ls})\dot{\tilde{B}}_q(t_{ls}), \quad (4.47)$$

$$\mathcal{G}(q) = -q\left(\frac{1}{2}a_{DG}(t_{ls})\dot{B}_q(t_{ls}) + \frac{1}{(1+3F(t_{ls}))a_{DG}(t_{ls})}\delta u_\gamma(t_{ls})\right), \quad (4.48)$$

$$\tilde{\mathcal{G}}(q) = -q\left(\frac{1}{2}a_{DG}(t_{ls})\dot{\tilde{B}}_q(t_{ls}) + \frac{1}{(1+3F(t_{ls}))a_{DG}(t_{ls})}\delta\tilde{u}_\gamma(t_{ls})\right). \quad (4.49)$$

where the TT CMB spectrum is given by the Equation (4.72). These formulas will be very useful [8].

These Form Factors can be rearranged using many new definitions that introduce physics notation. Before doing that, it is important to define many physical terms.

Angular distance d_A^{DG} The Etherington's distance duality [23] is preserved in DG: the relation between luminosity distance and angular distance that is expressed as

$$d_A^{DG} = \frac{d_L^{DG}}{(1+z)^2}. \quad (4.50)$$

From this relation, it is possible to find the Angular Distance in DG.

Note: in DG the angular distance appears naturally as $d_A = r_{ls}a_{DG}(t_{ls})$. This equation is the same definition given here, evaluated at the Last Scattering surface. The Angular Distance is crucial to define the physical meaning of the next equations.

Horizon distance d_H^{DG} We have to consider the Effective Metric. This will produce the same integrand as the Equation 1.48 but substituting $a(t) \to Y_{DG}(Y)$. Note that Y^{DG} depends on $Y(t)$. We have to apply the chain rule and also change the integral limits to $\int_0^{Y(z)}$. Finally, the Horizon distance in DG is given by

[8] The B_q, $\tilde{B}_q$ and E_q are scalar perturbative terms that appears in the SVT decomposition. For more details please see the preprint in https://arxiv.org/abs/2001.08354

$$d_H^{DG}(z, L_2, C) = \frac{\sqrt{C}}{(1+z)100\sqrt{h^2\Omega_{r,0}}} \int_0^{Y(z)} c_s \frac{Y}{\sqrt{Y+C}} \frac{dY}{Y_{DG}}, \tag{4.51}$$

$$d_H^{DG}(z, L_2, C) = \frac{\sqrt{1+C}}{(1+z)100h} \int_0^{Y(z)} c_s \frac{Y}{\sqrt{Y+C}} \frac{dY}{Y_{DG}}. \tag{4.52}$$

Note 1: the speed of light c has been replaced by c_s, where the subscript s represents the sound. This change is introduced because we want to use this equation to calculate the acoustic horizon distance and not the light's horizon distance. This acoustic horizon is the maximum distance that a fluid with speed c_s has traveled between redshift $\in (\infty, z)$.

Note 2: Do not confuse C in terms of GR densities that are not physical with physical densities labeled with ^{DG} or $_{DG}$. For example, $h^2\Omega_{r,0}$ is not a physical density.

This term (in standard cosmology) is given by

$$c_s^2 = \frac{\delta p}{\delta \rho} = \frac{1}{\sqrt{3(1+R)}}, \tag{4.53}$$

where $R = \frac{4\rho_b}{3\rho_\gamma}$ in GR. We emphasize that Delta matter and Delta radiation could change this equation. In the simplest case, Delta particles do not affect the speed of sound of the fluid because we are assuming that Delta particles behave like dark matter particles: they are non-interacting particles. Neither dark matter appears in this equation nor the Delta particles.

In DG, we use the following definition:

$$R = \frac{4h^2\Omega_{b,0}^{DG}}{3h^2\Omega_{\gamma,0}^{DG}}. \tag{4.54}$$

Now, R is a function of real densities. We did not include Delta matter or Delta radiation.

The procedure to determine the value of this integral is the same as given in Section 1.48 for d_L^{DG} (note the integral limits).

Unfortunately, due to all the approximations we have used, we need to add one more correction to the GR sector's solutions. We considered a sharp transition from the moment

when the Universe was opaque to transparent. However, this was not instantaneous, yet it could be considered gaussian. This normal distribution implies an effect known as Landau damping[33], and it is related to the distribution's dispersion of a plasma's wavefront. This consideration is relevant, and it is related to the standard deviation of temperature at the Last Scattering moment (labeled as ls). With these considerations, the solutions of the perturbations are given by:

$$\dot{\Psi}_q(t_{ls}) = -\frac{3q^2 t_{ls}\mathcal{R}_q^o \mathcal{T}(\kappa)}{5a_{DG}^2(t_{ls})}\,, \tag{4.55}$$

$$\begin{aligned}\delta_{\gamma q}(t_{ls}) &= \frac{3\mathcal{R}_q^o}{5}\left[\mathcal{T}(\kappa)(1+3R_{ls}) - (1+R_{ls})^{-1/4} e^{-q^2 d_D^2/a_{DG}^2(t_{ls})}\right. \\ &\times \left.\mathcal{S}(\kappa)\cos\left(q\int_0^{t_{ls}} \frac{dt}{\sqrt{3(1+R(t))}a_{DG}(t)} + \Delta(\kappa)\right)\right]\,,\end{aligned} \tag{4.56}$$

$$\begin{aligned}\delta u_{\gamma q}(t_{ls}) &= \frac{3\mathcal{R}_q^o}{5}\left[-t_{ls}\mathcal{T}(\kappa) + \frac{a_{DG}(t_{ls})}{\sqrt{3}q(1+R_{ls})^{3/4}} e^{-q^2 d_D^2/a_{DG}^2(t_{ls})}\right. \\ &\times \left.\mathcal{S}(\kappa)\sin\left(q\int_0^{t_{ls}} \frac{dt}{\sqrt{3(1+R(t))}a_{DG}(t)} + \Delta(\kappa)\right)\right]\,,\end{aligned} \tag{4.57}$$

where

$$d_D^2 = d_{Silk}^2 + d_{Landau}^2\,, \tag{4.58}$$

$$d_{Silk}^2 = Y_{DG}^2(t_{ls})\int_0^{t_{ls}} \frac{t_\gamma}{6Y_{DG}^2(1+R)}\left\{\frac{16}{15} + \frac{R^2}{(1+R)}\right\} dt\,, \tag{4.59}$$

$$d_{Landau}^2 = \frac{\sigma_t^2}{6(1+R_{ls})}\,, \tag{4.60}$$

and t_γ is the mean free time for photons and $R = 3\bar{\rho}_B^{DG}/4\bar{\rho}_\gamma^{DG} = 3h^2\Omega_{b,0}^{DG}Y_{DG}/4h^2\Omega_{\gamma,0}^{DG}$.
In order to evaluate the Silk damping, we have

$$t_\gamma = \frac{1}{n_e\sigma_T c}, \tag{4.61}$$

where n_e is the number density of electrons, and σ_T is the Thomson cross-section.

On the other hand

$$\begin{aligned} q\int_0^{r_{ls}} c_s dr &= q\int_0^{t_{ls}} \frac{dt}{\sqrt{3(1+R(t))}a_{DG}(t)} \equiv q r_{ls}^{SH} \\ &= \frac{q}{a_{DG}(t_{ls})}\cdot(a_{DG}(t_{ls})r_{ls}^{SH}) = \frac{q}{a_{DG}(t_{ls})}\cdot d_H(t_{ls}) \end{aligned} \tag{4.62}$$

where c_s is the speed of sound, r_{ls}^{SH} is the sound horizon radial coordinate and d_H is the horizon distance, and $\kappa = q d_T^{DG}/a_{DG}(t_{ls})$ (defined in Equation (4.33)) implies

$$d_T^{DG}(t_{ls}) \equiv c\frac{\sqrt{2}a_{DG}(t_{ls})}{a_{EQ}H_{EQ}} = c\frac{a_{DG}(t_{ls})\sqrt{\Omega_R}}{H_0\Omega_M} = c\frac{a_{DG}(t_{ls})}{100h}\sqrt{C(C+1)}. \tag{4.63}$$

The final consideration that we must include is that when $z_{reion} \sim 10$ (reionization), the neutral hydrogen left over from the time of recombination becomes reionized by ultraviolet light from the first generation of massive stars [67, 47]. The photons of the cosmic microwave background have a small but nonnegligible probability $1 - exp(-\tau_{reion})$ (where τ_{reion} is the optical depth of the reionized plasma) of being scattered by the electrons set free by this reionization. The TT spectrum is a quadratic function of the the temperature fluctuations, then we have to weigh the spectrum by a factor $exp(-2\tau_{reion})$[9].

On the other hand, we will use a standard parametrization of $\mathcal{R}_q^0$ given by

$$|\mathcal{R}_q^0|^2 = N^2 q^{-3}\left(\frac{q/R_0}{\kappa_{\mathcal{R}}}\right)^{n_s-1}, \tag{4.64}$$

where n_s is the spectral index. It is usual to take $\kappa_{\mathcal{R}} = 0.05$ Mpc^{-1}.

We emphasize that $d_A^{DG}(t_{ls}) = r_{ls}a_{DG}(t_{ls})$ is the angular diameter distance of the last scattering surface, because

[9] In the standard GR case, the observations from polarization spectrum suggests that $exp(-2\tau_{reion}) \approx 0.8$. We use this value to fit the spectrum. We did not study the reionization process and we did not develop the polarization spectrum.

$$d_A^{DG}(t_{ls}) = ca_{DG}(t_{ls})\int_{t_{ls}}^{t_0}\frac{dt'}{a_{DG}(t')} = c\frac{a_{DG}(t_0)}{1+z_{ls}}\int_{t_{ls}}^{t_0}\frac{dt'}{a_{DG}(t')} = c\frac{1}{1+z_{ls}}\int_{t_{ls}}^{t_0}\frac{dt'}{Y_{DG}(t')} \quad (4.65)$$

$$= c\frac{1}{1+z_{ls}}\int_{Y_{ls}}^{1}\frac{dY'}{Y_{DG}(Y')}\frac{dt}{dY'} = \frac{d_L^{DG}(t_{ls})}{(1+z_{ls})^2}. \quad (4.66)$$

This is consistent with the luminosity distance definition given in the Equation (1.48). Then, if we use $q = \beta l/r_{ls}$ we obtain

$$|\mathcal{R}^0_{\beta l/r_{ls}}|^2 = N^2\left(\frac{\beta l}{r_{ls}}\right)^{-3}\left(\frac{\beta l}{\kappa_{\mathcal{R}} r_{ls}}\right)^{n_s-1} = N^2\left(\frac{\beta l}{r_{ls}}\right)^{-3}\left(\frac{\beta l a_{DG}(t_{ls})}{\kappa_{\mathcal{R}} r_{ls} a_{DG}(t_{ls})}\right)^{n_s-1} \quad (4.67)$$

$$= N^2\left(\frac{\beta l}{r_{ls}}\right)^{-3}\left(\frac{\beta l a_{DG}(t_{ls})}{\kappa_{\mathcal{R}} d_A(t_{ls})}\right)^{n_s-1} \equiv N^2\left(\frac{\beta l}{r_{ls}}\right)^{-3}\left(\frac{\beta l}{l_R}\right)^{n_s-1}. \quad (4.68)$$

Using similar calculations for the other distances, the final form of the Form Factors are given by

$$\mathcal{F}(q) = \frac{\mathcal{R}_q^o}{5}\left[3\mathcal{T}(\beta l/l_T)R_{ls} - (1+R_{ls})^{-1/4}e^{-\beta^2 l^2/l_D^2}\mathcal{S}(\beta l/l_T)\cos\left(\beta l/l_H + \Delta(\beta l/l_T)\right)\right] \quad (4.69)$$

$$\mathcal{G}(q) = \frac{\sqrt{3}\mathcal{R}_q^o}{5(1+R_{ls})^{3/4}}e^{-\beta^2 l^2/l_D^2}\mathcal{S}(\beta l/l_T)\sin\left(\beta l/l_H + \Delta(\beta l/l_T)\right), \quad (4.70)$$

where

$$l_R = \frac{\kappa_{\mathcal{R}} d_A^{DG}(t_{ls})}{a_{DG}(t_{ls})}, \quad l_H = \frac{d_A^{DG}(t_{ls})}{d_H^{DG}(t_{ls})}, \quad l_T = \frac{d_A^{DG}(t_{ls})}{d_T^{DG}(t_{ls})}, \quad l_D = \frac{d_A^{DG}(t_{ls})}{d_D^{DG}(t_{ls})}. \quad (4.71)$$

To summarize, for reasonably large values of l, CMB multipoles are given by

$$\frac{l(l+1)C_{TT,l}^S}{2\pi} = \frac{4\pi T_0^2 l^3\exp(-2\tau_{reion})}{r_{ls}^3}\int_1^\infty\frac{\beta d\beta}{\sqrt{\beta^2-1}}$$
$$\times\left[\left(F\left(\frac{l\beta}{r_{ls}}\right)+\tilde{F}\left(\frac{l\beta}{r_{ls}}\right)\right)^2 + \frac{\beta^2-1}{\beta^2}\left(G\left(\frac{l\beta}{r_{ls}}\right)+\tilde{G}\left(\frac{l\beta}{r_{ls}}\right)\right)^2\right] \quad (4.72)$$

We emphasize that the structure of the Equation (4.72) considers that the Delta sector contributes additively inside the integral. If we set all Delta sector equal to zero, we recover the result for the scalar temperature-temperature multipole coefficients in GR given by Weinberg [67]. One of the purposes of this Thesis is to calculate the scalar TT CMB spectrum using the DG model. Thus, the Equation (4.72) is the main expression to implement the numerical analysis.

Finally, from SNe-Ia fit, we know that $C \ll 1$ and $L \approx 0.457$ [7][14], therefore we can estimate that Delta matter perturbation at the beginning of the Universe was much smaller than the Common matter fluctuation.[10] For example, at $y \sim 10^{-3}$ the ratio between components of the Universe is $|\tilde{\delta}_\alpha/\delta_\alpha| \sim 10^{-10}$. This does not mean that the intuitive fractional perturbation of Delta matter $\tilde{\delta}^{int}_{\alpha q} = \delta\tilde{\rho}_\alpha/(\tilde{\bar{\rho}}_\alpha + \tilde{\bar{p}})$ was much lower than the standard perturbations δ_α because $\tilde{\delta}_{\alpha q}(t) \propto (\tilde{\delta}^{int}_{\alpha q} - \delta_{\alpha q})$, implying that $\tilde{\delta}^{int}_{\alpha q} \sim \delta_{\alpha q}$.

4.4 DG contribution to the CMB spectrum

The DG contribution appears in many different forms in the Equation (4.72). The most notorious contribution is given by the functions $\tilde{F}$ and $\tilde{G}$. These functions are given by the functions f, r, d, g and $\tilde{f}, \tilde{r}, \tilde{d}, \tilde{g}$ through the Equations (4.35) - (4.38), and (4.39) - (4.42). They are related to the evolution of the perturbation, and all these functions are coupled with the GR solutions.

The standard way to solve this problem is to obtain an analytical solution for the approximated equations, like the equations given by the Transfer Functions given by the Equations (4.29) - (4.31), and then, solve the equations, for every κ (for example, from 0 to 100), thus match both results numerically, and solve for T, S and Δ as a function of κ.

It is crucial to understand that, at this moment, the solutions are approximations in the matter-dominated era, and they are independent of R and $\tilde{R}$. It is essential Then, if we apply this same methodology to the DG equations, we would include all the posterior effects produced by dampings and WKB effects (when the radiation and matter regime must match).

[10] See https://arxiv.org/abs/2001.08354.

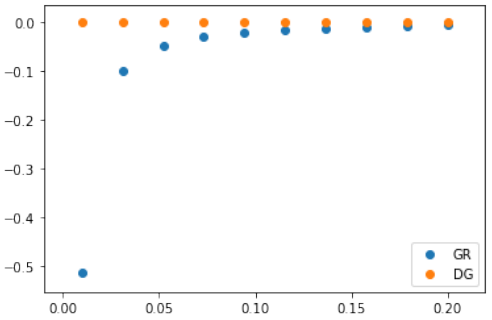

Figure 4.1: F.

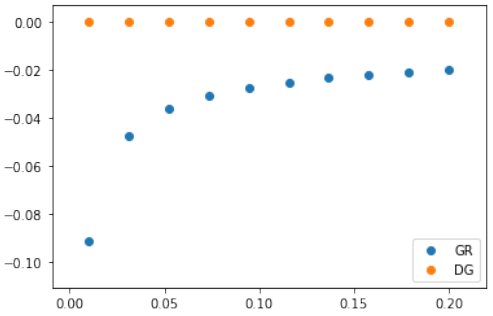

Figure 4.2: G.

Figure 4.3: Form Factors.

Besides, these equations evolve the perturbations given by the f, r, d, g and $\tilde{f}, \tilde{r}, \tilde{d}, \tilde{g}$ functions, and then they must be evaluated inside the matter regime. They start to evolve inside the matter-era but,very close the radiation era. This parametrization is given by $y = a/a_{EQ}$. The solutions were obtained starting from $y < 10^{-4}$ and stopping at $y \approx 10^2$. If the solutions are evaluated after the equality time, they could change, but, they are stable after $y \approx 10^2$.

The TT CMB spectrum needs these solutions because they build the Form Factors, and they are evaluated in an arbitrary κ that is related to β and l through the Equation (4.72).

First, we found the results for the numerical solutions of f, r, d, g and $\tilde{f}, \tilde{r}, \tilde{d}, \tilde{g}$, and then solve the expressions T, S and Δ. Then we calculate the Delta perturbations, and finally we obtain the Delta Form Factors. The Figure 4.3 shows the Delta Factors. They are tiny compared to the standard cosmological contributions given by F and G.

Numerically, the Delta contribution is $\approx 10^{39}$ times smaller than the Common Form Factor.

This result is crucial for the next steps. First of all, we can neglect those Delta terms, allowing us to forget about the posterior corrections that the hydrodynamic approach has.

For example, the dampings corrections and the WKB match never must be applied because the Delta part is neglected. Nevertheless, also, this creates more constraint over the DG model. This implies that any additional term, like a new damping term, cannot be applied to compensate a lousy fitting of the DG model. This constraint is essential.

Note: this allows us to avoid a damping definition for the Delta densities. We do not require that, and even more, it has no physical consequence in the physical observables.

However, the DG contribution appears in other exciting ways. The next stage is going to be divided in three parts. The first is about the l_i factors, the physics behind them, and the dependencies with physical processes. This is the biggest constraint that DG has. The second part is about the algorithm to include all the physical effects and the equations to obtain the TT CMB spectrum. The third and final part is about the results.

4.5 l_i coefficients

Here we analyze the l_i coefficients showed in the Equation (4.71). These are degrees of freedom that DG has to fit in order to find the TT CMB spectrum. These values are the arguments for the Form Factors $\mathcal{F}$ and $\mathcal{G}$.

Note 1: There are more free parameters, indicated at the beginning of the Equation (4.72) as a fraction in front of the integral.

Note 2: The full code is extensive. Then, I decided to include some essential parts of the code to understand the way that the TT CMB spectrum was fitted.

4.5.1 l_R

This coefficient depends on the angular distance and the DG Scale Factor a_{DG} evaluated at the Last Scattering time. This term is associated with the $\mathcal{F}$ and $\mathcal{G}$ functions and depends on n_s, the spectral index of the primordial spectrum. In the case where the contribution to the Delta Form Factors is ~ 0, then the coefficient given by the Equation (4.68) appears as a number powered to $n_s - 1$. This factor appears in the Equation (4.72) in front of the integral and regulates all the spectrum amplitude. In the case of $n_s \to 1$, these terms go to

0, and the l_R coefficient tends to be very unstable (for instance: if $n_s - 1 = 10^{-4}$, l_R has to compensate the small value of this exponent. This numerical part could take time because the initial guess must be close the correct value; in other cases could take too much time and could never converge). However, we decided to assume an arbitrary n_s to include the l_R coefficient. This assumption is important because, at first glance, these parameters appear to be correlated: N, n_s and l_R. This idea is incorrect because the l_R value depends on the Last Scattering moment, defined by z_{ls}, and this redshift appears in many other places of the Equation (4.72). If z_{ls} is not arbitrary, then the coefficient (4.68) is unique, and then N^2 have to compensate for the scale of the spectrum to fit the observable data.

In terms of the code, this part is defined as:

```
def factor1(beta,l,lR,ns):
    return np.power((beta*l/lR),ns-1)
```

Listing 4.1: factor1 depends on l_R and n_s.

The l_R function has been implemented in the code as

```
def lR(params):

    z,C = params[0],params[1]

    kappaR = 0.05
    Y  = float(Y_solve(z,C,Lfit))
    dA = da_DG(Y,C)

    return kappaR*dA/R_DG(Y,C,Lfit)
```

Listing 4.2: lR function depends on z and C. L_2 has been used as an established value. the dA function is the angular distance in DG: d_A^{DG}, and the R_DG function is the DG Scale Factor a_{DG}.

4.5.2 l_H

In [67], this parameter is defined as in the Equation (4.71), where the most known notation is $\theta = 1/l_H$. If we want to preserve the CMB TT spectrum, we must use a value close the

standard θ, but not strictly the same. In this context, it is essential to remember that in the SNe-Ia analysis, we worked with $C = 0$. This implies that there is no radiation and it is contradictory to the CMB procedure. Nonetheless, the SNe-Ia analysis is compatible with C small values. Then, we can try to fit the TT CMB spectrum assuming a small C value, where $M \approx -19.3$ and the H_0 local value is preserved. We are going to work only in this scenario. Then, the CMB fit assumes a fixed L_2 value from SNe-Ia (we do not want to change this value) and a C value close 0. After this process, we have to check that the C value found by this method is compatible with the SNe-Ia data.

The most notorious constraint from the CMB spectrum is the acoustic peak position. This parameter determines the TT CMB spectrum (in the l scale) and fits the hydrodynamic approach to the l-axis. Also, another important property of θ is that is obtained directly from the CMB spectrum. It's not a derived parameter [4]:

$$100\theta_{Planck} = 1.0411 \pm 0.0003. \tag{4.73}$$

This value almost always appears in the literature as θ_{MC}, where it was obtained by fitting the CMB data. However, in this work we calculate $l_H = 1/\theta$ as a function of d_H and d_A. In our case, θ is not constraining the peak position by itself, we are constraining the z_{ls}, C, and $h^2\Omega_{b,0}$ values.

This physical meaning of this parameter is: the angle that subtends the size of fluctuation respect to the distance to this fluctuation. d_H is the horizon distance (size of the Universe at a specific redshift given by when the photons were decoupled). d_A is the angular distance between us and the TT CMB fluctuation. This relation must be corrected changing the speed of light c by c_s (the speed of sound) because it is the growing fluctuation speed. [48, 49]. The correction has been introduced in Equations (4.54) and (4.52).

The Fourier modes give an easy way to understand the dependence between θ and l. For simplicity, in a flat Universe, the modes of wavelength $\lambda \sim 2\pi a(t_{ls})/k$ on the Last Scattering surface seen today under an angle $\theta = \lambda/d_A(t_{ls}) \sim 2\pi/l$ (the factor 2 appears because for a given multipole, π/l gives the angle between a maximum and a minimum. This is half of the wavelength of the perturbation on the surface). [34, p. 228] This position of the peak is very well determined; then, this parameter is very well constrained. This condition imposes

constraints over C or z_{ls} or c_s (the speed of sound in a specific period: from $z = \infty$ to z_{ls}). In this analysis L_2 is fixed, and is independent of any other value that we are changing.

From the Equation (4.53) and knowing the R value, we can obtain the $d_H(z)$ value in order to calculate θ. As we have seen, R is the baryons-photons relation. This factor considers particles that interact with the fluid, and then, the physical phenomena are described as sound waves. We can change this parameter if we suppose that more components interact in the fluid. But, we assume only the case where the photon-baryon relation determines the horizon distance.

Note: the R relation to calculate the speed of sound, is determined with $h^2\Omega_{b,0}^{DG}$ and $h^2\Omega_{\gamma,0}^{DG}$ values. This is essential because these parameters are physical and not apparent magnitudes. First of all, they depend on Y_{DG} and not directly on Y. Second, they are physical magnitudes, they represent the real density of energy per volume, and then the interactions determine a real speed of sound. This is the reason because we use these parameters. In any other case, the speed of sound (based in ρ_i) is not physical, therefore, it does not represent the speed of a wave sound.

The CMB radiation gives physical density of photons: the blackbody spectrum has associated the T_0 temperature, where the real density is described as $\rho_{r,0} \propto T_0^4$ (Stefan-Boltzmann law). We know that the real physical densities in DG evolve with Y_{DG}, then it is easy to evolve any physical parameter as a function of Y_{DG}[11].

Finally, the l_H parameter is a function of z_{ls}, C and $h^2\Omega_{b,0}^{DG}$.

```
1
2  def theta_DG(C,z,h2Ob):
3
4      Y = float(Y_solve(z,C,Lfit))
5
6      num = dH_DG(Y,C,h2Ob)
7
8      den = da_DG(Y,C)
9
10     return num/den
11
```

[11]Note: the parameters $h^2\Omega_{i,0}$ does not depend on H or any other cosmological parameters. They are pure physical densities because of the critical density definition.

```
12 def lH(params):
13
14     z,C,h2Ob = params[0],params[1],params[2]
15
16     return 1/theta_DG(C,z,h2Ob)
```

Listing 4.3: lH function depends on z_{ls}, C and $h^2\Omega_{b,0}^{DG}$. The calculation requires to call the angular distance and the horizon distance as da_DG and dH_DG, respectively.

The l_H parameter is like a kind of frequency-argument of the cos and sin functions in Equations (4.69) and (4.70).

4.5.3 l_T

The l_T parameters appear also inside of cos and sin functions in Equations (4.69) and (4.70). Nevertheless, they move the cos and sin on the horizontal axis through the Δ Transfer Function. They also appear outside the sinusoidal solutions, regulating the amplitude of these oscillations. The role of these parameters is to convert the arguments of the Transfer functions into the correct units. The origin of this normalization comes from Equations (4.33) and (4.63). Those definitions are important because it implies that $d_T \propto a_{DG}(t_{ls})$, where z_{ls} determines the DG Scale Factor at the moment of the Last Scattering. This normalization of the wave-number appears until this step of the numerical evaluation.

```
1
2 def lT(params):
3
4     z,C = params[0],params[1]
5
6     Y  = float(Y_solve(z,C,Lfit))
7
8     dT = np.divide(c*R_DG(Y,C,Lfit),100*hfit)*np.sqrt(C*(C+1))
9
10    dA = da_DG(Y,C)
11
12    return dA/dT
```

Listing 4.4: lT function depends on z_{ls} and C.

To evaluate this function, first the program solves Y as function of z_{ls}, and then evaluates $a_{DG}(t_{ls})$. Finally, it returns d_A^{DG}/d_T^{DG} for that particular combination of z_{ls} and C. Remember that l_T parameter modulates the position and the amplitude of the sin and cos functions. Thus it is not trivial to know if this parameter is degenerated with another. Also, this is the only parameter that appears as an argument for the Transfer functions. Then, the result depends on the numerical solution of the Transfer functions. The $\mathcal{T}, \mathcal{S}$ and Δ functions, can be solved numerically from the differential equations given by Equations (4.35) - (4.38) and the $\mathcal{T}, \mathcal{S}$ and Δ definitions.

```
1
2  def equations(p,*data):
3
4      T,S,D= p
5      k,y_stop = data
6
7      return (T-5*dk(k)/(8*y_stop),\
8      T-S*np.cos(2*k*(np.sqrt(1+y_stop)-1)/np.sqrt(3)+D)-5*k**2*rk(k)/12,\
9      -T+S*np.sqrt(3)*np.sin(2*k*(np.sqrt(1+y_stop)-1)/np.sqrt(3)+D)\
10     /(2*k*np.sqrt(y_stop))-5*k**2*gk(k)/(8*y_stop**(3/2)))
11
12 T_k = []
13 S_k = []
14 D_k = []
15
16 for i in tqdm(x):
17
18     data = (i,y_stop)
19
20     sol1,sol2,sol3 =  fsolve(equations, (0.01,2,0.003),args=data,xtol=0.00000001)
21
22     T_k.append(sol1)
23     S_k.append(sol2)
24     D_k.append(sol3)
```

Listing 4.5: $\mathcal{T}, \mathcal{S}$ and Δ definitions as functions of , r, d and g. k is the wavenumber, $y\_stop \approx 100$ and corresponds to evaluate the functions inside the matter-dominated era. The equations are solved for every k number, and then we obtain the Transfer functions depending on k.

These solutions can be fitted by a very useful analytical approximation given by [67]:

```
def Tk(k):

    return np.log(1+(0.124*k)**2)/(0.124*k)**2*\
    np.sqrt((1+(1.257*k)**2+(0.4452*k)**4+(0.2197*k)**6)\
    /(1+(1.606*k)**2+(0.8568*k)**4+(0.3927*k)**6))

def Sk(k):

    return ((1+(1.209*k)**2+(0.5116*k)**4+np.sqrt(5)*(0.1657*k)**6)/\
    (1+(0.9459*k)**2+(0.4249*k)**4+(0.1657*k)**6))**2

def Dk(k):

    return np.power(((0.1585*k)**2+(0.9702*k)**4+(0.2460*k)**6)/\
    (1+(1.180*k)**2+(1.540*k)**4+(0.9230*k)**6+(0.4197*k)**8),1/4)
```

Listing 4.6: $\mathcal{T}, \mathcal{S}$ and Δ definitions as functions of $, r, d$ and g. k is the wavenumber, $y\_stop \approx 100$ and corresponds to evaluate the functions inside the matter-dominated era. The equations are solved for every k number, and then we obtain the Transfer functions depending on k.

Finally, with the numerical approximations for every Transfer function, and evaluating them with the solution of l_T as a function of z_{ls} and C, it is possible to obtain the third step to evaluate the TT CMB spectrum.

4.5.4 l_D

Finally, the fourth parameter is incredibly difficult because it includes many steps that are physical and numerical (specific routines) processes.

Note: This explanation continues in the next section because it is related to the MCMC method. Here we explain the physical approaches to obtain the dampings, the functions needed, and the relation with the MCMC algorithm.

The l_D parameter appears as a result of the physical damping of the oscillations, which is related to both processes: Silk and Landau dampings. These effects only appear next to every cos and sin function in the Equation (4.72) as an exponential. The TT CMB spectrum is very sensitive to this value because it changes the whole spectrum's amplitude.

First, the Silk damping is described by a special-relativistic non-perfect fluid. This approximation implies damping. The cosmology part appears when the damping effect acts on a range of time, and the effect must be integrated and corrected by the expanding Universe. The expression that describes the Silk damping is the Equation (4.59), where the cosmological correction appears with Y_{DG}. This term appears inside and outside the integral. Take a look for a moment at this equation.

The instantaneous Silk damping, only appears like a damping length, where there is no integration and without the Y_{DG} term. This term is a length (multiply it by c to take length units). Each t variable must be scaled with c and then, d^2_{Silk} appears like a squared variable. This term is normalized instantaneously by the squared Scale Factor, and then it is evaluated when we want to know the Silk effect. This procedure is the same that GR uses, but where the scale factor is $a(t)$ instead of $Y_{DG}(t)$. This notation is useful to parametrize everything in terms of Y_{DG}. Also, it is important that Y_{DG} depends on C, L_2 and Y. L_2 is fixed, but C and Y are variables, and they have to be evaluated as z_{ls} changes.

Second, the calculation of Landau damping is challenging. Despite the Equation (4.60) is very short, its intrinsic relation with the dispersion of the temperature creates many calculations. σ_T is the standard deviation of the temperature at the Last Scattering moment when the transparency is a normal distribution function centered around the z_{ls}. This is a good approximation, but it requires many calculations provided by interactions related to the free electrons and photons. In terms of the dispersion,

$$\sigma_t = \frac{\sigma_T}{TH_{DG}}, \tag{4.74}$$

because,

$$\sigma_t dt = \sigma_T dT \rightarrow \frac{dt}{dT} = \frac{dt}{dY}\frac{dY}{dY_{DG}}\frac{dY_{DG}}{dT} \rightarrow \frac{dt}{dT} = \frac{1}{H_{DG}T}$$

With this transformation, we can express the time-dispersion in terms of temperature.

To obtain the dispersion, first, we have to find the visibility function in DG, and before that, we have to define the Opacity function. This function is described in by [67, 125p.] and it is defined as follows

$$\mathcal{O}(T) = 1 - exp\left(-\int_{t(T)}^{t_0} c\sigma_{\text{Thomson}} n_e(t) dt\right). \tag{4.75}$$

This describes the probability[12] that a photon present at a time $t(T)$ when the temperature is T will undergo at least one more scattering before the present. The exponent is related to the number of collisions; therefore, it is related to physical densities. In other words, the amount of electrons that describes a scattering process is related to the physical quantity of particles in a real volume in the DG context. We can integrate this equation changing the variable from t to T, but the time t depends on Y (and not Y_{DG}). However, the physical densities depends on Y_{DG}.

Another essential physical definition is the Visibility Function. The probability that the last scattering of a photon was before the temperature dropped to T is $1 - O(T)$, and the probability that the last scattering was after the temperature dropped further to $T - dT$ is $O(T - dT)$, then the probability that the last scattering of a photon was at a temperature between T and $T - dT$ is $1 - (1 - O(T)) - O(T - dT) = O'(T)dT$. Finally, the function $O(T)$ increases monotonically with temperature from $O = 0$ at $T = T_0$ because $O \to 1$ for $T \to \infty$. Therefore, $O'(T)$ behaves like a probability distribution. We try to fit a Normal distribution and obtain an estimation of σ_T using the Visibility function.

$$\mathcal{O}'_{fit}(T) \approx \frac{1}{\sigma_T\sqrt{2\pi}} e^{-\frac{(T-T_L)^2}{2\sigma_T^2}}. \tag{4.76}$$

There is another option to calculate the σ_T. It consist in evaluate the maximum of the distribution, where the $O'(T_{max}) \approx \frac{1}{\sigma_T\sqrt{2\pi}}$. This method is faster than the fitting algorithm. Then we decide to use it.

To calculate the Opacity function, we have to know the physical electron density at that epoch. This is strictly related to the H,e^-, and p abundances at that moment. These values can be easily correlated using an equation that describes the formation of the H. There are many methods to do this calculation. The most naive approximation is assuming an equilibrium through the Saha Equation. The equilibrium involves only atomic parameters, and it does not depend on cosmological parameters. Then, any assumption and equation in this calculation is preserved in DG. We emphasize that the evolution is given in terms of T.

[12] This definition is extracted from [67].

Furthermore, the relation between T and z in DG is the same as in GR. Then, this procedure is totally preserved. In order to clarify any doubt, we are going to show the general scheme.

The naive approximation [67, p. 113] begins at a time early enough so that protons, electrons, hydrogen, and helium atoms were in thermal equilibrium at the radiation's temperature. Then, the number density of any non-relativistic non-degenerate particle of type i is given by the Maxwell-Boltzmann distribution:

$$n_i = \frac{g_i}{(2\pi\hbar)^3} e^{\frac{\mu_i}{k_B T}} \int d^3q e^{-\frac{\left(m_i + \frac{q^2}{2m_i}\right)}{k_B T}} \tag{4.77}$$

where m_i is the particle mass, g_i is the number of its spin states, and μ_i is the chemical potential of particles of type i. $g_p = g_e = 2$ while the 1s ground state of the H has two hyperfine states with spins 0 and 1, so $g_{1s} = 1 + 3 = 4$. The most dominant reaction is given by $p + e \rightleftarrows H_{1s}$. The equilibrium is described by

$$\mu_p + \mu_e \rightleftarrows \mu_{1s}. \tag{4.78}$$

Then, the relation between the density numbers is described by

$$\frac{n_{1s}}{n_p n_e} = \left(\frac{m_e k_B T}{2\pi\hbar^2}\right)^{-3/2} e^{\frac{B_1}{k_B T}}, \tag{4.79}$$

where $B_1 \equiv m_p + m_e - m_H = 13.6$ eV is the binding energy of the 1s ground state of the hydrogen. Now, including that $n_e = n_p$ because the Universe has to be neutral, and also consider that 76% of the baryons were neutral or ionized hydrogen: $n_p + n_{1s} = 0.76 n_B$ [67, 114], we can define the fractional hydrogen ionization as $X \equiv n_p/(n_p + n_{1s})$, where the Saha equation is satisfied as:

$$X(1 + SX) = 1. \tag{4.80}$$

Finally, S can be expressed as

$$S = \frac{(n_p + n_{1s}) n_{1s}}{n_p^2} = 0.76 n_B \left(\frac{m_e k_B T}{2\pi\hbar^2}\right)^{-3/2} e^{B_1/k_B T}. \tag{4.81}$$

Note that S can be expressed in terms of T and $h^2\Omega_{b,0}^{DG}$ as

$$S = 1.747 \times 10^{-22} e^{157894/T} T^{3/2} h^2 \Omega_{b,0}^{DG}. \tag{4.82}$$

This dependence is significant for DG. First of all, the evolution is in terms of T and not cosmic time, and also, the fraction S depends on the baryon density parameter $h^2\Omega_{b,0}^{DG}$, then it will appear as a free parameter in the TT CMB spectrum. In DG, as we have said, the effect of Delta fields does not affect the spectrum (they are minimal). Only the evolution in time, represented by distances, can be affected by DG.

To improve the calculation, it is possible to add more corrections, including the $2p$ and $2s$ levels of the H atom. The full discussion about the decay and the emission processes can be found in [67, 116].

The differential equation that describes this process with all those corrections is given by

$$\frac{dX}{dT} = \frac{\alpha n}{H^{DG} T} \left(1 + \frac{\beta}{\Gamma_{2s} + \frac{8\pi H^{DG}}{\lambda_\alpha^3 n(1-X)}} \right)^{-1} \left(X^2 - \frac{1-X}{S} \right), \tag{4.83}$$

where $\alpha = \alpha(T)$, $\beta = \beta(T)$, $n = n(h^2\Omega_{b,0}^{DG}, T)$, $H^{DG} = H^{DG}(C, L_2, Y(T))$ are functions related to the transitions of the H and λ_α is the wavelength of Lyman α photons [13]. This equation depends on the Hubble parameter: H^{DG}. This is important because in the derivation of this equation, H^{DG} appears in two different places: the first term $1/TH^{DG}$ is a coefficient that comes from changing t to T (to evolve the equations in temperature instead of time) and the second term (where H^{DG} appears as $8\pi H^{DG}$) comes from the change of the frequency (or wavelength) produced by the cosmic expansion. Therefore, both of those corrections appear in DG as H^{DG} and not like the standard H (then, this equation looks similar, but it is different because the dependence between the variables is totally different) [67, p. 122].

In DG, this effect could be crucial because the evolution could change due to that the Hubble parameter is a function of the Effective Scale Factor Y^{DG}, and this is a function of $Y(t)$. Furthermore, the T preserves the standard dependence with the Effective Scale Factor Y^{DG}, in other words, in standard cosmology, we have $T = T_0(1+z)$ and this relation is preserved in DG, but the dependence between z in DG appears related to $a_{DG}(Y(t))$. Furthermore, the

[13] For more details see [67].

numerical solution with all these corrections changes the Saha approximation, and then also changes the GR solution. It is also essential to note that the differential equations are evolved in a high range of T, and DG tends to be very similar to the standard GR at the beginning. The Scale Factor tends to be the same because the Delta field contributions disappear when $Y \to 0$. Nevertheless, all these aspects must be taken into account to compute $X(T)$ in order to obtain an excellent numerical value to fix z_{ls} and n_e affecting the Visibility function: the peak position in redshift (z_{ls}) and the standard deviation (σ_T).

It is essential to highlight that the Visibility function appears two times in the code. First, these equations are useful to calculate the Landau damping, and second, they are also used to estimate the z_{ls} in the MCMC algorithm.

We show some crucial definitions related to these functions:

```
def S(T,h2Ob):

    return 1.747*10**(-22)*np.exp(157894/T)*T**(3/2)*h2Ob

def model(X,T,h2Ob,C):

    Y = Y_don_T(T,C)

    Coef = 1 + beta(T)/(Gamma_2s + ( 8*np.pi*H_DG(Y,C) ) \
    /( Lambda_alpha**3*n(T,h2Ob)*(1-X) ) )

    N = alpha(T)*n(T,h2Ob)/(T*H_DG(Y,C))

    dXdt = N*Coef**(-1)*(X**2-(1-X)/S(T,h2Ob))

    return dXdt

def equilibrium(X,T,h2Ob):

    return X*(1+S(T,h2Ob)*X)-1

def solve_ode_DG(C,h2Ob):

    X0 = X_solver(6000,h2Ob)

    if h2Ob < 0:
```

```
27
28          return np.full([len(temp)],np.nan)
29
30      else:
31
32          return odeint(model,X0,temp,args=(h2Ob,C),rtol=0.0000001)
```

Listing 4.7: These equations correspond to the DG modified equations to obtain the $X(T)$ fraction. The function "S" and "equilibrium" correspond to the Saha Solution, while the model and solve_ode_DG functions calculate the $X(T)$ fraction with all the modifications: including the DG effects and the two levels correction (for the H atom). Note: h2Ob represents a physical density in the code.

The $\alpha(T)$ and $\beta(T)$ are numerical functions of T [44]. They are exact, and there is no cosmological influence here, then it does not affect the DG calculations.

Finally, the Visibility function is calculated in a function called calc_vis_fun, which takes as arguments: C and $h^2\Omega_{b,0}^{DG}$. This function returns an array with the $O'(T)$ values at different T. We omit the code for this function because it is too long. All the code is attached in the Appendix F and G. This function is essential to find the z_{ls}: due to this, the Visibility function also appears in the following Section.

4.5.5 Tables

To compute all the l_i coefficient, we have to use all the equations described in the previous subsection. All the equations depend on only 3 parameters $C, h^2\Omega_{b,0}^{DG}, z_{ls}$, and 2 extra parameters that are n_s and N. There are differences between both kinds of parameters. The former type is used to calculate the l_i parameter, these calculations are hard because they use many equations, but the last two parameters are used straightforwardly. They are only needed to evaluate the TT CMB spectrum multiplying all the Form Factors by a simple fraction given by a function called factor1 in the code.

The procedure is the following; first, we calculate tables of the l_i coefficients that depend on $C, h^2\Omega_{b,0}^{DG}$, and z_{ls}, and then, we can interpolate the l_i coefficients with these values. We created the following arrays:

```
1 array_z = np.linspace(900,1200,50)
```

```
array_C = np.linspace(0.0001,0.0009,60)
array_h2Ob = np.linspace(0.01,0.04,100)
```

Listing 4.8: Arrays created to calculate the l_i tables.

then, we calculate all the l_i coefficient for all the previous combinations. The range of values was estimated after many attempts, polishing the mesh and the interpolation ranges.

4.6 Algorithm to obtain the CMB

The MCMC algorithm consists of a modified Adaptative Metropolis MCMC algorithm.

We explain briefly what it is. An MCMC is a method that uses Markov chains to sample from a probability distribution. A Markov chain is a chain of random values, where the next step always depends on the previous value. Each value is linked to the next value through an algorithm creating a chain. In a Metropolis algorithm, the prior or proposal distribution depends on the previous distribution of values. This algorithm is useful to find what value is better to describe a sample. The Monte Carlo algorithm adds some randomness to explore different values, where these values always depend on the previous probability distribution of values.

The more steps that are included, the more closely the sample's distribution matches the actual desired distribution.

Note: the predicted TT CMB spectrum requires interpolating the spectrum to find the best combination of parameters that fit the Planck satellite's data [14]. Due to this, the tables must be dense to create smooth interpolations, where the MCMC can estimate suitable parameters. This MCMC uses the tables generated by the code described in the previous subsection.

In our case, we want to find all the possible values that match, in the best way, the TT CMB spectrum. The algorithm works as follows: we propose an original distribution of values, called priors: $C, h^2\Omega_{b,0}^{DG}, z_{ls}, n_s$ and N. All the priors are normally distributed. We calculate the predicted TT CMB spectrum and comparing with the TT CMB spectrum from [49]; we calculate the squared error. Then we pick a random parameter based on each probability

[14] The data were obtained from https://pla.esac.esa.int/#cosmology.

distribution for every parameter. We calculate the squared error again and compare it with the last step. Strictly, we compare the $\sim e^{-\chi^2}$ values given by the following part of the code (for more details see Appendix G):

```
        val = np.random.rand()

        val2 = f(error_array[j],error_new)

        if val < val2:

            # we move to this new probability

        else:

            # we don't move to the new probability
```

Listing 4.9: How to advance to the next step.

where the error is calculated as

```

def f(o,n):

    return np.exp(o - n)

def error(a,sigma_dist):

    n = np.square(TT_planck_obs - a)

    return np.sum(n)/sigma_dist
```

Listing 4.10: Estimation of the acceptance ratio.

Essentially, if the next step's squared error is lower than the previous step, then the probability of that *val* would be less than *val*2 is high, then the algorithm moves to the next step (with a high probability).

Note: the squared errors tend to be big numbers, and the exponential tends to be 0 or ∞. To avoid this problem, we implement an adaptative Metropolis. This algorithm corrects the sigma_dist value to maintain the acceptance ratio close the interval $[0, 1]$. This method is based on that if the last seven steps of the MCMC always advanced to the next step or always stayed in the same values, then the acceptance ratio must be redefined. With this little modification, we maintain the MCMC working.

However, this is not sufficient, because the z_{ls} must be estimated differently. Originally, the spectrum is predicted using probability distributions that are centered based on a previous step for every parameter: $C, h^2\Omega_{b,0}^{DG}, z_{ls}, n_s$ and N. This is not true for the Last Scattering redshift, because we expect that z_{ls} must be close the peak of the Visibility function. Then, to add randomness to the election of z_{ls}, but constraining it close the Visibility function peak, we choose the probability of choosing z_{ls} based on a normal distribution centered in the previous visibility function peak. This function depends on C and $h^2\Omega_{b,0}^{DG}$. These two values constraint the z_{ls}, but they do not determine the z_{ls} value. It is not deterministic. The results (next section) shows that the peak of the visibility function and the z_{ls} that gives the best TT CMB spectrum, are similar, but not equal. Strictly speaking, we fit a z_{ls} near to the peak of the Visibility function, and we are using adaptative Metropolis MCMC only in the other four parameters that determine the l_i parameters.

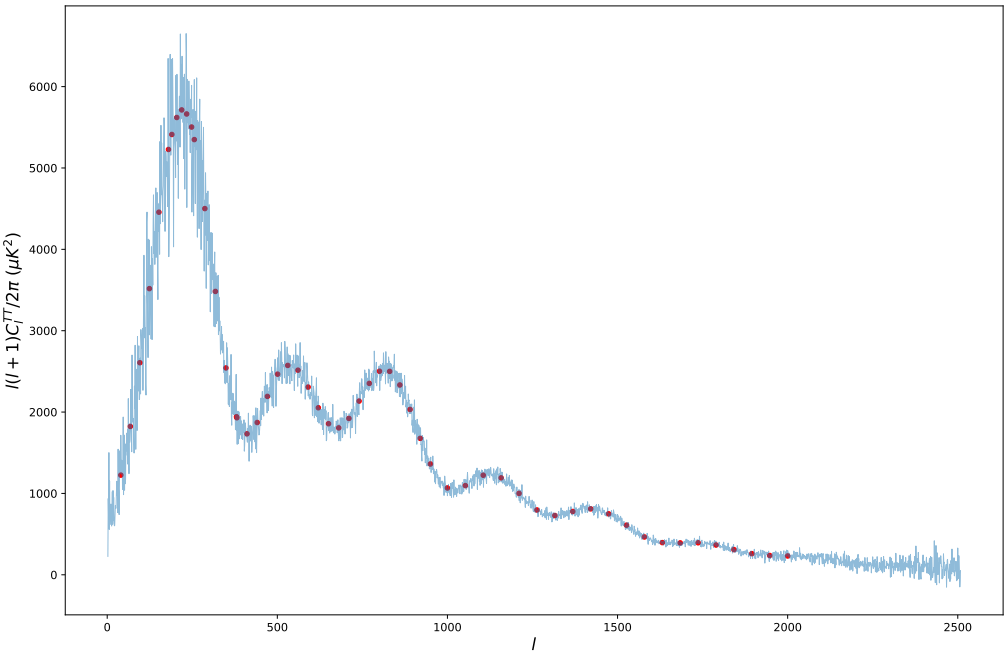

Figure 4.4: TT CMB spectrum. The blue line indicates the observational data and errors. The red dots were chose to fit the TT CMB spectrum.

The squared error calculated in every step is based on evaluating the differences of the predictions and the observation in that points determined by the l moments.

4.7 Results

Before presenting the results, it is crucial to clear that the right way to prove that the MCMC is working is to use the Gelman-Rubin convergence diagnostic. All the chains always converged to the same values; all are independent of the prior distributions. Now, we present the results. This corresponds to a chain with 20.000 steps for every parameter. The chains are plotted in Figure 4.5.

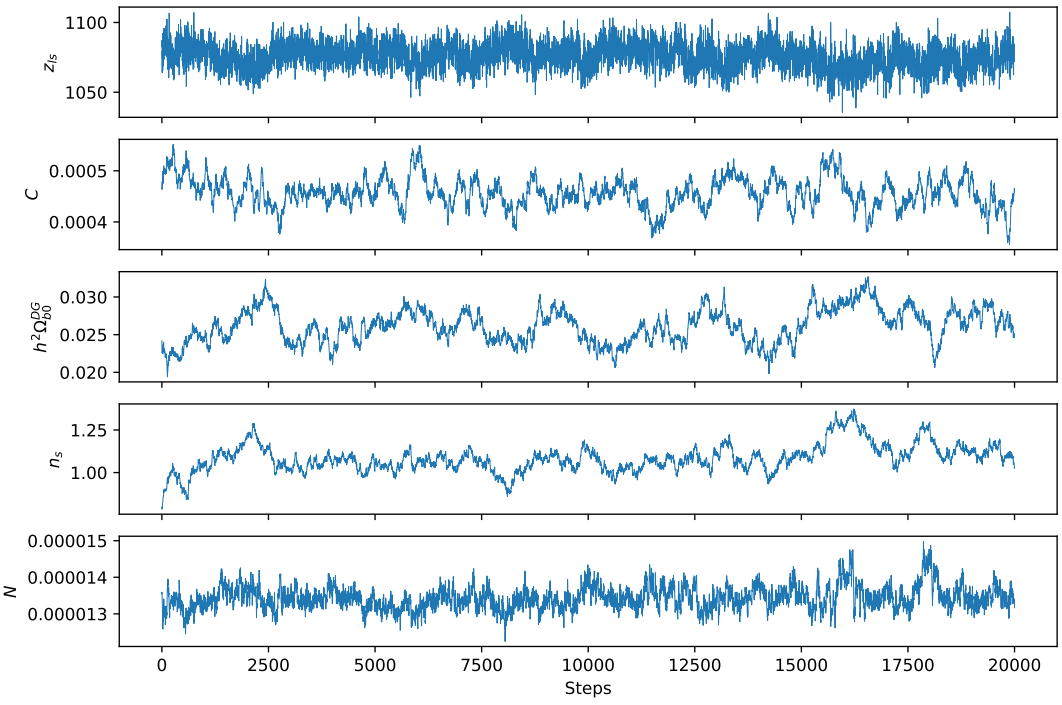

Figure 4.5: Chains for every parameter. This result was obtained after 20.000 steps.

The posterior distribution for every parameter are shown in Figures 4.6,4.7,4.8,4.9 and 4.10. All the distributions show only one peak, but some of them are not normally distributed at all. We specify the case of $h^2\Omega_{b,0}^{DG}$ and n_s. These parameters show multimodal distributions. We fit in both cases a normal distribution but the error was defined such that the σ_x includes the smallest multimodal distributions with its errors. Then, all the parameter have errors defined as $\pm 1\sigma_x$, with exception of $h^2\Omega_{b,0}^{DG}$ and n_s.

In every posterior distribution, we fitted a normal distribution where we calculated the mean and standard deviation. These results are shown also in Table 4.1

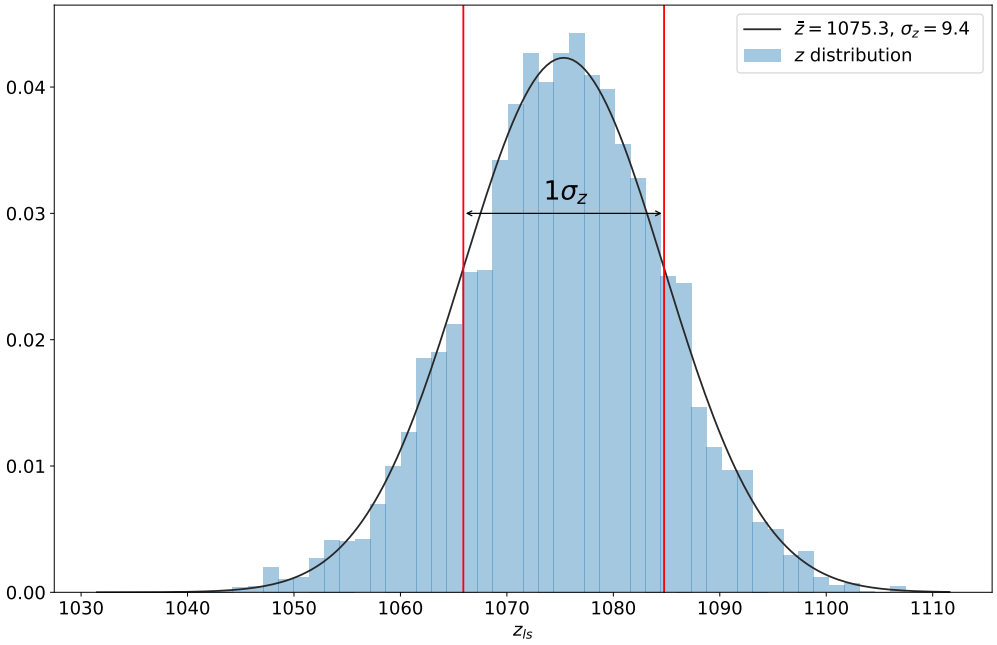

Figure 4.6: Posterior distribution for z_{ls}.

Table 4.1: MCMC fit results for the DG free parameters. These values are related to posterior distributions.

Parameter	Mean	Standard deviation
z_{ls}	1075.3	9.4
C	4.6×10^{-4}	0.3×10^{-4}
$h^2\Omega_{b,0}^{DG}$	0.026	0.002
n_s	1.09	0.08
N	1.34×10^{-5}	0.04×10^{-5}

Figure 4.11 shows all the combinations for the 5 free parameters. All the parameters are constrained to a normal-like distribution, and they are independent of each other.

Then, the shape of the TT CMB spectrum constraint all the parameters to "accurate" values. The fitted curve is shown in the Figure 4.12

These results are good according to the approximation given by Weinberg in [67]. This analytic and hydrodynamic approach shows a good fit for the most prominent three peaks, including the acoustic peak, but it is inaccurate at larger multipoles. The Figure 4.12 shows that DG prediction is very similar to the observable data, but the prediction is inaccurate from the third peak. However, the precision of the approximation includes that error scale.

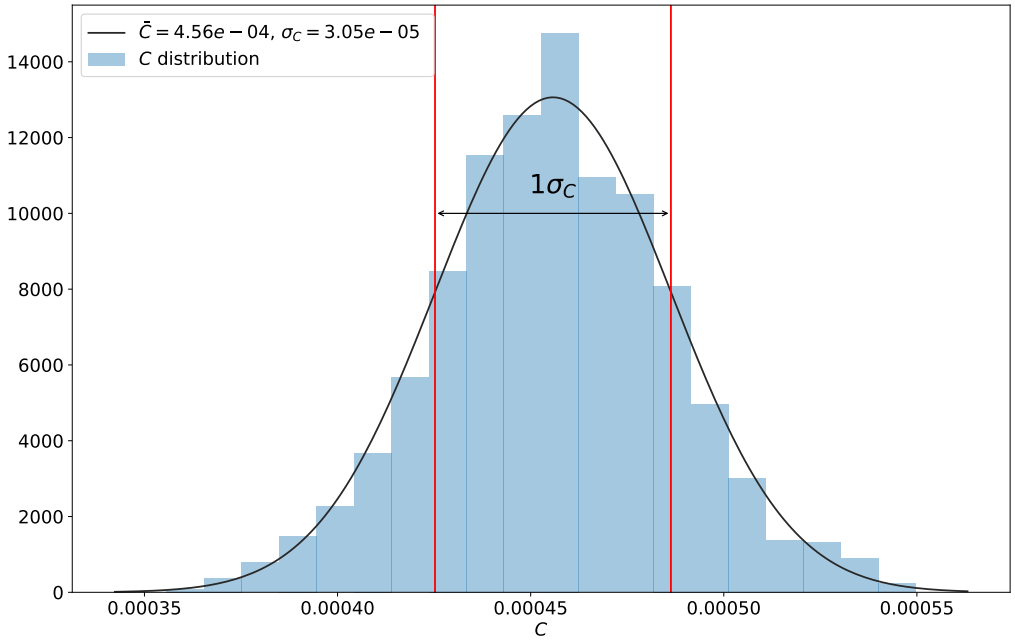

Figure 4.7: Posterior distribution for C.

In [67] the TT CMB spectrum has a similar error, and the differences also appear at larger multipoles.

Two important aspects must be checked: the C value and the Visibility function peak compatibility with the z_{ls} needed to fit the TT CMB spectrum.

Respect to the C value, the TT CMB spectrum fix this value around $C = 4.6 \times 10^{-4}$. This result is completely in concordance with the analysis presented in Chapter 3, and in Section 3.2. The C parameter is so small that the SNe-Ia analysis cannot detect a difference between 0 and $\approx 10^{-4}$. Then, the M and H_0 observables obtained from [56, 54, 55] are in concordance with our results, assuming a standard error in the approximation of the hydrodynamic approach similar to GR.

In the Last Scattering redshift case, we have to check if z_{ls} is near to the Visibility function peak. The Figure 4.13 shows how the fraction of free electrons X depends on T and z. At lower temperatures $X \to 0$, meanwhile at higher temperatures $X \to 1$. The X function depends on C, $h^2\Omega_{b,0}^{DG}$ and T, where the MCMC results have fixed the two first parameters. This case is shown in the Figure 4.13.

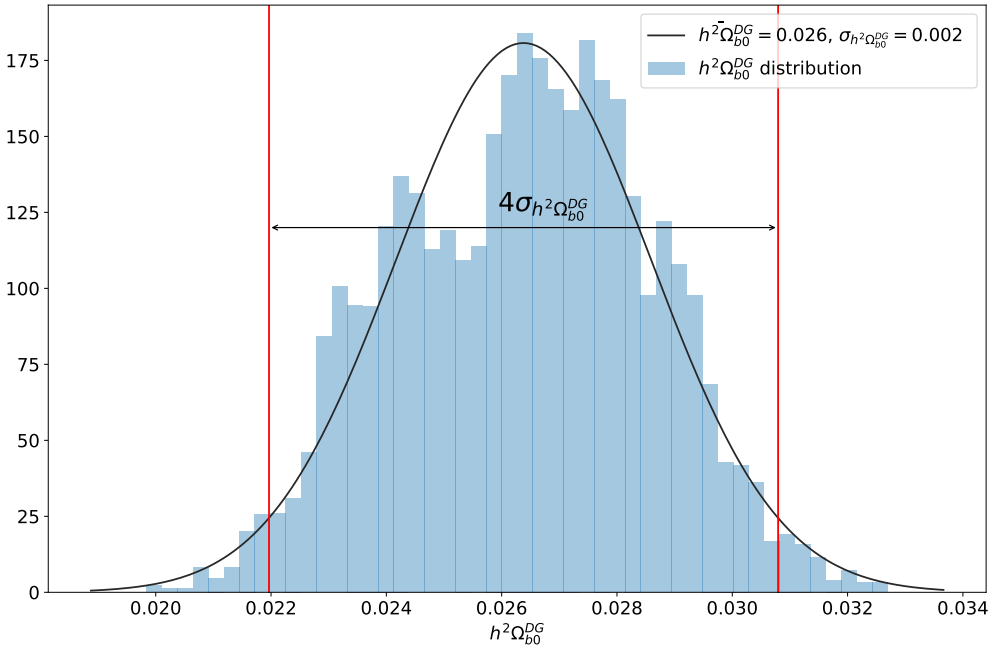

Figure 4.8: Posterior distribution for $h^2\Omega_{b,0}^{DG}$.

Then, the visibility function given by $X(T)$ has a maximum close $T_{max} \approx 2942$ K ($z_{max} \approx 1078$) with a temperature dispersion $\sigma_T \approx 244$ K. This function is shown in the Figure 4.14. Furthermore, we add a normal distribution centered at the same peak to show the similarity between the Visibility function and a normal distribution.

The σ_T was estimated from the height of the peak (not by fitting a distribution, FWHM, or any other method).

The GR case [67] finds $T_{max} \approx 2941$ K with a $\sigma_T \approx 248$ K.

The DG peak around $z \approx 1078$ is near to the MCMC results $z_{ls} \approx 1075$. Despite z_{ls} was obtained varying the redshift around the peak estimation, the z_{ls} is not exactly the peak associated with the Visibility function, but it is near.

Finally, the density of matter and radiation is related to the C and L_2 values through the definition of the physical densities.

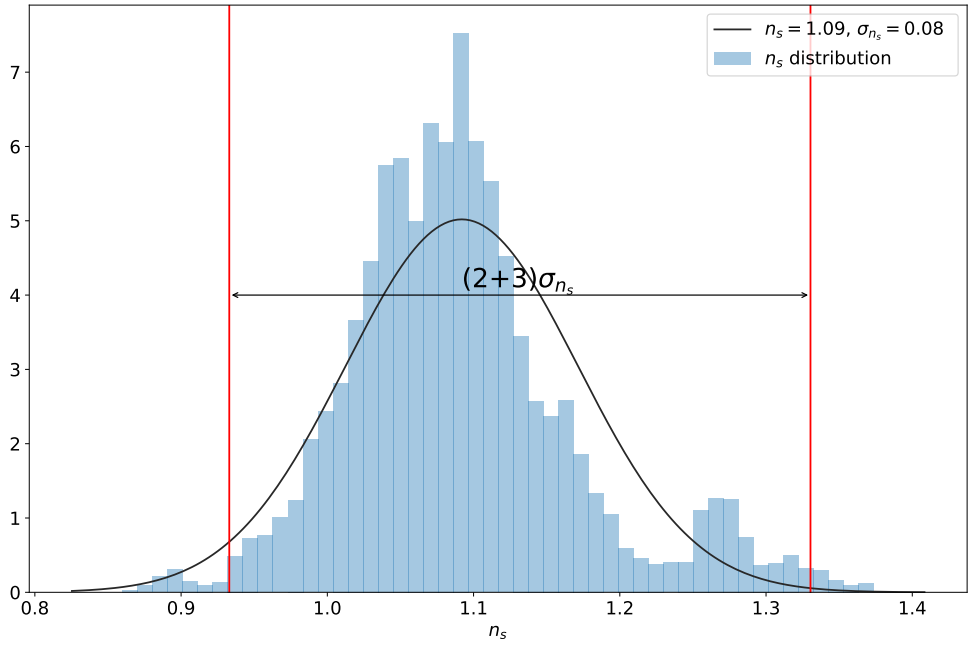

Figure 4.9: Posterior distribution for n_s.

In GR, the equality moment is vital because the hydrodynamic approach uses equality to match the equations when the Universe was dominated by radiation and dominated by matter. In the case of GR, naturally appears that

$$\frac{\rho_{GR\,m}}{\rho_{GR\,r}} = \frac{Y}{C}\,, \tag{4.84}$$

where $C = \Omega_{r,0}/\Omega_{m,0}$ by definition. Then the moment of equality in GR corresponds to $Y_{EQ} = C$. But, for DG densities, the physical densities depend on Y_{DG}, thus

$$\frac{\rho_{phys;m}}{\rho_{phys\,r}} = \frac{Y_{DG}}{C_{DG}}\,, \tag{4.85}$$

where $C_{DG} = \Omega^{DG}_{r,0}/\Omega^{DG}_{m,0}$. In DG, we imposed that the equality moment must occur in both sectors at the same time. In other words,

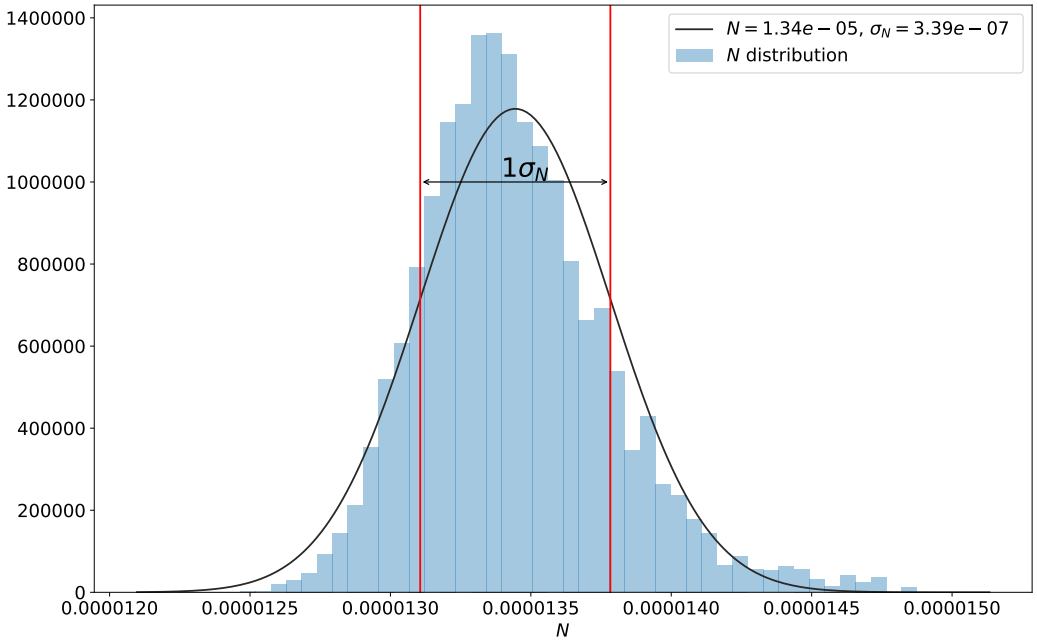

Figure 4.10: Posterior distribution for N.

$$Y_{DG}(Y_{EQ}) = C_{DG} \rightarrow C_{DG} = C\frac{\sqrt{\frac{1+F(C)}{1+3F(C)}}}{\sqrt{\frac{1+F(1)}{1+3F(1)}}}\ , \tag{4.86}$$

From the MCMC results, we know that $C \ll 1$ and $L_2 \approx 0.45$, then

$$C_{DG} \approx C\sqrt{\frac{1-L_2}{1-L_2/3}}. \tag{4.87}$$

This result is useful because if we know the physical density of radiation, we can find the physical density of matter. Then,

$$C_{DG} \approx C\sqrt{\frac{1-L_2}{1-L_2/3}} \approx 0.80C \approx 3.7 \times 10^{-4}. \tag{4.88}$$

Note 1: Henceforth, all the densities expressed as numbers with units energy per volume are physical quantities.

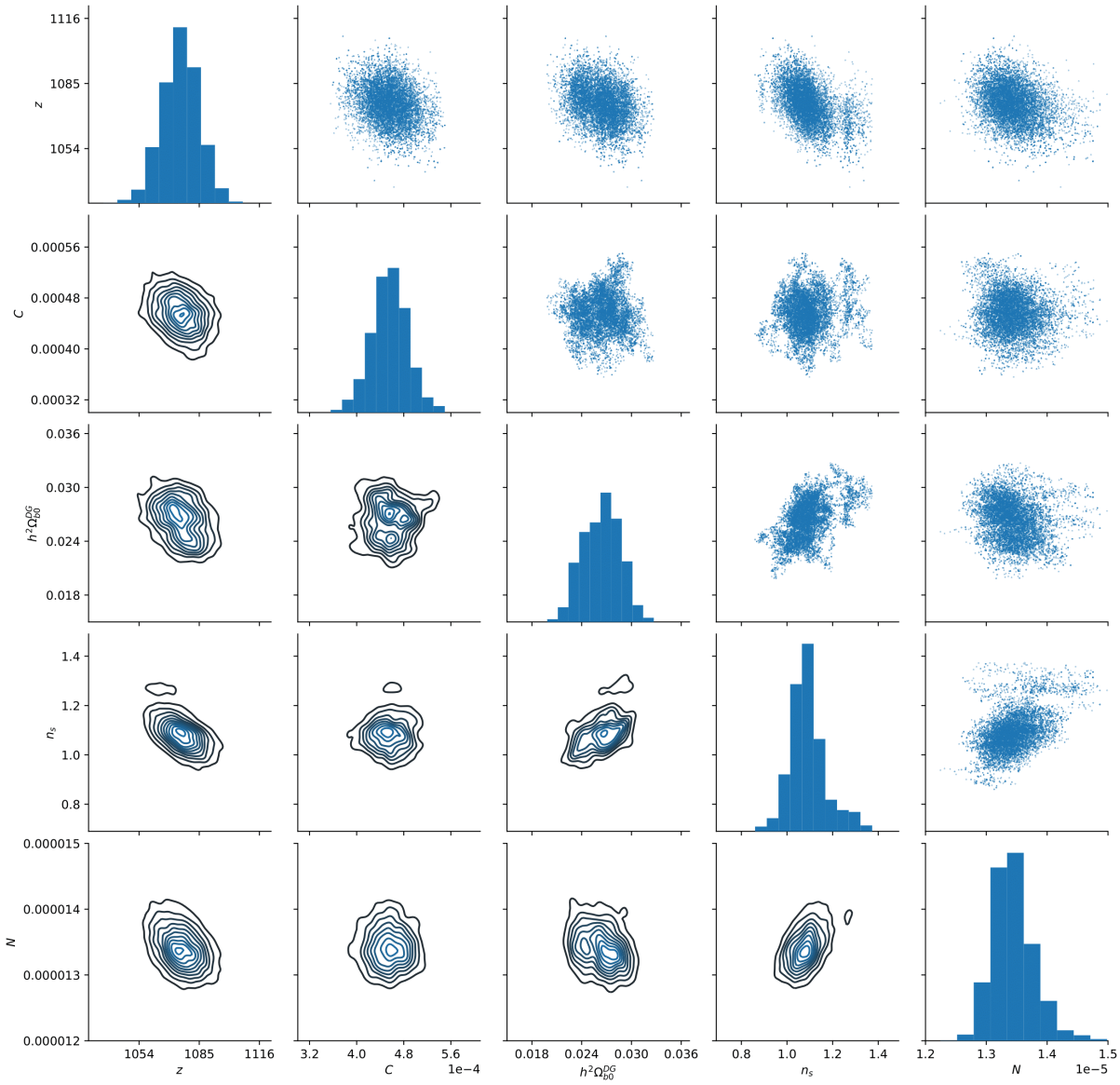

Figure 4.11: Contour plot for all posterior probabilities associated to the DG parameters.

Note 2: To be clear, in the next calculations we emphasize the observable (physical) densities with a DG sub or superscript.

To calculate the physical densities, we can use the photon density given by the black body spectrum integrated (based on the TT CMB spectrum):

$$\rho_{\gamma,0}^{DG} c^2 = a_B T_0^4, \tag{4.89}$$

,

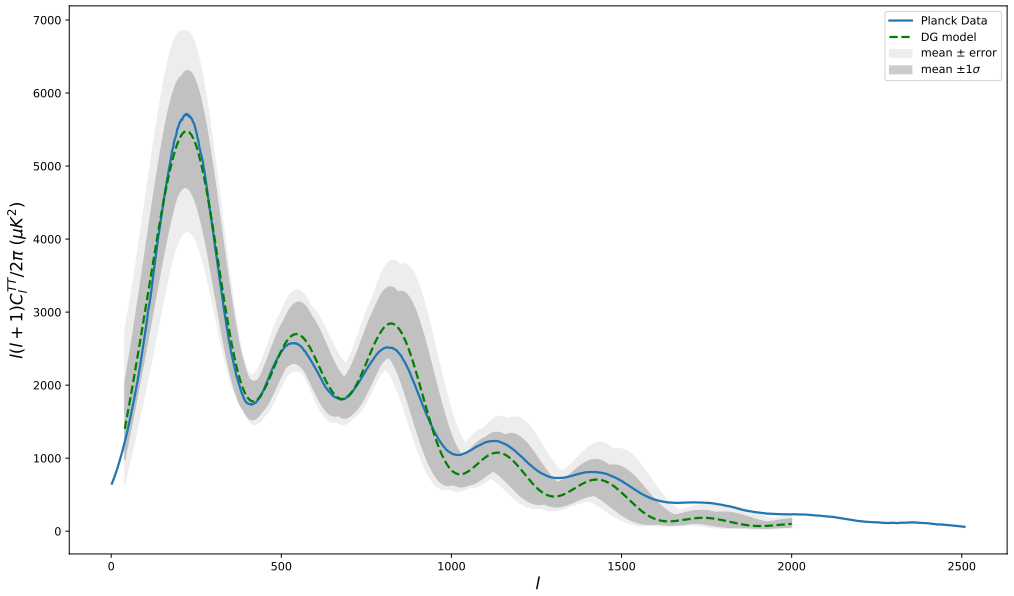

Figure 4.12: TT CMB spectrum was predicted by DG vs. the observed TT CMB spectrum. The blue line corresponds to the Planck observations, the green line is the DG prediction, and the greyscale is the error associated with the MCMC posterior probabilities.

where

$$a_B = \frac{8\pi^5 k_B^4}{15h^3c^3} = 7.56577 \times 10^{-16}\ \text{J m}^{-3}\ \text{K}^{-4}, \tag{4.90}$$

is the radiation energy constant. With $T_0 = 2.7255K$, we get the today density associated to the photons $\rho_{\gamma,0}^{DG} = a_B T_0^4/c^2 = 4.64511 \times 10^{-31}\text{kg m}^3$. This is a physical quantity.

The neutrinos density (physical quantity) is related to the photon density as following [2]

$$\rho_{\nu,0}^{DG} = N_{\text{eff}} \frac{7}{8} \left(\frac{4}{11}\right)^{4/3} \rho_{\gamma,0}^{DG}, \tag{4.91}$$

where $N_{\text{eff}}^{\text{Planck}} = 3.04678$ [49]. The relation given by the Equation (4.91) is based on statistical mechanics: photons and neutrinos are in thermal equilibrium, but neutrinos are fermions and photons are bosons. Thus,

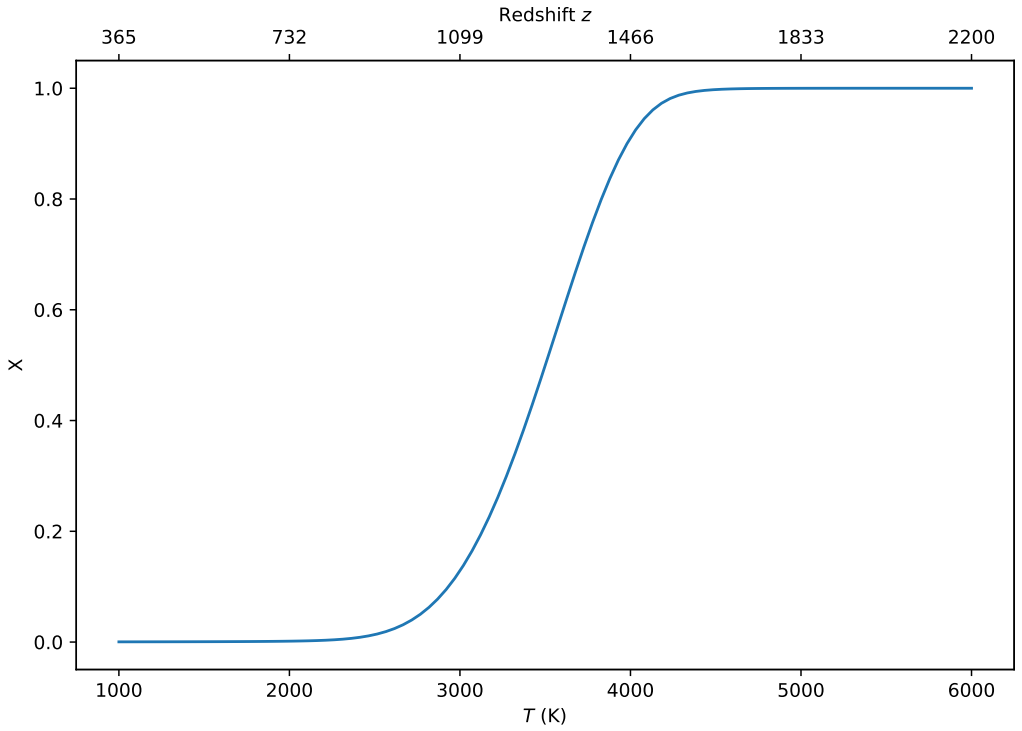

Figure 4.13: $X(T)$ fraction as function of temperature T and redshift z assuming C and $h^2\Omega_{b,0}^{DG}$ MCMC results.

$$\rho_{\nu,0}^{DG} = 3.21334 \times 10^{-31} \text{ kg m}^{-3}, \tag{4.92}$$

and the total radiation density (physical quantity) is given by

$$\rho_{\text{r},0}^{DG} = \rho_{\gamma,0}^{DG} + \rho_{\nu,0}^{DG} = 7.85846 \times 10^{-31} \text{ kg m}^{-3}. \tag{4.93}$$

Until here, we have assumed that neutrinos are relativistic particles and contribute to the radiation density. We can also write these values divided by the critical density given by:

$$\rho_{c,0} = \frac{3H_0^2}{8\pi G} = 1.87847h^2 \times 10^{-26} \text{ kg m}^{-3}, \tag{4.94}$$

where the GR Hubble Constant have been expressed in terms of the dimensionless parameter h, where $H_0 = 100h$ km s^{-1}Mpc^{-1}. Therefore, the density parameters are (these are

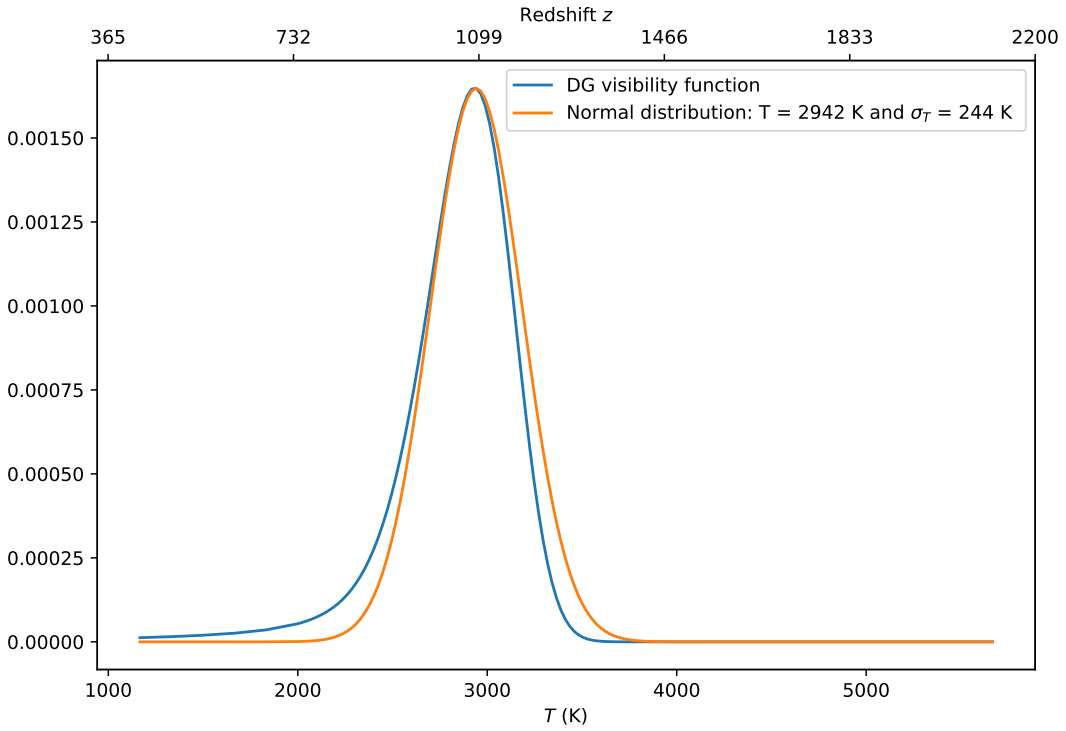

Figure 4.14: In blue color, the Visibility function is associated with the $X(T)$ obtained from the MCMC results. The orange line is a normal distribution centered in the peak of the DG solution.

physical!, we emphasize that the h constant is simplified, these parameters are independent of h.)

$$\begin{aligned} h^2\Omega_{\gamma,0}^{DG} &= \frac{\rho_{\gamma,0}^{DG}}{\rho_{c,0}}h^2 = 2.47\times10^{-5}, \\ h^2\Omega_{\nu,0}^{DG} &= \frac{\rho_{\nu,0}^{DG}}{\rho_{c,0}}h^2 = 1.71\times10^{-5}, \\ h^2\Omega_{r,0}^{DG} &= h^2\Omega_{\gamma,0}^{DG} + h^2\Omega_{\nu,0}^{DG} = 4.18\times10^{-5}, \end{aligned} \tag{4.95}$$

and (cdm is "cold dark matter")

$$h^2\Omega_{m,0}^{DG} \equiv h^2\Omega_{b,0}^{DG} + h^2\Omega_{cdm,0}^{DG} + (3-N_{\text{eff}})h^2\Omega_{r,0}^{DG} \approx h^2\Omega_{b,0}^{DG} + h^2\Omega_{cdm,0}^{DG}, \tag{4.96}$$

Finally, we assume that $N_{\rm eff} = 3$ (we emphasize, again, that $h^2\Omega_{x,0}^{DG}$ quantities are not related with H_0. They are related only with the physical density and $3 \times 100^2/8\pi G$) the quantities are:

$$h^2\Omega_{r,0}^{DG} = 4.18 \times 10^{-5}, \tag{4.97}$$

$$h^2\Omega_{b,0}^{DG} = 0.026, \tag{4.98}$$

$$h^2\Omega_{m,0}^{DG} = 0.113, \tag{4.99}$$

$$h^2\Omega_{cdm,0}^{DG} \equiv h^2\Omega_{m,0}^{DG} - h^2\Omega_{b,0}^{DG} = 0.087. \tag{4.100}$$

We include the relations between the five parameters and the shape of the TT CMB spectrum in Appendix E. This could be useful to understand how the parameters change the shape of the TT CMB spectrum.

Chapter 5

Conclusions

Here we have studied the cosmological implications for a modified gravity theory named Delta Gravity. The results from SNe-Ia analysis indicate that DG explains the accelerating expansion of the Universe without Λ or anything like "Dark Energy". The Delta Gravity equations naturally produce the acceleration .

In this work we performed a fit to the SNe-Ia data considering three free parameters M, C and L_2, finding that C is not relevant if it is small: less than 10^{-2}. Also we found that $L_2 \approx 0.457$ and $h \approx 0.496$.

In order to derive cosmological parameters, we assumed that $M = -19.23$ is a suitable value calculated from [56]. We want to emphasize that the local measurements and calibrations of SNe-Ia obtained this value: it is independent of any cosmological model. The procedure presented does not use ΛCDM assumptions. We only assume that the calibrations from Cepheids and SNe-Ia are correct; therefore, the absolute magnitude $M = -19.23$ for SNe-Ia is correct.

We emphasize that if C is small, the TT CMB spectrum will not be affected. This aspect is crucial because L_2 establishes the acceleration of the Universe in DG, as we have shown in Chapter 3; thus, even in the case where M could be wildly inaccurate, L_2 does not change because this parameter is independent of M, where M is degenerated with h. In this case, the Universe is accelerating as a result of $L_2 > 0$.

The acceleration in DG is given by $L_2 \neq 0$. L_2 also determines that the Universe contains Delta matter and Delta radiation. This can be associated with the new Delta fields. It is

not clear if this Delta Composition is made of real particles, or not. However, we can assume two different interpretations. The first is that the Universe only contains matter (baryonic and cold dark matter) and radiation. The other scenario is that the Universe also contains Delta matter and Delta radiation. In both scenarios, the Universe shows the same behavior, and it is accelerating, but the difference is that the Delta Sector could be invisible because the geometry provides the fundamental physics behind Delta Sector and not the particles. This is part of the interpretation, and for now, we cannot conclude more about this aspect.

Also, Delta Gravity is in concordance with a high H_0 value (assuming $M = -19.23$). This is a consequence of the local expansion in terms of the redshift of the luminosity distance $d_L^{DG}(z)$. This aspect is vital because the current H_0 value is in tension [56][54] between SNe-Ia analysis and the Planck satellite's data. GR also predicts a high H_0 value with the same assumptions, but it needs to include Λ to fit the SNe-Ia and also seems to be problems to explain all together: the CMB, BAOs and SNe-Ia [56, 54, 55, 49, 65, 21, 31].

The most crucial point is that the local measurement of H_0 is model-independent. Then, we want to preserve this constraint to analyze the TT CMB spectrum.

Another difference between Delta Gravity and GR models is that DG model predicts a Big Rip dominated by the L_2 value. This is a consequence of the accelerated expansion produced by L_2 (Delta Sector).

The TT CMB Spectrum is well-reproduced by the DG model. To fit the spectrum, we had to use 5 free parameters: $C, h^2\Omega_{b,0}^{DG}, z_{ls}, n_s$ and N.

The $l_H = 1/\theta$ parameter, which fixes the position of the first peak (it is not the only cause), is very sensitive to C and then constrains the C value. We can examine the C influence in the Appendix E. The position of the first peak is very well determined. Therefore the θ error or l_H error dominates the TT CMB fitting. The position of the peak is also related to $h^2\Omega_{b,0}^{DG}$ and z_{ls}. The other two peaks, in the GR case, tend to be fitted by the dark matter and baryon density [1] [1] (principally). Nevertheless, in the hydrodynamic approach [67], the dark matter evolution is assumed as dominant considering that all the gravitational potential is driven by dark matter. This approximation is useful because the equations are easy to solve, however it is not accurate according to [67, p. 358]: this approach introduced 10% errors or less. Despite this approximation, the TT CMB spectrum is very well described,

[1] Any dependence can be easily verified with https://camb.readthedocs.io/en/latest/CAMBdemo.html. Specifically, the dependence of the height peaks and its relative positions respect to the $h^2\Omega_x$.

but the large multipoles show deviations from the observable data. The integral limits of the equations constrain the z_{ls} value in Equation 4.52, and the angular distance is determined by the Equation (4.50). The z_{ls} obtained from the MCMC is compatible with the transition range showed in Figure 4.13, and the peak of the Visibility function showed in Figure 4.14. The amount of baryonic matter given by $h^2\Omega_{b,0}^{DG} = 0.026$ is close to the GR case: 0.022. It is important to contrast this value with other measurements, especially because DG has a very different description of the Universe, where other equations, different to GR, give the distances. Then, other observational constraints must be examined meticulously in order to conclude if DG fit those observations.

The parameters related to the primordial spectrum, A and n_s, are close to the standard values: the spectral index is close to 1, and the amplitude is $\sim 10^{-5}$. It is vital to consider that those values were obtained from an approximation called hydrodynamic approach, and then, the numerical values contain intrinsic errors associated with the approximations, then they are not accurate. Nonetheless, these values are very similar to the GR case.

An assumption that is essential for all the CMB analysis is that the plasma fluid, which is described with the speed of sound c_s within the horizon radius, is only affected by baryons and radiation. This aspect could indicate that Delta Components do not interact with common radiation and matter, but it would be interesting to analyze all the changes that introduce a Delta Sector that interacts with Common matter and radiation. This aspect may change many approximations and, then, could affect enormously the TT CMB spectrum. This could be part of future research.

The observable rate of expansion of the Universe in DG is given by H_0^{DG}. This parameter is determined by L_2 and h. In the context of the TT CMB analysis, if C is very small, then the SNe-Ia observations can be compatible with the TT CMB spectrum. The results show that $C \sim 10^{-4}$. In this regime, the SNe-Ia is not affected, and the compatibility between both observations is possible. It is important to emphasize that there are two values that are different. One is h, which is provided from the GR background, and second, the H_0^{DG}, that is the observable Hubble Constant in this model.

A relevant cosmological value that can be constrained from the observations, is the age of the Universe. The higher the Hubble Constant, the lower the age of the Universe. This relation is vital since if the local fit of supernovae radically changes H_0, then the age of the Universe changes. Therefore, there could be conflicts with some estimates of the age of the Universe that are independent of cosmology. We remark the fact that according to

local measurements of supernovae, the age of the Universe for DG and GR are: 13.1 Gyrs for DG and 13.0 Gyrs for GR. Instead, Planck's data imply a larger age of the Universe: 13.8 Gyrs. A crucial and precise estimation based on the measurement of globular clusters age in the Milky Way [42] [2], which is independent of cosmology, indicates that the Universe has to be older than 13.6 $\pm$ 0.8 Gyrs. DG and GR, assuming the results of SNe's local measurements, are on the verge of this observational constraint. According to this, one wonders if SNe can be in conflict with the age of the Universe. It is a very recent discussion, and we are only commenting on the problems when astrophysicists try to make SNe and CMB compatible. We emphasize that the problem goes beyond DG because a high Hubble Constant causes it, and it also involves other types of measurements that yield high values of the Hubble Constant. This discrepancy could be caused by the calibrations and methods used by Riess et al., but this tension between both observations has been widely discussed and until now there is no agreement. Even, other researchers have tried to measure the H_0 value using methods independent of distance ladders and the CMB. They found that the Hubble Constant exceeds the Planck results, with the confidence of 95% [46]. However, other measurements based on the tip of the red giant branch (TRGB) have found that H_0 is close to 69.6 km/(Mpc s) [24, 25]. Other methods based on lensed quasars found that $H_0 = 73.3$ Mpc/(km s) agrees with local measurements but tension with Planck observations [70].

All the TT CMB spectrum analyses were made in the DG context were the Delta contributions represented by $\tilde{F}$ and $\tilde{G}$ in Chapter 4 can be neglected. This is an essential part of the development of the perturbation theory, and it implied many simplifications when we want to calculate the spectrum and creates more constraints on the spectrum fitting.

Furthermore, the definition of what is a physical density was only possible when we developed the equations that describe physical processes such as the Thomson scattering or the evolution of the transparency of the Universe, described by the Visibility function. Before the CMB analysis, it was impossible to understand the meaning of physical density, and even we did not define a total composition of the Universe in terms of percentage. Now, we have a picture of the Universe, but the questions continue about what the Delta Components are. DG requires more development to compare with other constraints such as the He produced at the Big Bang nucleosynthesis, or the BAOs constraints, or even cosmological simulations. This last aspect could be relevant if the interpretation of the Delta Sector is given in terms

[2] https://www.eso.org/public/chile/news/eso0425/

of particles that create gravitational interactions. In fact, at the Newtonian limit, the Delta matter appears as a new source of the gravitational potential [11].

Finally, it is remarkable that DG finds a well-behaved TT CMB spectrum, where it is possible to constraint new parameters, even related to inflation. However, this analysis does not use all the numerical precision, because the equations are only an approximation, and even more, we are calculating only the scalar contributions to the total TT CMB spectrum. Furthermore, many other sources that contribute to the "spectrum" have been avoided to simplify the analytical solution, such as Sachs-Wolfe effect or lensing. This is only a first order approximation, and it shows that DG could fit the TT CMB spectrum, but it is essential to fit the spectrum with all the numerical precision without approximations because the conclusions drawn in that case could be different. Thus, these numerical results must be understood as values that are near to the correct value, not as a final and undeniable result.

The incompatibility between the SNe-Ia and CMB occurs when ΛCDM model is constrained using BAOs and SNe-Ia. Even when the model uses curvature: if all the parameters describe the same Universe, the whole model must be compatible with only one geometry given by Ω_k. For example, recently, it was published an article that shows a discrepancy between the Planck's data [49]. These differences can be caused by the assumption that the Universe is flat. Despite this curvature assumption in the ΛCDM model, the cosmological parameters are incompatible because some of them are compatible with a flat Universe, but others indicate a closed Universe [65]. Furthermore, regarding the SNe-Ia analysis, another article shows an anisotropy in the SNe-Ia distribution, and then, the acceleration measurement could be wrong [21]. All the DG analysis could change because the L_2 value will be different, and all the distances would change [31]. . In this context, it is relevant to emphasize that there are many approximations in our procedure, and DG must be contrasted with other observations to conclude with a good precision if this model is a solution for today's paradigm. BAOs could be an excellent option to verify the model, mainly because these observations are related to the angular distance and could constrain the DG model and verify if DG can survive to describe SNe-Ia and BAOs.

Despite these interpretations, problems, and approximations, DG can fit both SNe-Ia and TT CMB spectrum data, without Dark Energy. There are many open problems and interpretations: what is Delta matter and Delta radiation? BAOs can be explained without tension with SNe-Ia and Planck in the DG model? Can DG reproduce the Big Bang Nucleosynthesis without tension? What is the role, in terms of gravitation, of the Delta Sector?

What are the cosmological parameters obtained from a complete numerical fit of the CMB spectrum?

Appendix A

Local Expansion in terms of redshift

We develop the approximation for d_L in terms of redshift z up to the second order. The polynomial expansion is the same as in the Standard Cosmological Model.

The luminosity distance in DG is given by (1.48):

$$d_L^{DG}(z, L_2, C) = c\frac{a_{DG,0}(1+z)}{H_0\sqrt{\Omega_m}}\int_{Y(z)}^{1}\frac{Y}{\sqrt{Y+C}}\frac{dY}{a_{DG}}, \tag{A.1}$$

In the previous work, we found that $C \approx 0$, thus the d_L can be approximated to

$$d_L^{DG}(z, L_2) = c\frac{a_{DG,0}(1+z)}{H_0}\int_{Y(z)}^{1}\frac{\sqrt{Y}}{a_{DG}(Y)}dY, \tag{A.2}$$

where (by equation (1.43))

$$a_{DG} = \frac{a_{DG,0}}{1+z}. \tag{A.3}$$

If we expand Y around $z = 0$ (near today), we obtain

$$Y(z) = \underbrace{Y(0)}_{1} + \left.\frac{dY}{dz}\right|_{z=0} z + \frac{1}{2}\left.\frac{d^2Y}{dz^2}\right|_{z=0} z^2. \tag{A.4}$$

Furthermore, we define

$$F(u) \equiv \frac{\sqrt{u}}{a_{DG}(u)}, \tag{A.5}$$

then

$$f(Y) \equiv \int_Y^1 F(u)du \tag{A.6}$$

and

$$\left.\frac{df}{dY}\right|_{Y=1} = -\frac{1}{a_{DG,0}}. \tag{A.7}$$

If we define the deceleration parameter as

$$q_0 = -\frac{\ddot{R}_{DG,0}a_{DG,0}}{(\dot{R}_{DG,0})^2}, \tag{A.8}$$

the deceleration parameter today is given by:

$$q_0 = \frac{a_{DG,0}}{2R'_{DG,0}} - \frac{R_{DG,0}a''_{DG}}{(R'_{DG,0})^2}. \tag{A.9}$$

Finally, the $\frac{d^2f}{dz^2}$ term is given by

$$\frac{d^2f}{dz^2} = \frac{1}{a'_{DG,0}}(-1-q_0). \tag{A.10}$$

Finally, replacing all these equations into the luminosity distance, we obtain

$$d_L^{DG}(z, L_2, C) \approx \frac{c}{H_{DG,0}}\left(z + \frac{1}{2}(1-q_0)z^2\right). \tag{A.11}$$

This relation is important because it can be used to fit SNe-Ia at low redshift.

Note that H_0^{DG} in DG is the observable. This term describes the real expansion of the Universe on the effective metric. if we compare this expression with the standard expansion of

the luminosity distance in GR, we obtain the same term that appears in standard cosmology. [56, 54] Then, if we replace d_L^{DG} expression into d_L up to first order in z we find

$$m = 5 \log \frac{cz + \mathcal{O}(z^2)}{H_0^{DG}} + M + 25. \tag{A.12}$$

Appendix B

Friedmann Equations in GR

B.1 Friedmann Equations

The Friedmann equations are obtained from the Einstein Field Equations: (using the FLRW metric)

$$G_{\mu\nu} = R_{\mu\nu} - \frac{1}{2}Rg_{\mu\nu} + \Lambda g_{\mu\nu} = \frac{8\pi G}{c^4}T_{\mu\nu},$$

where Λ is called the Cosmological Constant or DE. To calculate $T_{\mu\nu}$ we can use the Fluid Perfect equation. Finally, the Friedmann Equations are

$$H^2 = \left(\frac{\dot{a}}{a}\right)^2 = \frac{8\pi G\rho + \Lambda}{3} - K\frac{c^2}{a^2} \tag{B.1}$$

$$3\frac{\ddot{a}}{a} = \Lambda - 4\pi G\left(\rho + \frac{3p}{c^2}\right) \tag{B.2}$$

B.2 $q(t)$ equation

By definition, the deceleration parameter is

$$q(t) \equiv -\frac{\ddot{a}a}{\dot{a}^2}.$$

We can use the Friedmann Equations given by to rewrite this terms in function of densities:

$$q(t) = -\frac{\ddot{a}}{a(\dot{a}/a)^2} = -\frac{\ddot{a}}{aH^2}$$

$$\frac{1}{a}\frac{d^2a}{dt^2} = -\frac{4\pi G}{3}\sum_i \left[\rho_i + \frac{3p_i}{c^2}\right] + \frac{\Lambda}{3}$$

$$q(t) = \frac{8\pi G}{3H^2}\left[\frac{1}{2}\rho_m + \rho_r - \rho_\Lambda\right]$$

Where we used r, m, Λ to denote radiation, matter and Dark Energy, and ρ and p for density and pressure, respectively. The critical density is

$$\rho_c \equiv \frac{3H^2}{8\pi G}.$$

Finally,

$$q(t) = \frac{1}{\rho_c}\left[\frac{1}{2}\rho_m + \rho_r - \rho_\Lambda\right] = \frac{1}{2}\sum_i \left((1+3\omega_i)\Omega_i(t)\right), \tag{B.3}$$

where $\omega_m = 0$, $\omega_r = 1/3$ y $\omega_\Lambda = -1$.

Appendix C

Convergence Test

A useful convergence test is the Gelman-Rubin statistic[27].

The Gelman-Rubin diagnostic uses an analysis of variance approach to assessing convergence. This diagnostic uses multiple chains to check for lack of convergence, and is based on the notion that if multiple chains have converged, by definition, they should appear very similar to one another; if not, one or more of the chains has failed to converge (see PyMC 2 documentation).

In practice, we look for values of $\hat{R}$ close to one because this is the indicator that shows convergence.

We ran 16 chains for the DG model. Figure C.1 shows the L_2 and C predicted values for every chain of the Monte Carlo simulation. Figure C.4a,b shows the convergence of L_2 and C. All the chains converge to a similar value assuming different priors. These final values predicted for every chain are shown in Figure C.1. From all these chains, it is clear that the Delta Gravity MCMC analysis is convergent for the two free parameters.

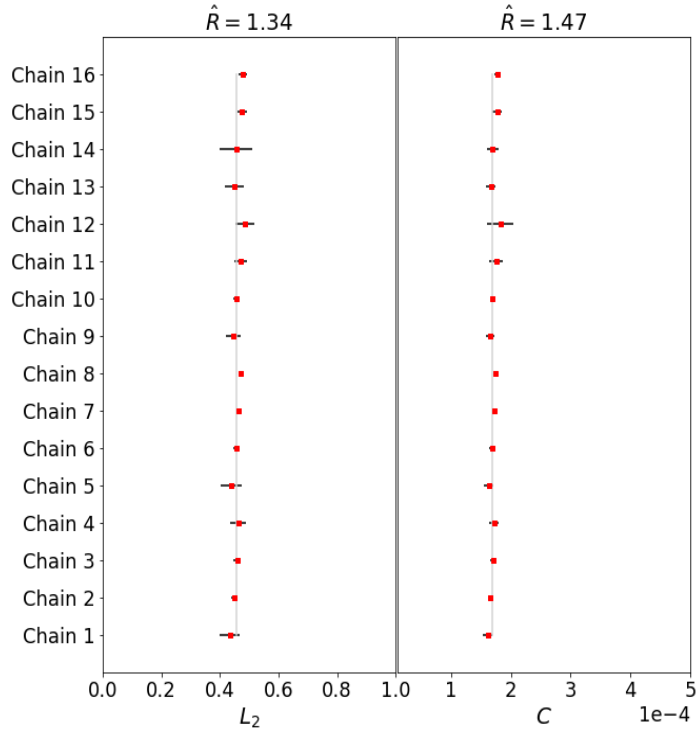

Figure C.1: Gelman-Rubin test for Delta Gravity model assuming $M_V = -19.23$. The Gelman-Rubin test was run with 16 different chains, all with different L_2 and C priors. The $\hat{R}$ coefficient (Gelman-Rubin coefficient) was calculated for each parameter.

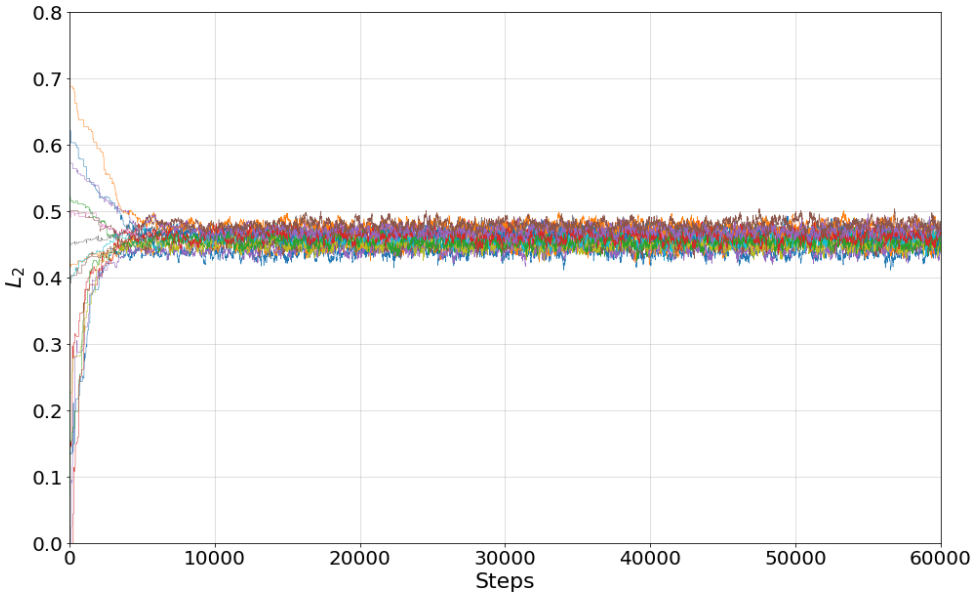

Figure C.2

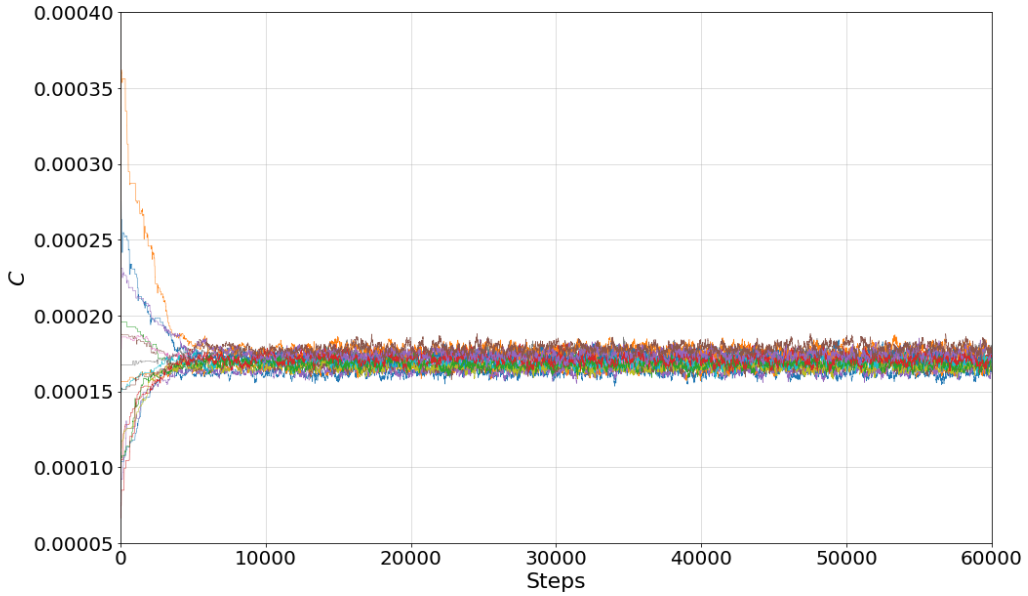

Figure C.3

Figure C.4: Gelman-Rubin test for Delta Gravity model. There are 16 chains with different priors. (**a**) All the chains converge to a $L_2 \approx 0.455$. (**b**) All the chains converge to a $C \approx 0.000169$.

Appendix D

Other parameters

D.1 Cosmic Time and Redshift

By using Equation (1.22) we obtain the Cosmic Time in Delta Gravity, where the redshift is obtained by numerical solution from Equation (1.44).

Meanwhile for GR model, we obtained the cosmic time from the integration of the first Friedmann equation and solving $t(\Omega_{m0}, H_0)$. Here we have included $\Omega_\Lambda = 1 - \Omega_{m0}$ and we did Ω_k ($k = 0$) and $\Omega_{r0} = 0$. The integral for the first Friedmann equation can be analytically solved:

$$t = \int_0^a \frac{1}{\sqrt{\frac{\Omega_{m0}}{x} + (1 - \Omega_{m0})x^2}} dx = \frac{2}{3\sqrt{1 - \Omega_{m0}}} \ln\left(\frac{\sqrt{-\Omega_{m0}a^3 + \Omega_{m0} + a^3} + \sqrt{1 - \Omega_{m0}}a^{3/2}}{\sqrt{\Omega_{m0}}}\right) \tag{D.1}$$

where t in (D.1) is the cosmic time for GR.

We plot the results in Figure D.1:

The behavior of cosmic time dependence with redshift for both models is very similar.

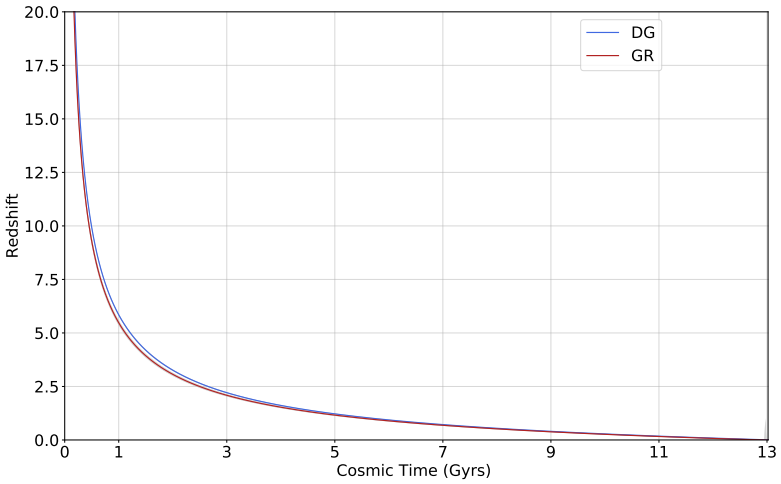

Figure D.1: Cosmic time for GR and Delta Gravity.

D.1.1 Age of the Universe

The age of the Universe in Delta Gravity is calculated using (1.22). $t(Y)$ only depends on C and not on L_2. In GR we calculate the age of the Universe using (D.1).

With these expressions, we can compare the behavior between cosmic time and the scale factor in GR (or the effective scale factor in Delta Gravity).

In Figure D.2, it is possible to see the evolution for $Y_{DG}(t)$ in time. At $t = 28.75$ Gyr, Y_{DG} goes to infinity, and the Universe ends with a Big Rip, then, in this model the Universe has an end (in time). Also, we see the dependence between the scale factor a and cosmic time t. The Universe has no end (in time) in GR.

D.2 Deceleration Parameter q_0

For Delta Gravity, we used Equation (1.56). For today, we evaluate $a = 1$ for GR, and $Y_{DG} = 1$ for Delta Gravity.

In Figure D.5, we can see the evolution in time for both GR and Delta Gravity models.

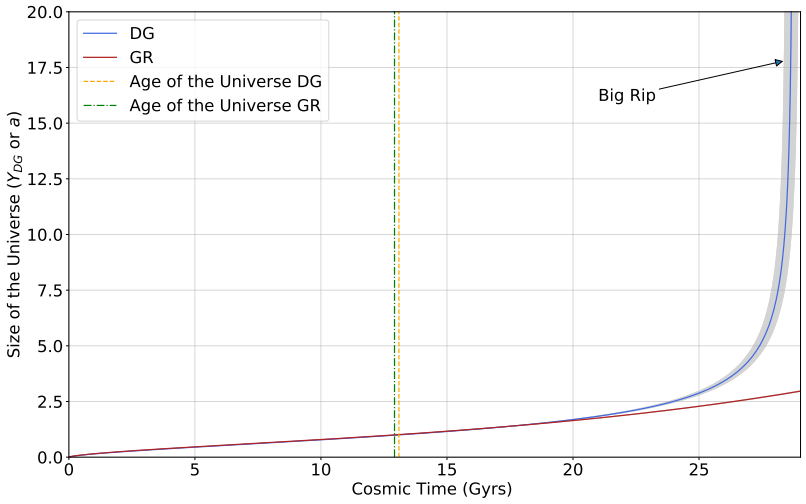

Figure D.2: The size of the Universe vs. age of the Universe. In the Delta Gravity model, the size of the Universe Y_{DG} depends on cosmic time t and on C. The blue line indicates the effective scale factor in Delta Gravity. The gray zone shows the error associated with Y_{DG}. For GR, the scale factor a depends on cosmic time t and on Ω_{m0}. The red line indicates the scale factor evolution in GR. The gray zone shows the error associated with a (these are tiny).

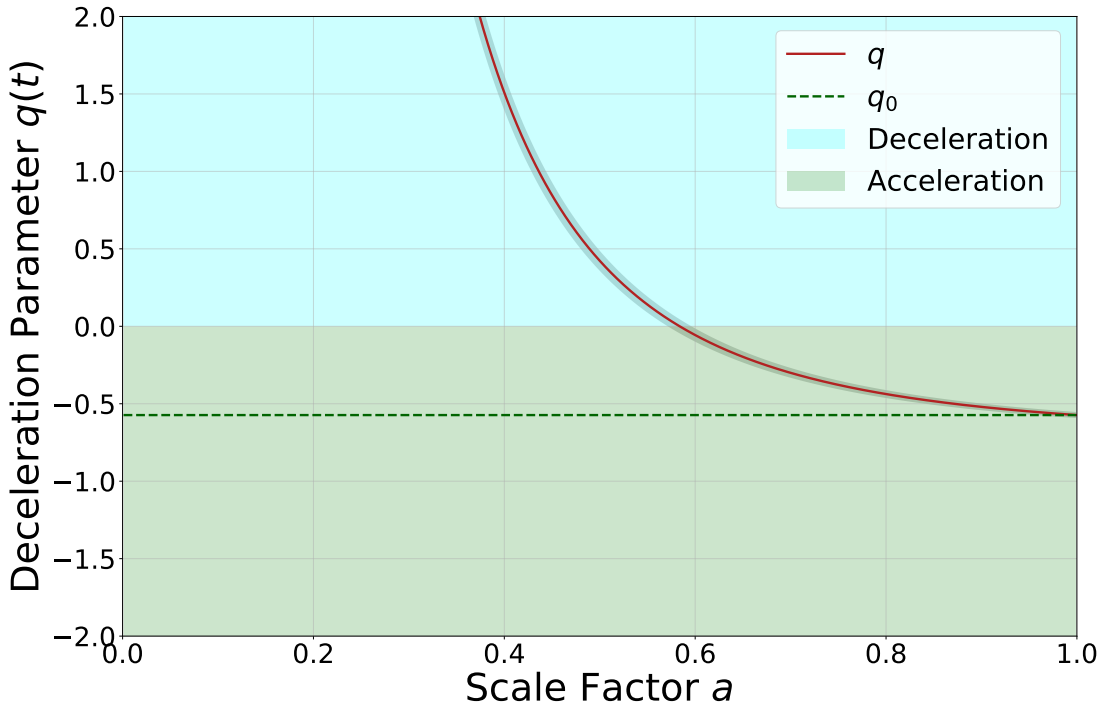

Figure D.3

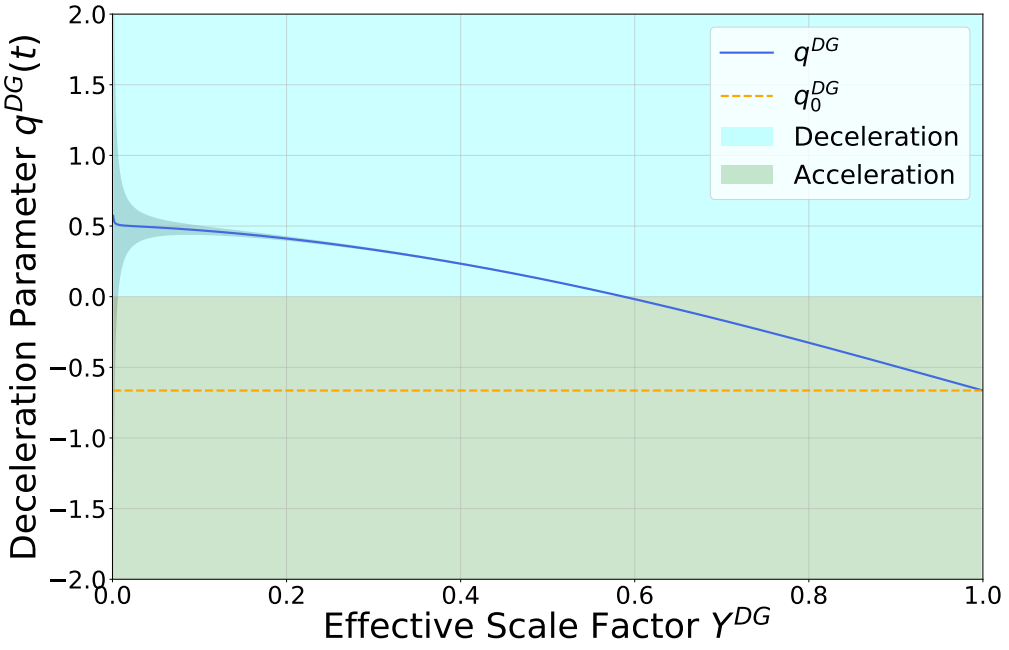

Figure D.4

Figure D.5: Deceleration parameter for both models. (**a**) Evolution of deceleration parameter in GR. (**b**) Evolution of deceleration parameter in Delta Gravity.

Appendix E

CMB and the free parameters

We plot the five relations with the free parameters used to fit the TT CMB spectrum. They are $C, h^2\Omega_{b,0}^{DG}, z_{ls}, n_s$ and N. To create the Figures, we fix all the parameters equal to the results obtained from the MCMC, and vary only one parameter around the mean of the posterior distribution.

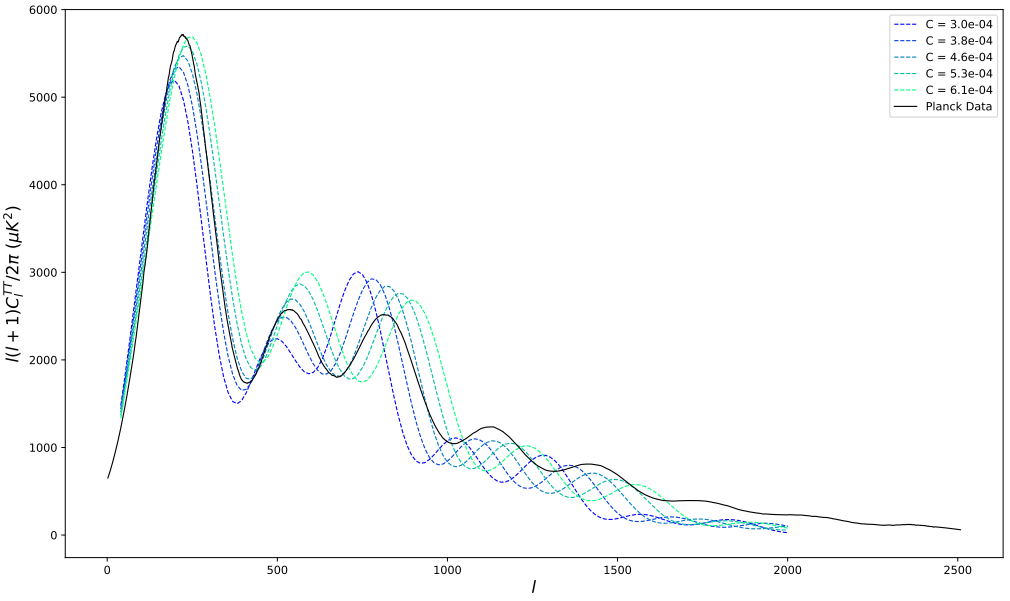

Figure E.1: TT CMB spectrum vs. C.

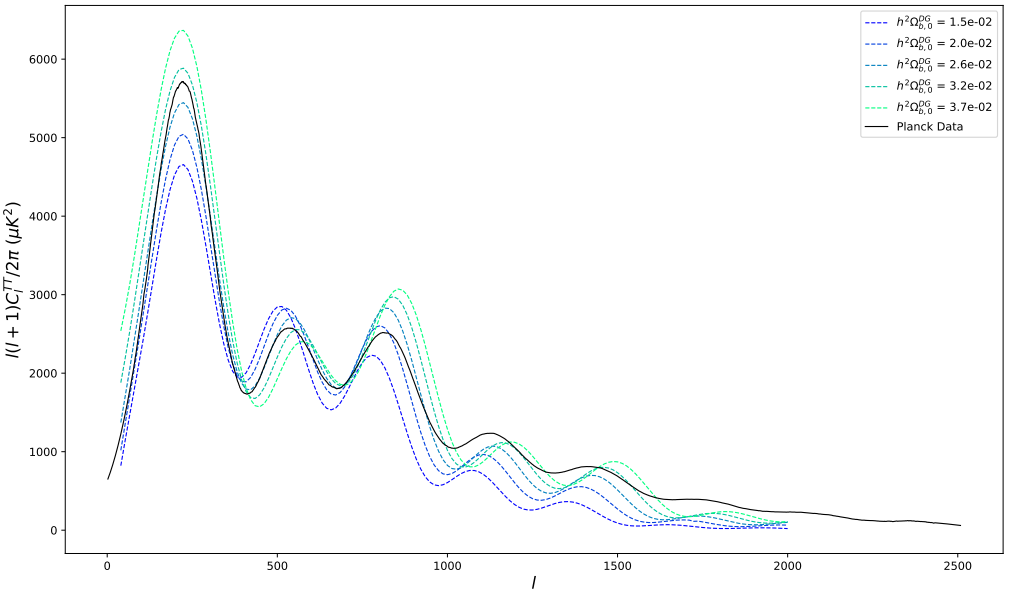

Figure E.2: TT CMB spectrum vs. $h^2\Omega_{b,0}^{DG}$.

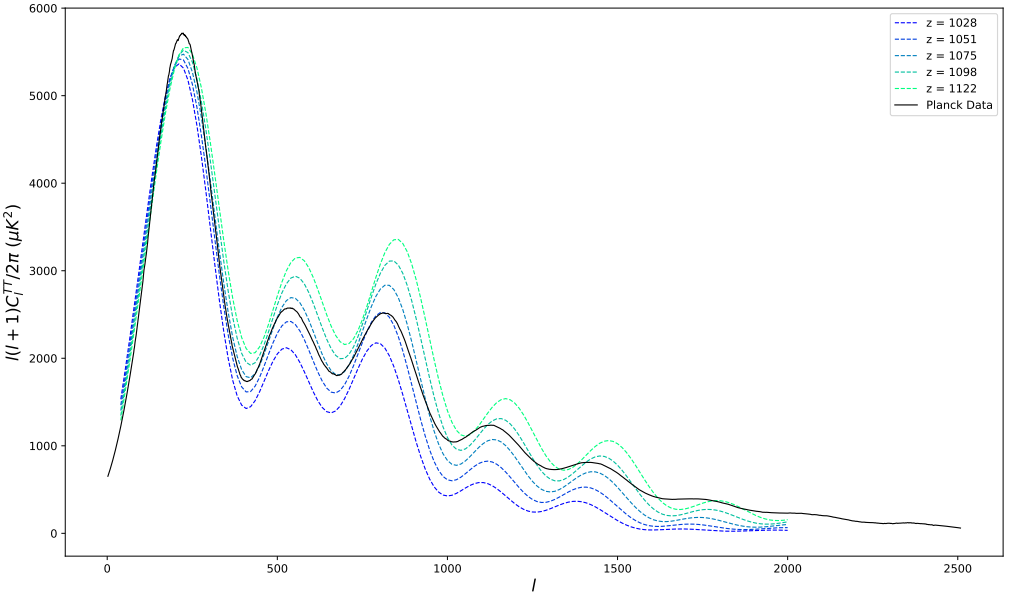

Figure E.3: TT CMB spectrum vs. z_{ls}.

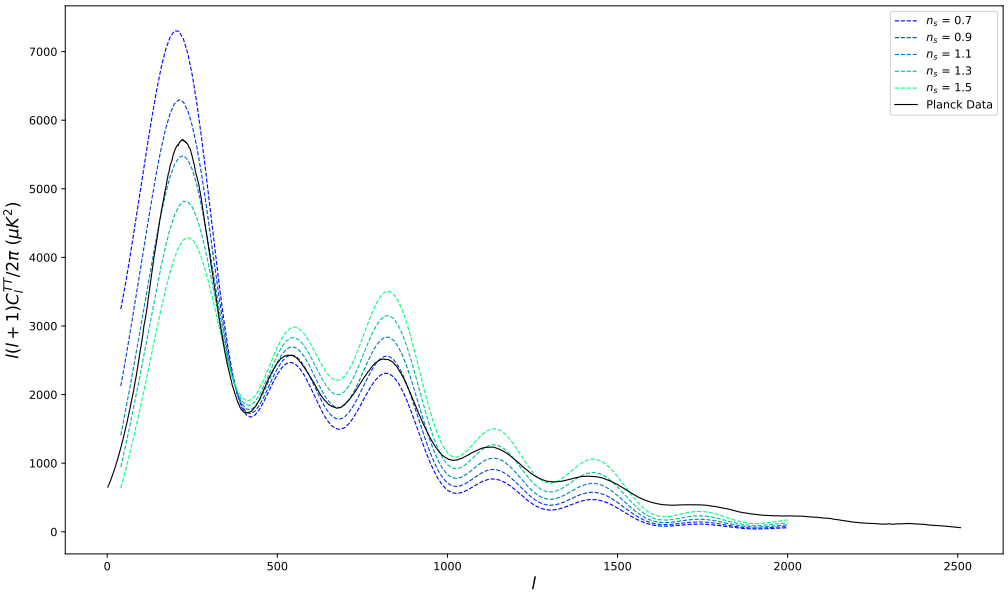

Figure E.4: TT CMB spectrum vs. n_s.

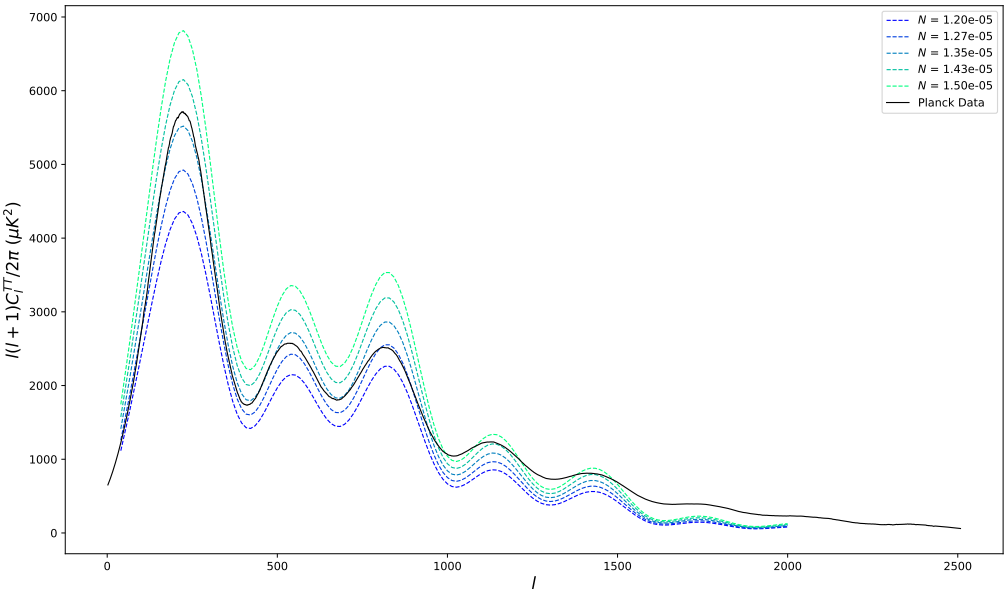

Figure E.5: TT CMB spectrum vs. N.

Appendix F

Table generator - Code

This code generates the tables from all the combinations given by the C, z_{ls} and $h^2\Omega_{b,0}^{DG}$ arrays.

```
# In[ ]:


import numpy as np
import csv
from tqdm import tqdm_notebook
from itertools import product
from joblib import Parallel, delayed
from scipy.optimize import fsolve, root_scalar, curve_fit
from scipy.integrate import quad, odeint, cumtrapz, quadrature
from scipy.misc import derivative
from scipy import interpolate
from matplotlib import pyplot as plt
plt.rcParams['figure.dpi']= 200


## PARAMETERS

# In[ ]:


array_z = np.linspace(900,1200,50)
array_C = np.linspace(0.0001,0.0009,60)
```

```
array_h2Ob = np.linspace(0.01,0.04,100)


# In[ ]:


with open("z.csv","w") as F1:
    writer = csv.writer(F1, delimiter=' ', lineterminator='\n')
    for i in tqdm_notebook(range(len(array_z))):
        writer.writerow([array_z[i]])


# In[ ]:


with open("C.csv","w") as F1:
    writer = csv.writer(F1, delimiter=' ', lineterminator='\n')
    for i in tqdm_notebook(range(len(array_C))):
        writer.writerow([array_C[i]])


# In[ ]:


with open("h2Ob.csv","w") as F1:
    writer = csv.writer(F1, delimiter=' ', lineterminator='\n')
    for i in tqdm_notebook(range(len(array_h2Ob))):
        writer.writerow([array_h2Ob[i]])


## $$\mathcal{l}_H$$

# In[ ]:
```

```
66
67
68 c = 299792.458 # light speed in km/s
69
70 T0 = 2.725 #Black Body Spectrum T CMB
71
72 Lfit = 0.45741271  # from SNe
73 hfit = 0.49638699  # from SNe
74
75 h2Og = 2.47*10**(-5) # photon density
76
77 # Mpc and km
78 mpc_to_km = 3.086*10**19
79 km_to_mpc = 3.24078*10**(-20)
80
81
82 # In[ ]:
83
84
85 #-----------------------------------------------
86
87 def EQ(Y,z,C,L):
88
89     return 1/(1+z) - Y_DG(Y,C,L)
90
91 #-----------------------------------------------
92
93 def F(Y,C,L):
94
95     value = - L*(Y/3)*np.sqrt(Y+C)
96
97     return  value
98
99 #-----------------------------------------------
100
101 def R_DG(Y,C,L):
102
103     try:
104
105         value = Y*np.sqrt( ( 1+F(Y,C,L) )/( 1+3*F(Y,C,L) ) )
106
107     except:
```

```
108
109         value = np.nan
110
111     return value
112
113 #-----------------------------------------------
114
115 def Y_solve(z,C,L):
116
117     outputs = fsolve(EQ, 0.3, args=(z,C,L),full_output=True,xtol=0.1)
118
119     if outputs[2] == 1:
120
121         return outputs[0]
122
123     else:
124
125         return np.nan
126
127 #-----------------------------------------------
128
129 def Y_DG(Y,C,L):
130
131     try:
132
133         value = R_DG(Y,C,L)/R_DG(1,C,L)
134
135     except:
136
137         value = np.nan
138
139     return value
140
141
142 # In[ ]:
143
144
145 def dt_dY(Y,C): # returns seconds
146
147     return np.sqrt(1+C)/(100*hfit)*Y/np.sqrt(Y+C)*mpc_to_km
148
149 #-----------------------------------
```

```
150 def dY_DGtodY(Y,C,L):
151
152     return derivative(Y_DG, args = (C,L), x0 = Y, dx = 1e-6)
153
154 #-------------------------------------------------------#
155
156 def H_DG(Y,C): #retorna en 1/s
157
158     return dY_DGtodY(Y,C,Lfit)/(dt_dY(Y,C)*Y_DG(Y,C,Lfit))
159
160
161 # In[ ]:
162
163
164 #---------------- DG Equations --------
165
166 def integrand_DG_sound(Y,C,h2Ob): # integration in seconds
167
168     R=3*h2Ob/(4*h2Og)*Y_DG(Y,C,Lfit)
169
170     integrand = dt_dY(Y,C)/(  Y_DG(Y,C,Lfit)*np.sqrt( 3*(1+R) )  )
171
172     return integrand
173
174 def dH_DG(Y,C,h2Ob): #returns in Mpc
175
176     return c*Y_DG(Y,C,Lfit)* \
177     (quad(integrand_DG_sound,0,Y,args=(C,h2Ob),epsrel=1))[0]/mpc_to_km
178
179 def integrand_DG(Y,C): # integration in seconds
180
181     integrand = Y/(np.sqrt(Y+C)*Y_DG(Y,C,Lfit))
182
183     return integrand
184
185 def da_DG(Y,C): # returns in Mpc
186
187     return Y_DG(Y,C,Lfit)*c*np.sqrt(1+C)/(100*hfit)* \
188     (quad(integrand_DG,Y,1,args=(C),epsrel=0.001)[0])
189
190 def theta_DG(C,z,h2Ob):
191
```

```
192     Y = float(Y_solve(z,C,Lfit))
193
194     num = dH_DG(Y,C,h2Ob)
195
196     den = da_DG(Y,C)
197
198     return num/den
199
200
201 # ## $$l_H$$
202
203 # In[ ]:
204
205
206 def lH(params):
207
208     z,C,h2Ob = params[0],params[1],params[2]
209
210     return 1/theta_DG(C,z,h2Ob)
211
212
213 # In[ ]:
214
215
216 paramlist=list(product(array_z,array_C,array_h2Ob))
217
218 results_lin = \
219 Parallel(n_jobs = 6)(delayed(lH)(e) for e in tqdm_notebook(paramlist))
220
221
222 # In[ ]:
223
224
225 k = 0
226
227 with open("lH.csv","w") as F1:
228
229     writer = csv.writer(F1, delimiter=' ', lineterminator='\n')
230
231     for i in tqdm_notebook(product(range(len(array_z)) \
232     ,range(len(array_C)),range(len(array_h2Ob))),\
233     total=len(array_z)*len(array_C)*len(array_h2Ob) ):
```

```
234
235             writer.writerow([i[0],i[1],i[2],float(results_lin[k])])
236
237             k += 1
238
239
240
241 # ## $$l_T$$
242
243 # In[ ]:
244
245
246 def lT(params):
247
248     z,C = params[0],params[1]
249
250     Y  = float(Y_solve(z,C,Lfit))
251
252     dT = np.divide(c*R_DG(Y,C,Lfit),100*hfit)*np.sqrt(C*(C+1))      # Mpc
253
254     dA = da_DG(Y,C)
255
256     return dA/dT
257
258
259 # In[ ]:
260
261
262 paramlist=list(product(array_z,array_C))
263
264 results_lin = Parallel(n_jobs = 6) (delayed(lT)(e) \
265 for e in tqdm_notebook(paramlist))
266
267
268 # In[ ]:
269
270
271 k = 0
272
273 with open("lT.csv","w") as F1:
274
275     writer=csv.writer(F1,delimiter=" ",lineterminator="\n",)
```

```
276
277     for i in tqdm_notebook(product(range(len(array_z)) \
278     ,range(len(array_C))),total=len(array_z)*len(array_C)):
279
280         writer.writerow([i[0],i[1],results_lin[k]])
281
282         k += 1
283
284
285 # ## $$l_R$$
286
287 # In[ ]:
288
289
290 def lR(params):
291
292     z,C = params[0],params[1]
293
294     kappaR = 0.05
295     Y  = float(Y_solve(z,C,Lfit))
296     dA = da_DG(Y,C)
297
298     return kappaR*dA/R_DG(Y,C,Lfit)
299
300
301 # In[ ]:
302
303
304 paramlist=list(product(array_z,array_C))
305
306 results_lin = \
307 Parallel(n_jobs = 6) (delayed(lR)(e) for e in tqdm_notebook(paramlist))
308
309
310 # In[ ]:
311
312
313 k = 0
314
315 with open("lR.csv","w") as F1:
316
317     writer=csv.writer(F1,delimiter=" ",lineterminator="\n",)
```

```
318
319     for i in tqdm_notebook(product(range(len(array_z)) \
320     ,range(len(array_C))),total=len(array_z)*len(array_C)):
321
322         writer.writerow([i[0],i[1],results_lin[k]])
323
324         k += 1
325
326
327 # In[ ]:
328
329
330 #---------- don = depends on ----------------
331
332 def z_don_T(T):
333
334     return T/T0 - 1
335
336 z_don_T = np.vectorize(z_don_T)
337
338 #--------------------------------------------
339
340 def T_don_z(z):
341
342     return T0*(1+z)
343
344 T_don_z = np.vectorize(T_don_z)
345
346 #--------------------------------------------
347
348 def Y_don_T(T,C):
349
350     YDG = T0/T
351
352     z = 1/YDG - 1
353
354     return Y_solve(z,C,Lfit)
355
356 #--------------------------------------------
357
358 def T_don_Y(Y,C):
359
```

```
360         return T0/Y_DG(Y,C,Lfit)
361 
362 
363 # ## $$l_D$$
364 
365 # In[ ]:
366 
367 
368 # Some constants:
369 
370 T_g = 2.725 # T CMB in K
371 
372 G = 6.67430*10**(-11) *100**3 # Gravitational constant cm^3 kg^-1 s^-2
373 
374 m_p = 1.6726219*10**(-27) # Proton mass kg
375 
376 Lambda_alpha = 1215.682*10**(-8) # cm
377 
378 frac = 0.76 # H fraction (vs He)
379 
380 Gamma_2s = 8.22458 # s^-1
381 
382 sigma_thomson = 0.66524*10**(-24)  # thomson cross section cm^2
383 
384 c = 2.99792458*10**10 # speed of light cm/s
385 
386 
387 # In[ ]:
388 
389 
390 def n(T,h2Ob):    # returns cm^-3  eq 2.3.29 Weinberg's book
391 
392     #return km_to_Mpc**2*frac*3*100**2*h2Ob/(8*np.pi*G*m_p)*(T/T_g)**3
393 
394     return 4.218*10**(-7)*h2Ob*T**3
395 #-----------------------------------------------------
396 
397 def alpha(T):  # returns en cm^3 s^-1 eq.2.3.31 Weinberg's book
398 
399     return 1.4377*10**(-10)*T**(-0.6166)/(1+5.085*10**(-3)*T**0.5300)
400 
401     #return 2.84*10**(-11)*T**(-1/2)
```

```
402
403 #-----------------------------------------------
404
405 def beta(T): # returns cm^-3 K^3/2 * alpha eq 2.3.32 Weinberg's book
406
407     return 2.4147*10**(15) *T**(3/2)*np.exp(-39474/T)*alpha(T)
408
409 #-----------------------------------------------
410
411 def S(T,h2Ob): # eq 2.3.8 Weinberg's book
412
413     return 1.747*10**(-22)*np.exp(157894/T)*T**(3/2)*h2Ob
414
415 #-----------------------------------------------
416
417 def model(X,T,h2Ob,C): # eq 2.3.27 Weinberg's book
418
419     # X is the fraction of H ionized
420     # T is the temperature
421
422     Y = Y_don_T(T,C)
423
424     Coef = 1 + beta(T)/(Gamma_2s + ( 8*np.pi*H_DG(Y,C) ) \
425     /( Lambda_alpha**3*n(T,h2Ob)*(1-X) ) )
426
427     N = alpha(T)*n(T,h2Ob)/(T*H_DG(Y,C))
428
429     dXdt = N*Coef**(-1)*(X**2-(1-X)/S(T,h2Ob))
430
431     return dXdt
432
433 #-----------------------------------------------
434
435 def equilibrium(X,T,h2Ob):
436
437     return X*(1+S(T,h2Ob)*X)-1
438
439 #-----------------------------------------------
440
441 def X_solver(T,h2Ob):
442
443     value=root_scalar(equilibrium,bracket=[0.9,3], \
```

```
444         method="brentq",args=(T,h2Ob),rtol=0.01)
445 
446         if value.root > 1:
447 
448             return 0.9999999
449 
450         else:
451 
452             return float(value.root)
453 
454     X_solver = np.vectorize(X_solver)
455 
456     #-----------------------------------------------
457 
458     temp = np.linspace(6000,1000,100)
459 
460     def solve_ode_DG(params):
461 
462         C,h2Ob = params[0],params[1]
463 
464         X0 = X_solver(6000,h2Ob)
465 
466         if h2Ob < 0:
467 
468             return np.full([len(temp)],np.nan)
469 
470         else:
471 
472             return odeint(model,X0,temp,args=(h2Ob,C),rtol=0.0000001)
473 
474 
475     # In[ ]:
476 
477 
478     paramlist=list(product(array_C,array_h2Ob))
479 
480     results_lin = Parallel(n_jobs = 4) \
481     (delayed(solve_ode_DG)(e) for e in tqdm_notebook(paramlist))
482 
483 
484     # In[ ]:
485 
```

```
486
487 k = 0
488
489 with open("sol_ode_DG.csv","w") as F1:
490
491     writer = csv.writer(F1, delimiter=' ', lineterminator='\n')
492
493     for i in tqdm_notebook(product(range(len(array_C)) \
494     ,range(len(array_h2Ob))),total=len(array_C)*len(array_h2Ob) ):
495
496         writer.writerow(results_lin[k].reshape(100))
497
498         k += 1
499
500
501 # In[ ]:
502
503
504 with open("sol_ode_DG.csv", "r") as F1:
505
506     lines1 = F1.readlines()
507
508
509 # In[ ]:
510
511 k = 0
512
513 arreglo_sol_ode_DG = []
514
515 for i in tqdm_notebook(lines1):
516
517     temp = np.fromstring(i, dtype=float, sep=' ')
518     arreglo_sol_ode_DG.append(temp)
519
520 # In[ ]:
521
522
523 def calc_vis_fun(C,h2Ob,array_X_DG):
524
525     if h2Ob < 0:
526
527         return np.full([98],np.nan),np.full([98],np.nan)
```

```
528
529     else:
530
531         temp = np.linspace(6000,1000,100)
532
533         temp = np.reshape(temp,100)
534
535         temp =  temp.tolist() + [800,600,400,200,0]
536
537         array_X_DG = np.reshape(array_X_DG,100)
538
539         array_X_DG = array_X_DG.tolist() + [0,0,0,0,0]
540
541         X_funcion = interpolate.interp1d(temp, array_X_DG, kind='quadratic')
542
543         def integrand(T):
544
545             Y = Y_don_T(T,C)
546
547             return c*sigma_thomson*X_funcion(T)*n(T,h2Ob)/(T*H_DG(Y,C))
548
549         integrand = np.vectorize(integrand)
550
551         def function(integral):
552
553             if integral > 12:
554
555                 return 1
556
557             else:
558
559                 return 1 - np.exp(-integral)
560
561         function = np.vectorize(function)
562
563         A1=np.linspace(1000,1999,50)
564
565         A2= np.linspace(2000,4000,300)
566
567         A3= np.linspace(4001,6000,100)
568
569         T_array_0 = np.concatenate((A1,A2,A3))
```

```
570
571         integral = cumtrapz(integrand(T_array_0),T_array_0)
572
573         integral = np.insert(integral,0,0,axis=0)
574
575         O = interpolate.interp1d(T_array_0,function(integral),kind='quadratic')
576
577         def dOdT(T):
578
579             return float(derivative(O, x0 = T, dx = 1e-6))
580
581         dOdT = np.vectorize(dOdT)
582
583         B1=np.linspace(1000,2000,7)
584
585         B2= np.linspace(2001,4000,86)
586
587         B3= np.linspace(4001,6000,7)
588
589         T_array = np.concatenate((B1,B2,B3))
590
591         return T_array[1:99],dOdT(T_array[1:99])
592
593
594 # In[ ]:
595
596
597 def cuadratica(x,a0,b0,c0):
598
599     return a0*x**2+b0*x+c0
600
601
602 # In[ ]:
603
604
605 sigma_array = np.full((len(array_C),len(array_h2Ob)),np.nan)
606
607
608 # In[ ]:
609
610
611 def sigma_f(i):
```

```
612
613     C = array_C[int(i[0])]
614     h2Ob = array_h2Ob[int(i[1])]
615     fila = int(i[0])*len(array_h2Ob)+int(i[1])
616
617     # fila is the index associated with i[0],i[1],i[2].
618     # This order matchs with the output's product
619
620     array_X_DG = arreglo_sol_ode_DG[fila]
621
622     if np.isnan(np.sum(array_X_DG)):
623
624         return np.nan
625
626     else:
627
628         eje_T,eje_dOdT = calc_vis_fun(C,h2Ob,array_X_DG)
629
630         peak=np.where(np.nanmax(eje_dOdT) == eje_dOdT)[0]
631
632         near_x = eje_T[int(peak)-2:int(peak)+3]
633         near_y = eje_dOdT[int(peak)-2:int(peak)+3]
634
635         popt, pcov = curve_fit(cuadratica,near_x,near_y)
636
637         value = -popt[1]/(2*popt[0])
638
639         return float(1/(np.sqrt(2*np.pi)*cuadratica(value,*popt)))
640
641
642 # In[ ]:
643
644
645 for p in tqdm_notebook(product(range(len(array_C)) \
646 ,range(len(array_h2Ob))),total=len(array_C)*len(array_h2Ob)):
647
648     i = list([p[0],p[1]])
649
650     sigma_array[p[0]][p[1]] = sigma_f(i)
651
652
653
```

```
654 # In[ ]:
655
656
657 k = 0
658
659 with open("sigma.csv","w") as F1:
660
661     writer = csv.writer(F1, delimiter=' ', lineterminator='\n')
662
663     for i in tqdm_notebook(product(range(len(array_C)) \
664     ,range(len(array_h2Ob))),total=len(array_C)*len(array_h2Ob) ):
665
666         writer.writerow([i[0],i[1],sigma_array[i[0]][i[1]]])
667
668         k += 1
669
670
671 # In[ ]:
672
673 # lines2[fila]  is equivalent to, for example: sigma_array[100,34,23]
674
675 with open("sigma.csv", "r") as F2:
676
677     lines2 = F2.readlines()
678
679
680 # In[ ]:
681
682 k = 0
683
684 # for example: arreglo_sigma[int(100)*len(array_C)*len(array_ht2Ob) ...
685 # +int(34)*len(array_ht2Ob)+int(23)] == sigma_array[100][34][23]
686
687 arreglo_sigma = []
688
689 for i in tqdm_notebook(lines2):
690     temp = np.fromstring(i, dtype=float, sep=' ')[2]
691     arreglo_sigma.append(temp)
692
693 # ## SILK
694
695 # In[ ]:
```

```
696
697
698 c = 299792458 # m/s
699 sigma_thomson = 6.652458*10**(-29)  #m^2
700 m_to_mpc = 3.24078*10**(-23)
701
702 def silk_damping2(z,C,h2Ob,temp,array_X_DG):
703
704     X_frac=interpolate.interp1d(temp,array_X_DG)
705
706     def R(Y):
707
708         return 3*h2Ob/(4*h2Og)*Y_DG(Y,C,Lfit)
709
710     def factor(Y):
711
712         return float(dt_dY(Y,C) \
713         /(Y_DG(Y,C,Lfit)**2*(1+R(Y)))*(16/15+R(Y)**2/(1+R(Y))))
714
715     def nelectron(Y): # 1/m^3
716
717         T=T_don_Y(Y,C)
718
719         if T>5999:
720
721             return 1*n(T,h2Ob)*10**6
722
723         else:
724
725             return float(X_frac(T))*n(T,h2Ob)*10**6
726
727     def tgamma(Y): # s
728
729         return float(1/(sigma_thomson*c*nelectron(Y)))
730
731     def integrand(Y):
732
733         return tgamma(Y)*factor(Y)
734
735     integrand = np.vectorize(integrand)
736
737     YDG = 1/(1+z)
```

```
738
739         val = c**2*YDG**2/6* \
740         quadrature(integrand,0,float(Y_solve(z,C,Lfit)), \
741         rtol=10**(-4),maxiter=100)[0]*m_to_mpc**2
742
743         # error is approx 0.014% with rtol = E-5
744
745         return val
746
747
748 # ## Landau
749
750 # In[ ]:
751
752
753 def d_landau2(z,C,h2Ob,sigma_T): # Landau Damping in Mpc^2
754
755         Y = Y_solve(z,C,Lfit)
756
757         R = 3*float(h2Ob)/(4*h2Og)*Y_DG(Y,C,Lfit)
758
759         T = T_don_z(z)
760
761         sigma_t = sigma_T/(T*H_DG(Y,C))
762         # it comes from sigmat/dt = sigmaT/dT    dt/dT = YDG*dYDG/dT*dt/dYDG/YDG
763
764         return float(c**2*sigma_t**2/(6*(1+R))*m_to_mpc**2)
765
766
767 # In[ ]:
768
769
770 def l_D(z,C,d_D):
771
772         Y=float(Y_solve(z,C,Lfit))
773
774         dA = da_DG(Y,C)/1000
775
776         return dA/d_D
777
778
779 # ## Damping total
```

```
780
781 # In[ ]:
782
783
784 Damping_Total = []
785 array_lD = np.full((len(array_z),len(array_C),len(array_h2Ob)),np.nan)
786 array_D = np.full((len(array_z),len(array_C),len(array_h2Ob)),np.nan)
787
788 temp = np.linspace(6000,1000,100)
789
790 for i in tqdm_notebook(product(range(len(array_z)) \
791 ,range(len(array_C)),range(len(array_h2Ob))), \
792 total=len(array_z)*len(array_C)*len(array_h2Ob) ):
793
794     z = array_z[i[0]]
795     C = array_C[i[1]]
796     h2Ob = array_h2Ob[i[2]]
797
798     fila = int(i[1])*len(array_h2Ob)+int(i[2])
799
800     array_X_DG = arreglo_sol_ode_DG[fila]
801     sigma_T = arreglo_sigma[fila]
802
803     Silk_2    = silk_damping2(z,C,h2Ob,temp,array_X_DG)
804     Landau_2 = d_landau2(z,C,h2Ob,sigma_T)
805
806     array_D[i[0],i[1],i[2]] = np.sqrt( Silk_2+Landau_2 )
807
808     array_lD[i[0],i[1],i[2]] = l_D(z,C,array_D[i[0],i[1],i[2]])
809
810
811
812
813 # In[ ]:
814
815
816 k = 0
817
818 with open("array_D.csv","w") as F1:
819
820     writer = csv.writer(F1, delimiter=' ', lineterminator='\n')
821
```

```
822     for i in tqdm_notebook(product(range(len(array_z)) \
823     ,range(len(array_C)) \
824     ,range(len(array_h2Ob))),total=len(array_z)*len(array_C)*len(array_h2Ob) ):
825 
826         writer.writerow([i[0],i[1],i[2],array_D[i[0]][i[1]][i[2]]])
827 
828         k += 1
829 
830 
831 # In[ ]:
832 
833 
834 k = 0
835 
836 with open("lD.csv","w") as F1:
837 
838     writer = csv.writer(F1, delimiter=' ', lineterminator='\n')
839 
840     for i in tqdm_notebook(product(range(len(array_z)), \
841     range(len(array_C)),range(len(array_h2Ob))), \
842     total=len(array_z)*len(array_C)*len(array_h2Ob) ):
843 
844         writer.writerow([i[0],i[1],i[2],array_lD[i[0]][i[1]][i[2]]])
845 
846         k += 1
847 
848 
849 # In[ ]:
850 
851 
852 # for example: fila =
853 # int(100)*len(array_C)*len(array_ht2Omegab)
854 # +int(34)*len(array_ht2Omegab)+int(23)
855 # is equivalent to lines2[fila] ---> sigma_array[100,34,23]
856 
857 with open("lD.csv", "r") as F1:
858 
859     lines3 = F1.readlines()
860 
861 
862 # In[ ]:
863 
```

```
k = 0

arreglo_l_D = []

for i in tqdm_notebook(lines3):
    temp = np.fromstring(i, dtype=float, sep=' ')[3]
    arreglo_l_D.append(temp)


## PARAMETRO $$R_L$$

# In[ ]:


array_RL = np.full((len(array_z),len(array_C),len(array_h2Ob)),np.nan)

for i in tqdm_notebook(product(range(len(array_z)) \
,range(len(array_C)),range(len(array_h2Ob))), \
total=len(array_z)*len(array_C)*len(array_h2Ob) ):

    z = array_z[i[0]]
    C = array_C[i[1]]
    h2Ob = array_h2Ob[i[2]]

    Y = Y_solve(z,C,Lfit)

    array_RL[i[0],i[1],i[2]] = 3*float(h2Ob)/(4*h2Og)*Y_DG(Y,C,Lfit)


# In[ ]:


k = 0

with open("RL.csv","w") as F1:

    writer = csv.writer(F1, delimiter=' ', lineterminator='\n')

    for i in tqdm_notebook(product(range(len(array_z)) \
    ,range(len(array_C)),range(len(array_h2Ob))), \
    total=len(array_z)*len(array_C)*len(array_h2Ob) ):

```

```
906             writer.writerow([i[0],i[1],i[2],array_RL[i[0]][i[1]][i[2]]])
907 
908             k += 1
909 
910 
911 # ## $Z_{ls}$
912 
913 # In[ ]:
914 
915 
916 # Some constants:
917 
918 T_g = 2.725 # T CMB in K
919 
920 G = 6.67430*10**(-11) *100**3 # Gravitational constant cm^3 kg^-1 s^-2
921 
922 m_p = 1.6726219*10**(-27) # Proton mass kg
923 
924 Lambda_alpha = 1215.682*10**(-8) # cm
925 
926 frac = 0.76 # H fraction (vs He)
927 
928 Gamma_2s = 8.22458 # s^-1
929 
930 sigma_thomson = 0.66524*10**(-24)  # thomson cross section cm^2
931 
932 c = 2.99792458*10**10 # speed of light cm/s
933 
934 
935 # In[ ]:
936 
937 
938 def n(T,h2Ob):    # returns cm^-3  eq 2.3.29 Weinberg's book
939 
940     #return km_to_Mpc**2*frac*3*100**2*h2Ob/(8*np.pi*G*m_p)*(T/T_g)**3
941 
942     return 4.218*10**(-7)*h2Ob*T**3
943 #-----------------------------------------------
944 
945 def alpha(T):  # returns en cm^3 s^-1 eq.2.3.31 Weinberg's book
946 
947     return 1.4377*10**(-10)*T**(-0.6166)/(1+5.085*10**(-3)*T**0.5300)
```

```
948
949     #return 2.84*10**(-11)*T**(-1/2)
950
951 #-----------------------------------------------
952
953 def beta(T): # returns cm^-3 K^3/2 * alpha eq 2.3.32 Weinberg's book
954
955     return 2.4147*10**(15) *T**(3/2)*np.exp(-39474/T)*alpha(T)
956
957 #-----------------------------------------------
958
959 def S(T,h2Ob): # eq 2.3.8 Weinberg's book
960
961     return 1.747*10**(-22)*np.exp(157894/T)*T**(3/2)*h2Ob
962
963 #-----------------------------------------------
964
965 def model(X,T,h2Ob,C): # eq 2.3.27 Weinberg's book
966
967     # X is the fraction of H ionized
968     # T is the temperature
969
970     Y = Y_don_T(T,C)
971
972     Coef = 1 + beta(T)/(Gamma_2s + ( 8*np.pi*H_DG(Y,C) ) \
973     /( Lambda_alpha**3*n(T,h2Ob)*(1-X) ) )
974
975     N = alpha(T)*n(T,h2Ob)/(T*H_DG(Y,C))
976
977     dXdt = N*Coef**(-1)*(X**2-(1-X)/S(T,h2Ob))
978
979     return dXdt
980
981 #-----------------------------------------------
982
983 def equilibrium(X,T,h2Ob):
984
985     return X*(1+S(T,h2Ob)*X)-1
986
987 #-----------------------------------------------
988
989 def X_solver(T,h2Ob):
```

```
990
991         value=root_scalar(equilibrium,bracket=[0.9,3],method="brentq", \
992         args=(T,h2Ob),rtol=0.01)
993
994         if value.root > 1:
995
996             return 0.9999999
997
998         else:
999
1000            return float(value.root)
1001
1002    X_solver = np.vectorize(X_solver)
1003
1004    #-----------------------------------------------
1005
1006    temp = np.linspace(6000,1000,100)
1007
1008    def solve_ode_DG(C,h2Ob):
1009
1010        X0 = X_solver(6000,h2Ob)
1011
1012        if h2Ob < 0:
1013
1014            return np.full([len(temp)],np.nan)
1015
1016        else:
1017
1018            return odeint(model,X0,temp,args=(h2Ob,C),rtol=0.0000001)
1019
1020
1021    # In[ ]:
1022
1023
1024    # we chose $C$ and $h^2 \Omega_{b,0}^{DG}$ from the MCMC results
1025
1026    X_sol = solve_ode_DG(0.00045577097697686473,0.026379909222130012)
1027
1028
1029    # In[ ]:
1030
1031
```

```
1032 fig,ax1 = plt.subplots(figsize=(9, 6))
1033
1034 ax2 = ax1.twiny()
1035
1036 X = temp
1037
1038 Y = X_sol
1039
1040 ax1.plot(X,Y)
1041 ax1.set_xlabel(r"$T$ (K)")
1042 ax1.set_ylabel(r"X")
1043
1044
1045 new_tick_locations = np.linspace(1000,6000,6)
1046
1047 def tick_function(X):
1048     V = z_don_T(X)
1049
1050     return ["%d" % z for z in V]
1051
1052 ax2.set_xlim(ax1.get_xlim())
1053 ax2.set_xticks(new_tick_locations)
1054 ax2.set_xticklabels(tick_function(new_tick_locations))
1055 ax2.set_xlabel(r"Redshift $z$")
1056 fig.savefig('X_de_T.pdf')
1057 plt.show()
1058
1059
1060 # In[ ]:
1061
1062
1063 def calc_vis_fun(C,h2Ob,array_X_DG):
1064
1065     if h2Ob < 0:
1066
1067         return np.full([98],np.nan),np.full([98],np.nan)
1068
1069     else:
1070
1071         temp = np.linspace(6000,1000,100)
1072
1073         temp = np.reshape(temp,100)
```

```
1074
1075        temp =  temp.tolist() + [800,600,400,200,0]
1076
1077        array_X_DG = np.reshape(array_X_DG,100)
1078
1079        array_X_DG = array_X_DG.tolist() + [0,0,0,0,0]
1080
1081        X_funcion = interpolate.interp1d(temp, array_X_DG, kind='quadratic')
1082
1083        def integrand(T):
1084
1085            Y = Y_don_T(T,C)
1086
1087            return c*sigma_thomson*X_funcion(T)*n( T, h2Ob )/(T*H_DG(Y,C))
1088
1089        integrand = np.vectorize(integrand)
1090
1091        def function(integral):
1092
1093            if integral > 12:
1094
1095                return 1
1096
1097            else:
1098
1099                return 1 - np.exp(-integral)
1100
1101        function = np.vectorize(function)
1102
1103        A1=np.linspace(1000,1999,50)
1104
1105        A2= np.linspace(2000,4000,300)
1106
1107        A3= np.linspace(4001,6000,100)
1108
1109        T_array_0 = np.concatenate((A1,A2,A3))
1110
1111        integral = cumtrapz(integrand(T_array_0),T_array_0)
1112
1113        integral = np.insert(integral,0,0,axis=0)
1114
1115       O = interpolate.interp1d(T_array_0,function(integral),kind='quadratic')
```

```
1116
1117            def dOdT(T):
1118
1119                return float(derivative(O, x0 = T, dx = 1e-6))
1120
1121            dOdT = np.vectorize(dOdT)
1122
1123            B1=np.linspace(1000,2000,7)
1124
1125            B2= np.linspace(2001,4000,86)
1126
1127            B3= np.linspace(4001,6000,7)
1128
1129            T_array = np.concatenate((B1,B2,B3))
1130
1131            return T_array[1:99],dOdT(T_array[1:99])
1132
1133
1134 # In[ ]:
1135
1136
1137 X,Y = calc_vis_fun(0.00045577097697686473,0.026379909222130012,X_sol)
1138
1139
1140 # In[ ]:
1141
1142
1143 def normal_dist(x,sigma,mu):
1144
1145     return 1/(sigma*np.sqrt(2*np.pi))*np.exp(-(x-mu)**2/(2*sigma**2))
1146
1147 normal_dist = np.vectorize(normal_dist)
1148
1149
1150 # In[ ]:
1151
1152
1153 mu = X[np.where(np.max(Y)== Y)[0][0]]  # T peak
1154 sigma = 1/(np.max(Y)*np.sqrt(2*np.pi))  # T sigma
1155
1156
1157 # In[ ]:
```

```
1158
1159
1160 fig,ax1 = plt.subplots(figsize=(9, 6))
1161
1162 ax2 = ax1.twiny()
1163
1164 ax1.plot(X,Y,label = 'DG visibility function')
1165 ax1.plot(X, normal_dist(X,sigma,mu), \
1166 label = 'Normal distribution: T = 2942 K and $\sigma_T$ = 244 K ')
1167 ax1.set_xlabel(r"$T$ (K)")
1168
1169 new_tick_locations = np.linspace(1000,6000,6)
1170
1171 def tick_function(X):
1172
1173     V = z_don_T(X)
1174
1175     return ["%d" % z for z in V]
1176
1177 ax2.set_xlim(ax1.get_xlim())
1178 ax2.set_xticks(new_tick_locations)
1179 ax2.set_xticklabels(tick_function(new_tick_locations))
1180 ax2.set_xlabel(r"Redshift $z$")
1181
1182 ax1.legend()
1183
1184 fig.savefig('Vis_fun.pdf')
1185 plt.show()
1186
1187
1188 # In[ ]:
1189
1190
1191 print("Redshift of the peak position: ",z_don_T(X[np.where(np.max(Y)== Y)[0][0]]))
1192
1193
1194 # In[ ]:
1195
1196
1197 print("Temperature of the peak position: ",X[np.where(np.max(Y)== Y)[0][0]])
1198
1199
```

```
1200 # In[ ]:
1201
1202
1203 print("Peak maximum: ",Y[np.where(np.max(Y) == Y)[0][0]])
1204
1205
1206 # In[ ]:
1207
1208
1209 print("Temperature standard deviation: ",sigma)
1210
1211
1212 # In[ ]:
```

Listing F.1: The code to generates the tables

Appendix G

Adaptative Metropolis MCMC - Code

The code read the tables generated in F to run the adaptative Metropolis MCMC algorithm. This code runs executing $result = mcmc_complex(N, M)$, where N is the total number of steps, and M is the whole parallel MCMC processes that the user wants to run. This function returns this object: $[z_chain, C_chain, h2Ob_chain, ns_chain, N_chain]$, where the user can access to every chain and step.

```
import numpy as np
import matplotlib.pyplot as plt
from scipy.signal import savgol_filter
from scipy.interpolate import interp1d, RegularGridInterpolator
from tqdm import tqdm_notebook
from itertools import product
from scipy.optimize import root_scalar, fsolve, curve_fit
from scipy.integrate import odeint, cumtrapz, quad
from scipy.misc import derivative
from scipy import interpolate
import random
import itertools

def Tk(k):

    return np.log(1+(0.124*k)**2)/(0.124*k)**2* \
    np.sqrt((1+(1.257*k)**2+(0.4452*k)**4+(0.2197*k)**6)   \
    /(1+(1.606*k)**2+(0.8568*k)**4+(0.3927*k)**6))

```

```
20 def Sk(k):
21
22     return ((1+(1.209*k)**2+(0.5116*k)**4+np.sqrt(5)* \
23     (0.1657*k)**6)/(1+(0.9459*k)**2+(0.4249*k)**4+(0.1657*k)**6))**2
24
25 def Dk(k):
26
27     return np.power(((0.1585*k)**2+(0.9702*k)**4+ \
28     (0.2460*k)**6)/(1+(1.180*k)**2+(1.540*k)**4
29     +(0.9230*k)**6+(0.4197*k)**8),1/4)
30
31 T0 = 2.725 #T CMB
32 R_ion = 0.80209 # reionization parameter
33
34 def factor1(beta,l,lR,ns):
35     return np.power((beta*l/lR),ns-1)
36
37 def factor2(beta,l,lH,lT,lD,RL):
38     return 1/(beta**2*np.sqrt(beta**2-1))* \
39     (3*Tk(beta*l/lT)*RL-np.power(1+RL,-1/4)*Sk(beta*l/lT)* \
40     np.exp(-beta**2*l**2/lD**2)*np.cos(beta*l/lH+Dk(beta*l/lT)))**2
41
42 def factor3(beta,l,lH,lT,lD,RL):
43     return 3*np.sqrt(beta**2-1)/(beta**4*np.power(1+RL,3/2))* \
44     np.exp(-2*beta**2*l**2/lD**2)* \
45     Sk(beta*l/lT)**2*np.sin(beta*l/lH+Dk(beta*l/lT))**2
46
47 def integrand(beta,l,lH,lT,lR,lD,RL,ns):
48
49     return factor1(beta,l,lR,ns) \
50     *(factor2(beta,l,lH,lT,lD,RL)+factor3(beta,l,lH,lT,lD,RL))
51
52 def integration(l,lH,lT,lR,lD,RL,ns,N):
53
54     resultado_integral = \
55     quad(integrand, 1, 10 ,args=(l,lH,lT,lR,lD,RL,ns) \
56     ,epsrel=0.001,full_output=True )
57
58     try:
59
60         resultado_integral[3]
61
```

```
62          return np.nan
63
64      except:
65
66          pass
67
68      if np.isnan(resultado_integral[0]):
69
70          return np.nan
71
72      return R_ion*4*np.pi*T0**2*N**2/25*resultado_integral[0]*10**(12)
73
74  multipoles = np.concatenate((np.linspace(40,180,6), \
75  np.linspace(190,248,5),np.linspace(256,380,5) \
76  ,np.linspace(381,950,20),np.linspace(1000,2000,20)))
77
78  integration = np.vectorize(integration)
79
80  # read the Planck data
81  data = np.loadtxt('COM_PowerSpect_CMB-TT-full_R3.01.txt',dtype=float)
82  l,TT,TT_min,TT_max = data[:,0],data[:,1],data[:,2],data[:,3]
83
84  #smooth the data with a Savitzky-Gola filter
85  TT_planck_filtered = savgol_filter(TT, 151,2)
86  # window size 151, polynomial order 2
87
88  TT_planck_interp = interp1d(l,TT_planck_filtered)
89
90  # These points will be used to evaluate the error in th MCMC
91  TT_planck_obs = TT_planck_interp(multipoles)
92
93  with open("z.csv", "r") as F1:
94
95      lines = F1.readlines()
96
97  array_z = np.full(len(lines),np.nan)
98
99  for i in range(len(lines)):
100
101     array_z[i] = np.fromstring(lines[i], dtype=float, sep=' ')[0]
102
103 with open("C.csv", "r") as F1:
```

```
104
105     lines = F1.readlines()
106
107 array_C = np.full(len(lines),np.nan)
108
109 for i in range(len(lines)):
110
111     array_C[i] = np.fromstring(lines[i], dtype=float, sep=' ')[0]
112
113 with open("h2Ob.csv", "r") as F1:
114
115     lines = F1.readlines()
116
117 array_h2Ob = np.full(len(lines),np.nan)
118
119 for i in range(len(lines)):
120
121     array_h2Ob[i] = np.fromstring(lines[i], dtype=float, sep=' ')[0]
122
123 with open("lH.csv", "r") as F1: # depends on z,C,array_ht2Ob
124
125     lines = F1.readlines()
126
127 array_lH = np.full((len(array_z) \
128 ,len(array_C),len(array_h2Ob)),np.nan)
129
130 for p in tqdm_notebook(product(range(len(array_z)) \
131 ,range(len(array_C)),range(len(array_h2Ob))),  \
132 total=len(array_z)*len(array_C)*len(array_h2Ob)):
133
134     fila = int(p[0])*len(array_C)* \
135     len(array_h2Ob)+int(p[1])*len(array_h2Ob)+int(p[2])
136
137     array_lH[p[0],p[1],p[2]] = \
138     np.fromstring(lines[fila], dtype=float, sep=' ')[3]
139
140 with open("lT.csv", "r") as F1:  # depends on z,C
141
142     lines = F1.readlines()
143
144 array_lT = np.full((len(array_z),len(array_C)),np.nan)
145
```

```
146 for p in tqdm_notebook(product(range(len(array_z)) \
147 ,range(len(array_C)) ),total=len(array_z)*len(array_C)):
148
149
150     fila = int(p[0])*len(array_C)+int(p[1])
151
152     array_lT[p[0],p[1]] = \
153     np.fromstring(lines[fila], dtype=float, sep=' ')[2]
154
155 with open("lR.csv", "r") as F1:  # depends on z,C
156
157     lines = F1.readlines()
158
159 array_lR = np.full((len(array_z),len(array_C)),np.nan)
160
161 for p in tqdm_notebook(product(range(len(array_z)) \
162 ,range(len(array_C))),total=len(array_z)*len(array_C)):
163
164     fila = int(p[0])*len(array_C)+int(p[1])
165
166     array_lR[p[0],p[1]] = \
167     np.fromstring(lines[fila], dtype=float, sep=' ')[2]
168
169 with open("lD.csv", "r") as F1: # depends on z,C,array_ht2Ob
170
171     lines = F1.readlines()
172
173 array_lD = np.full((len(array_z),len(array_C) \
174 ,len(array_h2Ob)),np.nan)
175
176 for p in tqdm_notebook(product(range(len(array_z)), \
177 range(len(array_C)),range(len(array_h2Ob))) \
178 ,total=len(array_z)*len(array_C)*len(array_h2Ob)):
179
180     fila = int(p[0])*len(array_C)*len(array_h2Ob) \
181     +int(p[1])*len(array_h2Ob)+int(p[2])
182
183     array_lD[p[0],p[1],p[2]] = \
184     np.fromstring(lines[fila], dtype=float, sep=' ')[3]
185
186 with open("Rl.csv", "r") as F1: # depends on z,C,array_ht2Ob
187
```

```
188     lines = F1.readlines()
189
190 array_Rl = np.full((len(array_z) \
191 ,len(array_C),len(array_h2Ob)),np.nan)
192
193 for p in tqdm_notebook(product(range(len(array_z)) \
194 ,range(len(array_C)),range(len(array_h2Ob))), \
195 total=len(array_z)*len(array_C)*len(array_h2Ob)):
196
197     fila = int(p[0])*len(array_C)*len(array_h2Ob) \
198     +int(p[1])*len(array_h2Ob)+int(p[2])
199
200     array_Rl[p[0],p[1],p[2]] = \
201     np.fromstring(lines[fila], dtype=float, sep=' ')[3]
202
203 # we define the interpolations in multiple dimensions
204
205 interp_lH = \
206 RegularGridInterpolator((array_z, array_C, array_h2Ob), array_lH)
207 interp_lT = RegularGridInterpolator((array_z, array_C), array_lT)
208 interp_lR = RegularGridInterpolator((array_z, array_C), array_lR)
209 interp_lD = \
210 RegularGridInterpolator((array_z, array_C, array_h2Ob), array_lD)
211 interp_Rl = \
212 RegularGridInterpolator((array_z, array_C, array_h2Ob), array_Rl)
213
214 Lfit = 0.45741271
215 hfit = 0.49638699
216 # conversion de Mpc to km
217 mpc_to_km = 3.086*10**19
218 km_to_mpc = 3.24078*10**(-20)
219
220 #-----------------------------------------------
221
222 def EQ(Y,z,C,L):
223
224     return 1/(1+z) - Y_DG(Y,C,L)
225
226 #-----------------------------------------------
227
228 def F(Y,C,L):
229
```

```
230     value = - L*(Y/3)*np.sqrt(Y+C)
231
232     return  value
233
234 #-----------------------------------------------
235
236 def R_DG(Y,C,L):
237
238     try:
239
240         value = Y*np.sqrt( ( 1+F(Y,C,L) )/( 1+3*F(Y,C,L) ) )
241
242     except:
243
244         value = np.nan
245
246     return value
247
248 #-----------------------------------------------
249
250 def Y_solve(z,C,L):
251
252     outputs = fsolve(EQ, 0.3, args=(z,C,L),full_output=True,xtol=0.1)
253
254     if outputs[2] == 1:
255
256         return outputs[0]
257
258     else:
259
260         return np.nan
261
262 #-----------------------------------------------
263
264 def Y_DG(Y,C,L):
265
266     try:
267
268         value = R_DG(Y,C,L)/R_DG(1,C,L)
269
270     except:
271
```

```
272             value = np.nan
273
274         return value
275
276 def dt_dY(Y,C): #lo retorna en s
277
278         return 1/(100*hfit*np.sqrt(1+C))*Y/np.sqrt(Y+C)*mpc_to_km
279
280 #-------------------------------------
281 def dY_DGtodY(Y,C,L):
282
283         return derivative(Y_DG, args = (C,L), x0 = Y, dx = 1e-6)
284
285 #-------------------------------------------------------#
286
287 def H_DG(Y,C): # 1/s
288
289         return dY_DGtodY(Y,C,Lfit)/(dt_dY(Y,C)*Y_DG(Y,C,Lfit))
290
291 #---------- don = depends on ----------------
292
293 def z_don_T(T):
294
295         return T/T_g - 1
296
297 z_don_T = np.vectorize(z_don_T)
298
299 #-----------------------------------------
300
301 def Y_don_T(T,C):
302
303         YDG = T0/T
304
305         z = 1/YDG - 1
306
307         return Y_solve(z,C,Lfit)
308
309 # we include the calculation of the visibility
310 # function to obtain a better fit associated
311 # to z. z is going to be constrained by the
312 # peak of the visibility function.
313 # to do this we have to include
```

```
314 # solve_ode_DG and calc_vis_fun
315
316 T_g = 2.725 # T CMB in K
317
318 G = 6.67430*10**(-11) *100**3 #  G: cm^3 kg^-1 s^-2
319
320 m_p = 1.6726219*10**(-27) # proton mass: kg
321
322 Lambda_alpha = 1215.682*10**(-8) # cm
323
324 frac = 0.76
325
326 Gamma_2s = 8.22458 # s^-1
327
328 sigma_thomson = 0.66524*10**(-24)  # thomson cross section cm^2
329
330 c = 2.99792458*10**10 # speed of light cm/s
331
332 #Black Body Spectrum T CMB
333 T0 = 2.725
334
335 def n(T,h2Ob):    #  cm^-3  eq 2.3.29 Weinberg's book
336
337     #return km_to_Mpc**2*frac*3*100**2*h2Ob/(8*np.pi*G*m_p)*(T/T_g)**3
338
339     return 4.218*10**(-7)*h2Ob*T**3
340
341 #-----------------------------------------------
342
343 def alpha(T):  # cm^3 s^-1 eq.2.3.31 Weinberg's book
344
345     return 1.4377*10**(-10)*T**(-0.6166)/(1+5.085*10**(-3)*T**0.5300)
346
347     #return 2.84*10**(-11)*T**(-1/2)
348
349 #-----------------------------------------------
350
351 def beta(T): # cm^-3 K^3/2 * alpha eq 2.3.32 Weinberg's book
352
353     return 2.4147*10**(15) *T**(3/2)*np.exp(-39474/T)*alpha(T)
354
355 #-----------------------------------------------
```

```
356
357 def S(T,h2Ob): #eq 2.3.8 Weinberg's book
358
359     return 1.747*10**(-22)*np.exp(157894/T)*T**(3/2)*h2Ob
360
361 #-----------------------------------------------
362
363 def model(X,T,h2Ob,C): # eq 2.3.27 Weinberg's book
364
365     # X is the fraction of H ionized
366     # T is the temperature
367
368     Y = Y_don_T(T,C)
369
370     Coef = 1 + beta(T)/(Gamma_2s + ( 8*np.pi*H_DG(Y,C) ) \
371     /( Lambda_alpha**3*n(T,h2Ob)*(1-X) ) )
372
373     N = alpha(T)*n(T,h2Ob)/(T*H_DG(Y,C))
374
375     dXdt = N*Coef**(-1)*(X**2-(1-X)/S(T,h2Ob))
376
377     return dXdt
378
379 #-----------------------------------------------
380
381 def equilibrium(X,T,h2Ob):
382
383     return X*(1+S(T,h2Ob)*X)-1
384
385 #-----------------------------------------------
386
387 def X_solver(T,h2Ob):
388
389     value=root_scalar(equilibrium,bracket=[0.9,3], \
390     method="brentq",args=(T,h2Ob),rtol=0.01)
391
392     if value.root > 1:
393
394         return 0.9999999
395
396     else:
397
```

```
398             return float(value.root)
399 
400 X_solver = np.vectorize(X_solver)
401 
402 #-----------------------------------------------
403 
404 temp = np.linspace(6000,1000,100)
405 
406 def solve_ode_DG(C,h2Ob):
407 
408     X0 = X_solver(6000,h2Ob)
409 
410     if h2Ob < 0:
411 
412         return np.full([len(temp)],np.nan)
413 
414     else:
415 
416         return odeint(model,X0,temp,args=(h2Ob,C),rtol=0.0000001)
417 
418 def calc_vis_fun(C,h2Ob,array_X_DG):
419 
420     if h2Ob < 0:
421 
422         return np.full([98],np.nan),np.full([98],np.nan)
423 
424     else:
425 
426         temp = np.linspace(6000,1000,100)
427 
428         temp = np.reshape(temp,100)
429 
430         temp =  temp.tolist() + [800,600,400,200,0]
431 
432         array_X_DG = np.reshape(array_X_DG,100)
433 
434         array_X_DG = array_X_DG.tolist() + [0,0,0,0,0]
435 
436         X_funcion = interpolate.interp1d(temp, array_X_DG, kind='quadratic')
437 
438         def integrand(T):
439 
```

```
440             Y = Y_don_T(T,C)
441
442             return c*sigma_thomson*X_funcion(T)*n( T, h2Ob )/(T*H_DG(Y,C))
443
444         integrand = np.vectorize(integrand)
445
446         def function(integral):
447
448             if integral > 12:
449
450                 return 1
451
452             else:
453
454                 return 1 - np.exp(-integral)
455
456         function = np.vectorize(function)
457
458         A1=np.linspace(1000,1999,50)
459
460         A2= np.linspace(2000,4000,300)
461
462         A3= np.linspace(4001,6000,100)
463
464         T_array_0 = np.concatenate((A1,A2,A3))
465
466         integral = cumtrapz(integrand(T_array_0),T_array_0)
467
468         integral = np.insert(integral,0,0,axis=0)
469
470         O = interpolate.interp1d(T_array_0,function(integral),kind='quadratic')
471
472         def dOdT(T):
473
474             return float(derivative(O, x0 = T, dx = 1e-6))
475
476         dOdT = np.vectorize(dOdT)
477
478         B1=np.linspace(1000,2000,7)
479
480         B2= np.linspace(2001,4000,86)
481
```

```
482         B3= np.linspace(4001,6000,7)
483
484         T_array = np.concatenate((B1,B2,B3))
485
486         return T_array[1:99],dOdT(T_array[1:99])
487
488 ######## modified adaptative metropolis MCMC algorithm #############
489
490 z_min,z_max = np.min(array_z),np.max(array_z)
491 C_min,C_max = np.min(array_C),np.max(array_C)
492 h2Ob_min,h2Ob_max = np.min(array_h2Ob),np.max(array_h2Ob)
493
494 # seeds
495
496 z_o = 1076
497 C_o = 4.67E-4
498 h2Ob_o = 0.024
499 ns_o = 1.02
500 N_o = 1.34E-5
501
502 sigma_z = 10
503 sigma_C = C_o/100
504 sigma_h2Ob = h2Ob_o/100
505 sigma_ns = ns_o/100
506 sigma_N = N_o/100
507
508 def f(o,n):
509
510     val = np.exp(o - n)
511
512     return val
513
514 def error(a,sigma_dist):
515
516     n = np.square(TT_planck_obs - a)
517
518     return np.sum(n)/sigma_dist
519
520 def cuadratica(x,a0,b0,c0):
521
522     return a0*x**2+b0*x+c0
523
```

```
524 def z_estimation(C_prob,h2Ob_prob):
525 
526     X_sol = solve_ode_DG(C_prob,h2Ob_prob)
527 
528     X,Y = calc_vis_fun(C_prob,h2Ob_prob,X_sol)
529 
530     peak=np.where(np.nanmax(Y) == Y)[0]
531 
532     near_x = X[int(peak)-4:int(peak)+5]
533     near_y = Y[int(peak)-4:int(peak)+5]
534 
535     popt, pcov = curve_fit(cuadratica,near_x,near_y)
536 
537     value = -popt[1]/(2*popt[0])
538 
539     return z_don_T(value)
540 
541 # MCMC metropolis
542 
543 def mcmc_complex(steps,chains):
544 
545     C_prob = np.random.normal(C_o, sigma_C, chains)
546     h2Ob_prob = np.random.normal(h2Ob_o, sigma_h2Ob, chains)
547     ns_prob = np.random.normal(ns_o, sigma_ns, chains)
548     N_prob = np.random.normal(N_o, sigma_N, chains)
549 
550     sigma_dist = 2849858
551 
552     z_o = z_estimation(C_o,h2Ob_o)
553 
554     z_prob = np.random.normal(z_o, sigma_z, chains)
555 
556     # initialization for every chain
557 
558     error_array = np.full((chains), np.nan)
559 
560     for i in range(chains):
561 
562         lH_prob = float(interp_lH([z_prob[i],C_prob[i],h2Ob_prob[i]]))
563         lT_prob = float(interp_lT([z_prob[i],C_prob[i]]))
564         lR_prob = float(interp_lR([z_prob[i],C_prob[i]]))
565         lD_prob = float(interp_lD([z_prob[i],C_prob[i],h2Ob_prob[i]]))
```

```
566         Rl_prob = float(interp_Rl([z_prob[i],C_prob[i],h2Ob_prob[i]]))
567
568         predict = integration(multipoles, \
569         lH_prob,lT_prob,lR_prob,lD_prob,Rl_prob,ns_prob[i],N_prob[i])
570
571         while np.isnan(error(predict,sigma_dist)):
572
573             C_prob[i] = np.random.normal(C_o, sigma_C)
574             h2Ob_prob[i] = np.random.normal(h2Ob_o, sigma_h2Ob)
575             ns_prob[i] = np.random.normal(ns_o, sigma_ns)
576             N_prob[i] = np.random.normal(N_o, sigma_N)
577
578             lH_prob = float(interp_lH([z_prob[i],C_prob[i],h2Ob_prob[i]]))
579             lT_prob = float(interp_lT([z_prob[i],C_prob[i]]))
580             lR_prob = float(interp_lR([z_prob[i],C_prob[i]]))
581             lD_prob = float(interp_lD([z_prob[i],C_prob[i],h2Ob_prob[i]]))
582             Rl_prob = float(interp_Rl([z_prob[i],C_prob[i],h2Ob_prob[i]]))
583
584             predict = integration(multipoles,lH_prob, \
585             lT_prob,lR_prob,lD_prob,Rl_prob,ns_prob[i],N_prob[i])
586
587         error_array[i] = error(predict,sigma_dist)
588
589     z_old,C_old,h2Ob_old,ns_old,N_old = \
590     z_prob,C_prob,h2Ob_prob,ns_prob,N_prob
591
592     z_chain = np.full((steps,chains), np.nan)
593     C_chain = np.full((steps,chains), np.nan)
594     h2Ob_chain = np.full((steps,chains), np.nan)
595     ns_chain = np.full((steps,chains), np.nan)
596     N_chain = np.full((steps,chains), np.nan)
597
598     adaptative_array = np.full((chains), 0)
599
600     for p in tqdm(itertools.product(range(steps) \
601     ,range(chains)),total = steps*chains):
602
603         i = p[0]
604         j = p[1]
605
606         C_new = float(np.random.normal(C_old[j], sigma_C))
607         h2Ob_new = float(np.random.normal(h2Ob_old[j], sigma_h2Ob))
```

```
608         ns_new = float(np.random.normal(ns_old[j], sigma_ns))
609         N_new = float(np.random.normal(N_old[j], sigma_N))
610 
611         z_o = z_estimation(C_new,h2Ob_new)
612         z_new = float(np.random.normal(z_o, sigma_z))
613 
614         while z_new<z_min or C_new<C_min or h2Ob_new<h2Ob_min or \
615         z_new>z_max or C_new>C_max or h2Ob_new>h2Ob_max or  N_new < 0:
616 
617             C_new = float(np.random.normal(C_old[j], sigma_C))
618             h2Ob_new = float(np.random.normal(h2Ob_old[j], sigma_h2Ob))
619             N_new = float(np.random.normal(N_old[j], sigma_N))
620 
621             z_o = z_estimation(C_new,h2Ob_new)
622             z_new = float(np.random.normal(z_o, sigma_z))
623         lH_new = float(interp_lH([z_new,C_new,h2Ob_new]))
624         lT_new = float(interp_lT([z_new,C_new]))
625         lR_new = float(interp_lR([z_new,C_new]))
626         lD_new = float(interp_lD([z_new,C_new,h2Ob_new]))
627         Rl_new = float(interp_Rl([z_new,C_new,h2Ob_new]))
628 
629         predict_new = integration(multipoles,lH_new, \
630         lT_new,lR_new,lD_new,Rl_new,ns_new,N_new)
631 
632         error_new = error(predict_new,sigma_dist)
633 
634         if np.isnan(error_new):
635 
636             print('NAN ERROR')
637 
638         val = np.random.rand()
639 
640         val2 = f(error_array[j],error_new)
641 
642         if val < val2:
643 
644             adaptative_array[j] += 1
645 
646             error_array[j] = error_new
647 
648             z_old[j] = z_new
649             C_old[j] = C_new
```

```
650             h2Ob_old[j] = h2Ob_new
651             ns_old[j] = ns_new
652             N_old[j] = N_new
653 
654         else:
655 
656             adaptative_array[j] -= 1
657 
658         if adaptative_array[j] ≥ 7:
659 
660             sigma_dist = 0.9*sigma_dist
661 
662             adaptative_array[j] -= 1
663 
664         elif adaptative_array[j] ≤ -7:
665 
666             sigma_dist = 1.1*sigma_dist
667 
668             adaptative_array[j] += 1
669 
670         z_chain[i][j] = z_old[j]
671         C_chain[i][j] = C_old[j]
672         h2Ob_chain[i][j] = h2Ob_old[j]
673         ns_chain[i][j] = ns_old[j]
674         N_chain[i][j] = N_old[j]
675 
676     return [z_chain, C_chain, h2Ob_chain, ns_chain, N_chain]
```

Listing G.1: This code runs the adaptative Metropolis MCMC algorithm based on the tables.

Bibliography

[1] Camb, 2019 (accessed March 20, 2019). URL https://camb.readthedocs.io/en/latest/.

[2] P. A. R. Ade et al. Planck 2013 results. XVI. Cosmological parameters. *Astron. Astrophys.*, 571:A16, 2014. doi: 10.1051/0004-6361/201321591.

[3] Stephen L. Adler. Einstein gravity as a symmetry-breaking effect in quantum field theory. *Reviews of Modern Physics*, 54(3):729–766, jul 1982. doi: 10.1103/revmodphys.54.729. URL https://doi.org/10.1103/revmodphys.54.729.

[4] N. Aghanim et al. Planck 2018 results. VI. Cosmological parameters. 7 2018.

[5] Andreas Albrecht, Gary Bernstein, Robert Cahn, Wendy L. Freedman, Jacqueline Hewitt, Wayne Hu, John Huth, Marc Kamionkowski, Edward W. Kolb, Lloyd Knox, John C. Mather, Suzanne Staggs, and Nicholas B. Suntzeff. Report of the Dark Energy Task Force. *arXiv e-prints*, art. astro-ph/0609591, September 2006.

[6] Jorge Alfaro. BV gauge theories. *ArXiv e-prints*, 1997.

[7] Jorge Alfaro. Delta-gravity, dark energy and the accelerated expansion of the universe. *Journal of Physics: Conference Series*, 384:012027, sep 2012. doi: 10.1088/1742-6596/384/1/012027. URL https://doi.org/10.1088%2F1742-6596%2F384%2F1%2F012027.

[8] Jorge Alfaro and Pablo González. Cosmology in delta-gravity. *Classical and Quantum Gravity*, 30(8):085002, March 2013. doi: 10.1088/0264-9381/30/8/085002. URL https://doi.org/10.1088/0264-9381/30/8/085002.

[9] Jorge Alfaro and Pablo González. Cosmology in delta-gravity. *Classical and Quantum Gravity*, 30(8):085002, mar 2013. doi: 10.1088/0264-9381/30/8/085002. URL https://doi.org/10.1088%2F0264-9381%2F30%2F8%2F085002.

[10] Jorge Alfaro and Pablo González. Cosmology in delta-gravity. *Classical and Quantum Gravity*, 30(8):085002, 2013. URL http://stacks.iop.org/0264-9381/30/i=8/a=085002.

[11] Jorge Alfaro and Pablo González. δ Gravity: Dark Sector, Post-Newtonian Limit and Schwarzschild Solution. *Universe*, 5(5):96, 2019. doi: 10.3390/universe5050096.

[12] Jorge Alfaro and Pablo González. $\tilde{\delta}$ gravity, $\tilde{\delta}$ matter and the accelerated expansion of the universe. *Gravitation and Cosmology*, 25(3):259–267, July 2019. doi: 10.1134/s0202289319030022. URL https://doi.org/10.1134/s0202289319030022.

[13] Jorge Alfaro and Pedro Labrana. Semiclassical gauge theories. *Phys. Rev.*, D65:045002, 2002. doi: 10.1103/PhysRevD.65.045002.

[14] Jorge Alfaro, Marco San Martín, and Joaquín Sureda. An accelerating universe without lambda: Delta gravity using monte carlo. *Universe*, 5(2), 2019. ISSN 2218-1997. doi: 10.3390/universe5020051. URL https://www.mdpi.com/2218-1997/5/2/51.

[15] Athem W. Alsabti and Paul Murdin. *Handbook of supernovae*. Springer, 2017.

[16] J. Ambjørn, J. Jurkiewicz, and R. Loll. Nonperturbative lorentzian path integral for gravity. *Physical Review Letters*, 85(5):924–927, jul 2000. doi: 10.1103/physrevlett.85.924. URL https://doi.org/10.1103/physrevlett.85.924.

[17] A Avgoustidis, G Luzzi, C.J.A.P Martins, and A.M.R.V.L Monteiro. Constraints on the CMB temperature-redshift dependence from SZ and distance measurements. *Journal of Cosmology and Astroparticle Physics*, 2012(02):013–013, feb 2012. doi: 10.1088/1475-7516/2012/02/013. URL https://doi.org/10.1088%2F1475-7516%2F2012%2F02%2F013.

[18] Jacob D. Bekenstein. Relativistic gravitation theory for the modified newtonian dynamics paradigm. *Phys. Rev. D*, 70:083509, Oct 2004. doi: 10.1103/PhysRevD.70.083509. URL https://link.aps.org/doi/10.1103/PhysRevD.70.083509.

[19] M. Betoule et al. Improved cosmological constraints from a joint analysis of the SDSS-II and SNLS supernova samples. *Astron. Astrophys.*, 568:A22, 2014. doi: 10.1051/0004-6361/201423413.

[20] Robert R. Caldwell and Marc Kamionkowski. The physics of cosmic acceleration. *Annual Review of Nuclear and Particle Science*, 59(1):397–429,

2009. doi: 10.1146/annurev-nucl-010709-151330. URL https://doi.org/10.1146/annurev-nucl-010709-151330.

[21] Colin, Jacques, Mohayaee, Roya, Rameez, Mohamed, and Sarkar, Subir. Evidence for anisotropy of cosmic acceleration. *A&A*, 631:L13, 2019. doi: 10.1051/0004-6361/201936373. URL https://doi.org/10.1051/0004-6361/201936373.

[22] I. de Martino, F. Atrio-Barandela, A. da Silva, H. Ebeling, A. Kashlinsky, D. Kocevski, and C. J. A. P. Martins. Measuring the Redshift Dependence of the Cosmic Microwave Background Monopole Temperature with Planck Data. *Astro-Ph*, 757(2):144, October 2012. doi: 10.1088/0004-637X/757/2/144.

[23] I.M.H. Etherington. Lx. on the definition of distance in general relativity. *The London, Edinburgh, and Dublin Philosophical Magazine and Journal of Science*, 15(100): 761–773, 1933. doi: 10.1080/14786443309462220. URL https://doi.org/10.1080/14786443309462220.

[24] Wendy L. Freedman, Barry F. Madore, Dylan Hatt, Taylor J. Hoyt, In Sung Jang, Rachael L. Beaton, Christopher R. Burns, Myung Gyoon Lee, Andrew J. Monson, Jillian R. Neeley, M. M. Phillips, Jeffrey A. Rich, and Mark Seibert. The carnegie-chicago hubble program. VIII. an independent determination of the hubble constant based on the tip of the red giant branch. *The Astrophysical Journal*, 882(1):34, aug 2019. doi: 10.3847/1538-4357/ab2f73. URL https://doi.org/10.3847%2F1538-4357%2Fab2f73.

[25] Wendy L. Freedman, Barry F. Madore, Taylor Hoyt, In Sung Jang, Rachael Beaton, Myung Gyoon Lee, Andrew Monson, Jill Neeley, and Jeffrey Rich. Calibration of the tip of the red giant branch. *The Astrophysical Journal*, 891(1):57, mar 2020. doi: 10.3847/1538-4357/ab7339. URL https://doi.org/10.3847%2F1538-4357%2Fab7339.

[26] J. A. Frieman, M. S. Turner, and D. Huterer. Dark energy and the accelerating universe. *Annual Review of Astronomy and Astrophysics*, 46:385–432, September 2008. doi: 10.1146/annurev.astro.46.060407.145243.

[27] A. Gelman, X.L. Meng, and H. Stern. Posterior predictive assessment of model fitness via realized discrepancies. *Statistica Sinica*, 6:733–759, 1996.

[28] Michael B. Green, J. H. Schwarz, and Edward Witten. *Superstring Theory. Vol. 1,2.* Cambridge Monographs on Mathematical Physics. Wiley, 1988. ISBN 9780521357524. URL http://www.cambridge.org/us/academic/subjects/physics/theoretical-physics-and-mathematical-physics/superstring-theory-volume-1.

[29] Joseph M. Hilbe, Rafael S. de Souza, and Emille E. O. Ishida. *Bayesian Models for Astrophysical Data*. Cambridge University Press, 2017. doi: 10.1017/cbo9781316459515. URL https://doi.org/10.1017/cbo9781316459515.

[30] N. Kaiser. Small-angle anisotropy of the microwave background radiation in the adiabatic theory. *MNRAS*, 202:1169–1180, March 1983. doi: 10.1093/mnras/202.4.1169.

[31] Yijung Kang, Young-Wook Lee, Young-Lo Kim, Chul Chung, and Chang Hee Ree. Early-type Host Galaxies of Type Ia Supernovae. II. Evidence for Luminosity Evolution in Supernova Cosmology. *arXiv e-prints*, art. arXiv:1912.04903, Dec 2019.

[32] O Klein. Generalization of einstein's principle of equivalence so as to embrace the field equations of gravitation. *Physica Scripta*, 9(2):69, 1974. URL http://stacks.iop.org/1402-4896/9/i=2/a=001.

[33] Lev Davidovich Landau. On the vibrations of the electronic plasma. *Yad. Fiz.*, 10:25, 1946. URL https://cds.cern.ch/record/437300.

[34] Julien Lesgourgues, Gianpiero Mangano, Gennaro Miele, and Sergio Pastor. *Neutrino Cosmology*. Cambridge University Press, 2013. doi: 10.1017/CBO9781139012874.

[35] Antony Lewis, Anthony Challinor, and Anthony Lasenby. Efficient Computation of Cosmic Microwave Background Anisotropies in Closed Friedmann-Robertson-Walker Models. *ApJ*, 538(2):473–476, Aug 2000. doi: 10.1086/309179.

[36] J. A. S. Lima, A. I. Silva, and S. M. Viegas. Is the radiation temperature-redshift relation of the standard cosmology in accordance with the data? *Monthly Notices of the Royal Astronomical Society*, 312(4):747–752, 03 2000. ISSN 0035-8711. doi: 10.1046/j.1365-8711.2000.03172.x. URL https://doi.org/10.1046/j.1365-8711.2000.03172.x.

[37] Daniel F. Litim. Fixed points of quantum gravity. *Physical Review Letters*, 92(20), may 2004. doi: 10.1103/physrevlett.92.201301. URL https://doi.org/10.1103/physrevlett.92.201301.

[38] Jerome Martin. Everything You Always Wanted To Know About The Cosmological Constant Problem (But Were Afraid To Ask). *Comptes Rendus Physique*, 13:566–665, 2012. doi: 10.1016/j.crhy.2012.04.008.

[39] M. Milgrom. A modification of the Newtonian dynamics as a possible alternative to the hidden mass hypothesis. *Astrophysical Journal*, 270:365–370, July 1983. doi: 10.1086/161130.

[40] V. Mukhanov. "CMB-slow" or how to determine cosmological parameters by hand? *International Journal of Theoretical Physics*, 43(3):623–668, March 2004. doi: 10.1023/b:ijtp.0000048168.90282.db. URL https://doi.org/10.1023/b:ijtp.0000048168.90282.db.

[41] Io Odderskov, Steen Hannestad, and Troels Haugbølle. On the local variation of the hubble constant. *Journal of Cosmology and Astroparticle Physics*, 2014(10):028, 2014. URL http://stacks.iop.org/1475-7516/2014/i=10/a=028.

[42] Pasquini, L., Bonifacio, P., Randich, S., Galli, D., and Gratton, R. G. Beryllium in turnoff stars of ngc 6397: Early galaxy spallation, cosmochronology and cluster formation ***. *A&A*, 426(2):651–657, 2004. doi: 10.1051/0004-6361:20041254. URL https://doi.org/10.1051/0004-6361:20041254.

[43] John A. Peacock, Peter Schneider, George Efstathiou, Jonathan R. Ellis, Bruno Leibundgut, Simon J. Lilly, and Yannick Mellier. Report by the ESA-ESO Working Group on Fundamental Cosmology. *"ESA-ESO Working Group on "Fundamental Cosmology", Edited by J.A. Peacock et al. ESA, 2006."*, 2006.

[44] D. Pequignot, P. Petitjean, and C. Boisson. Total and effective radiative recombination coefficients. *Astronomy & Astrophysics*, 251:680–688, November 1991.

[45] S. Perlmutter et al. Measurements of Ω and Λ from 42 High-Redshift Supernovae. *Astrophysical Journal*, 517:565–586, June 1999. doi: 10.1086/307221.

[46] D. W. Pesce, J. A. Braatz, M. J. Reid, A. G. Riess, D. Scolnic, J. J. Condon, F. Gao, C. Henkel, C. M. V. Impellizzeri, C. Y. Kuo, and K. Y. Lo. The megamaser cosmology project. XIII. combined hubble constant constraints. *The Astrophysical Journal*, 891(1):L1, feb 2020. doi: 10.3847/2041-8213/ab75f0. URL https://doi.org/10.3847%2F2041-8213%2Fab75f0.

[47] Oliver F. Piattella. *Lecture Notes in Cosmology*. UNITEXT for Physics. Springer, Cham, 2018. doi: 10.1007/978-3-319-95570-4.

[48] Planck Collaboration. Planck2015 results. *Astronomy & Astrophysics*, 594:A13, sep 2016. doi: 10.1051/0004-6361/201525830. URL https://doi.org/10.1051/0004-6361/201525830.

[49] Planck Collaboration. Planck 2018 results. VI. Cosmological parameters. *ArXiv e-prints*, 2018.

[50] J. Polchinski. *String theory. Vol. 1: An introduction to the bosonic string*. Cambridge Monographs on Mathematical Physics. Cambridge University Press, 2007. ISBN 9780511252273, 9780521672276, 9780521633031. doi: 10.1017/CBO9780511816079.

[51] Martin Reuter and Frank Saueressig. Functional Renormalization Group Equations, Asymptotic Safety, and Quantum Einstein Gravity. In *Geometric and topological methods for quantum field theory*, pages 288–329, 2010. doi: 10.1017/CBO9780511712135.008.

[52] Dean Richardson, Robert L. Jenkins, John Wright, and Larry Maddox. Absolute-Magnitude Distributions of Supernovae. *Astron. J.*, 147:118, 2014. doi: 10.1088/0004-6256/147/5/118.

[53] Adam G. Riess, Alexei V. Filippenko, Peter Challis, Alejandro Clocchiatti, Alan Diercks, Peter M. Garnavich, Ron L. Gilliland, Craig J. Hogan, Saurabh Jha, Robert P. Kirshner, B. Leibundgut, M. M. Phillips, David Reiss, Brian P. Schmidt, Robert A. Schommer, R. Chris Smith, J. Spyromilio, Christopher Stubbs, Nicholas B. Suntzeff, and John Tonry. Observational Evidence from Supernovae for an Accelerating Universe and a Cosmological Constant. *Astron.J.*, 116(3):1009–1038, Sep 1998. doi: 10.1086/300499.

[54] Adam G. Riess, Stefano Casertano, Wenlong Yuan, Lucas Macri, Jay Anderson, John W. MacKenty, J. Bradley Bowers, Kelsey I. Clubb, Alexei V. Filippenko, David O. Jones, and Brad E. Tucker. New parallaxes of galactic cepheids from spatially scanning the hubble space telescope : Implications for the hubble constant. *The Astrophysical Journal*, 855(2):136, 2018. URL http://stacks.iop.org/0004-637X/855/i=2/a=136.

[55] Adam G. Riess, Stefano Casertano, Wenlong Yuan, Lucas M. Macri, and Dan Scolnic. Large magellanic cloud cepheid standards provide a 1% foundation for the determination of the hubble constant and stronger evidence for physics beyond λCDM. *The*

Astrophysical Journal, 876(1):85, may 2019. doi: 10.3847/1538-4357/ab1422. URL https://doi.org/10.3847%2F1538-4357%2Fab1422.

[56] Adam G. Riess et al. A 2.4% Determination of the Local Value of the Hubble Constant. *Astrophys. J.*, 826(1):56, 2016. doi: 10.3847/0004-637X/826/1/56.

[57] A. D. Sakharov. Vacuum Quantum Fluctuations in Curved Space and the Theory of Gravitation. *Soviet Physics Doklady*, 12:1040, May 1968.

[58] D. M. Scolnic, D. O. Jones, et al. The complete light-curve sample of spectroscopically confirmed sne ia from pan-starrs1 and cosmological constraints from the combined pantheon sample. *The Astrophysical Journal*, 859(2):101, 2018. URL http://stacks.iop.org/0004-637X/859/i=2/a=101.

[59] Uros Seljak and Matias Zaldarriaga. A Line-of-Sight Integration Approach to Cosmic Microwave Background Anisotropies. *ApJ*, 469:437, Oct 1996. doi: 10.1086/177793.

[60] Joseph Silk. Cosmic black body radiation and galaxy formation. *Astrophys. J.*, 151: 459–471, 1968. doi: 10.1086/149449.

[61] Gerard 't Hooft and M. J. G. Veltman. One loop divergencies in the theory of gravitation. *Ann. Inst. H. Poincare Phys. Theor.*, A20:69–94, 1974.

[62] S. Tsujikawa. Modified gravity models of dark energy. In *Lectures on Cosmology*, pages 99–145. Springer Berlin Heidelberg, 2010. doi: 10.1007/978-3-642-10598-2_3. URL https://doi.org/10.1007/978-3-642-10598-2_3.

[63] Slava G. Turyshev. Experimental tests of general relativity. *Annual Review of Nuclear and Particle Science*, 58(1):207–248, 2008. doi: 10.1146/annurev.nucl.58.020807.111839. URL https://doi.org/10.1146/annurev.nucl.58.020807.111839.

[64] Makoto Uemura, Koji S. Kawabata, Shiro Ikeda, and Keiichi Maeda. Variable selection for modeling the absolute magnitude at maximum of type ia supernovae. *Publications of the Astronomical Society of Japan*, 67(3):55, jun 2015. doi: 10.1093/pasj/psv031. URL https://doi.org/10.1093/pasj/psv031.

[65] Eleonora Di Valentino, Alessandro Melchiorri, and Joseph Silk. Planck evidence for a closed universe and a possible crisis for cosmology. *Nature Astronomy*, November 2019. doi: 10.1038/s41550-019-0906-9. URL https://doi.org/10.1038/s41550-019-0906-9.

[66] S Weinberg. -. In S. Hawking and W. Israel, editors, *General Relativity: an Einstein Centenary Survey*, chapter 16, page 790. Cambridge University Press, Cambridge, 1979.

[67] S. Weinberg. *Cosmology*. Cosmology. OUP Oxford, 2008. ISBN 9780191523601. URL https://books.google.cl/books?id=nqQZdg020fsC.

[68] Steven Weinberg. Entropy Generation and the Survival of Protogalaxies in an Expanding Universe. *Astro-Ph*, 168:175, September 1971. doi: 10.1086/151073.

[69] Clifford M. Will. The confrontation between general relativity and experiment. *Living Reviews in Relativity*, 9(1):3, Mar 2006. ISSN 1433-8351. doi: 10.12942/lrr-2006-3. URL https://doi.org/10.12942/lrr-2006-3.

[70] Kenneth C Wong, Sherry H Suyu, Geoff C-F Chen, Cristian E Rusu, Martin Millon, Dominique Sluse, Vivien Bonvin, Christopher D Fassnacht, Stefan Taubenberger, Matthew W Auger, Simon Birrer, James H H Chan, Frederic Courbin, Stefan Hilbert, Olga Tihhonova, Tommaso Treu, Adriano Agnello, Xuheng Ding, Inh Jee, Eiichiro Komatsu, Anowar J Shajib, Alessandro Sonnenfeld, Roger D Blandford, Léon V E Koopmans, Philip J Marshall, and Georges Meylan. H0LiCOW XIII. A 2.4% measurement of H0 from lensed quasars: 5.3 tension between early and late-Universe probes. *Monthly Notices of the Royal Astronomical Society*, 06 2020. ISSN 0035-8711. doi: 10.1093/mnras/stz3094. URL https://doi.org/10.1093/mnras/stz3094. stz3094.

[71] Matias Zaldarriaga, Uroš Seljak, and Edmund Bertschinger. Integral solution for the microwave background anisotropies in nonflat universes. *The Astrophysical Journal*, 494(2):491–502, feb 1998. doi: 10.1086/305223. URL https://doi.org/10.1086%2F305223.

[72] Y. B. Zeldovich. Cosmological Constant and Elementary Particles. *JETP Lett.*, 6:316, 1967. [Pisma Zh. Eksp. Teor. Fiz.6,883(1967)].